

G3/05      Unclass  
24159

National Aeronautics and  
Space Administration

---

# A Mathematical Simulation Model of a CH-47B Helicopter

---

Jeanine M. Weber, Ames Research Center, Moffett Field, California

Tung Y. Liu and William Chung, Computer Sciences Corporation, Mountain View, California



National Aeronautics and  
Space Administration

**Ames Research Center**

Moffett Field, California 94035

# TABLE OF CONTENTS

	Page
SUMMARY . . . . .	1
NOMENCLATURE . . . . .	1
INTRODUCTION . . . . .	2
MATHEMATICAL MODEL DESCRIPTION . . . . .	
Rotors . . . . .	3
Fuselage Aerodynamics . . . . .	3
Engine and Governor . . . . .	13
Mechanical Controls . . . . .	16
Stability Augmentation System . . . . .	17
Electronic Control System . . . . .	18
Slung Load . . . . .	19
OPERATIONAL CONSIDERATIONS . . . . .	20
CONCLUSIONS . . . . .	24
APPENDIX A: FLAPPING AND CONING EQUATIONS . . . . .	24
APPENDIX B: INFLOW DYNAMICS SOLUTION . . . . .	25
REFERENCES . . . . .	28
TABLES . . . . .	31
FIGURES . . . . .	32
	95

PRECEDING PAGE BLANK NOT FILLED

## SUMMARY

A nonlinear simulation model of the CH-47B helicopter, developed by the Boeing Vertol Company (ref. 1), has been adapted for use in the NASA Ames Research Center (ARC) simulation facility. The model represents the specific configuration of the ARC variable stability CH-47B helicopter (fig. 1) and will be used in ground simulation research and to expedite and verify flight experiment design.

Modeling of the helicopter uses a total force approach in six rigid body degrees of freedom. Rotor dynamics are simulated using the Wheatley-Bailey equations, including steady-state flapping dynamics. Also included in the model is the option for simulation of external suspension, slung-load equations of motion.

Validation of the model (discussed in Volume II of this report) has been accomplished using static and dynamic data from the original Boeing Vertol mathematical model and flight test data from references 2 and 3, as reproduced in reference 4. The model is appropriate for use in real-time piloted simulation and is implemented on the ARC Sigma IX computer where it may be operated with a digital cycle time of 0.03 sec.

## NOMENCLATURE

AERO	fuselage aerodynamics subroutine
ARC	Ames Research Center
BV	Boeing Vertol Company
c.g.	center of gravity
CONTROL	mechanical control system subroutine
DCPT	differential collective pitch trim
ECS	electronic control system
ENGINE	engine and governor subroutine
$N_{\beta}$	change in helicopter yawing moment per sideslip angle
rpm	revolutions per minute
ROTOR	rotor dynamics subroutine
SAS	stability augmentation system
SLING	sling load dynamics subroutine

SNP        shaft-normal-plane  
SNPW      shaft-normal-plane-wind  
 $V_{eq}$       equivalent velocity

## INTRODUCTION

At Ames Research Center (ARC), the CH-47B provides a unique capability for generic flight research in flight controls and displays for rotorcraft and VTOL aircraft. In addition to the existing potential for variable-stability flight, a programmable display system and a variable force-feel system are being developed. The purpose of this mathematical model development is to provide the capability for real-time simulation and for the preliminary check-out of in-flight research experiments for the variable-stability CH-47B helicopter.

Subroutines that comprise the mathematical model describe the rotor systems, fuselage aerodynamics, engine and governor, mechanical control system, the option for either an electronic control system or the basic stability augmentation system (SAS), and the option for externally suspended, slung-load dynamics. Forward and rear rotor dynamics are simulated in a shaft-normal-plane-wind (SNPW) reference frame with the Wheatley-Bailey (modified tip path plane) equations of references 5, 6, and 7. Steady state flapping dynamics are represented with these equations; however, in-plane motions are neglected. Forces and moments at the rotor hubs are then calculated as a function of rotor aerodynamic conditions and dynamics, after which they are resolved to the helicopter center of gravity. Six rigid-body forces and moments resulting from fuselage aerodynamics are found from tabular data interpolated as a function of fuselage angle of attack and sideslip angle.

Each engine is represented with nonlinear, second-order dynamics; left and right engine models are identical, yet are modeled separately. The fuel control system and gas generator are each modeled as a first-order system, the latter including a variable time constant dependent upon power and power error. The engine governor, whose purpose is to regulate rotor rpm, is modeled as a linear, third-order system.

Modeling of the hardware from the cockpit controls to the swashplate comprises the mechanical controls subroutine. Included are upstream limiters on each control input, first- and second-stage mixing, swashplate limits, and swiveling and pivoting actuation dynamics (first order).

Stability augmentation in the form of longitudinal, lateral, and directional rate damping is modeled. Additional features of the directional SAS include turn coordination and feedback of sideslip angle to obtain a stable yawing moment change with sideslip ( $N_\beta$ ).

The provision for an electronic control system (ECS) model has been included in this program. Although no specific ECS configuration has been documented in this report, the information necessary to integrate such a subroutine into the simulation model is discussed in the section concerning the ECS.

A model of an externally suspended, slung load has been developed and is available for use with the helicopter simulation model. Three state variables, defining the position of the load and suspension cables relative to the helicopter, are represented

with nonlinear, second-order equations of motion. Thus, the combined system (helicopter and slung load), is represented with nine coupled, differential equations modeling the two rigid bodies.

The specifications of the real-time simulation model are presented in this report, organized by subroutine. Documentation of each subroutine is characterized by an engineering explanation, input/output variable lists, and the definition of computer mnemonics in terms of engineering variables. The subroutines are discussed in the following order: rotor dynamics (ROTOR), fuselage aerodynamics (AERO), engine and governor (ENGINE), mechanical control system (CONTROL), stability augmentation system (SAS), electronic control system (ECS) and slung-load dynamics (SLING).

Operational considerations are discussed, including the specification of input constants and other information necessary for a piloted simulation using a simulator cab and a visual display.

Finally, in Volume II of this report, results of the ARC static and dynamic model validation are discussed. ARC static trim and stability derivative data are tabulated; also, ARC dynamic data are compared with a Boeing Vertol Company (BV) model and CH-47 flight-test data from references 2 and 3 (reproduced in ref. 4).

## MATHEMATICAL MODEL DESCRIPTION

### Rotors

Wheatley-Bailey (modified tip-path plane) equations (refs. 5, 6, and 7) form the basis for the simulation of the rotors in this mathematical model. In subroutine ROTOR, total forces and moments resulting from each helicopter rotor are computed in the SNPW reference frame. These are then transformed to the body reference frame at the helicopter center of gravity (c.g.) for incorporation into the six degree-of-freedom rigid-body equations (which are part of the established Ames simulation facility and are known as subroutine SMART (refs. 8 and 9)).

Figure 2 shows a signal flow diagram of the rotor subroutine (in terms of computer mnemonics), including variable inputs and outputs to and from other model subroutines. The equations are executed sequentially as indicated by the numbered modules in the figure. Since the calculation of rotor hub forces and moments is required for this model, it is necessary to perform transformations between the helicopter body and the SNPW reference frames. To do this, the position of the actual rotor c.g. relative to the actual helicopter c.g. (fig. 3) is computed using equation (1),

$$\begin{matrix} \text{SLFR,SLRR} \\ \text{SDFR,SDRR} \\ \text{SHFR,SHRR} \end{matrix} \begin{bmatrix} f_{F,R} \\ d_{F,R} \\ h_{F,R} \end{bmatrix} = \begin{bmatrix} f_{F,R_x} \\ d_{F,R_x} \\ h_{F,R_x} \end{bmatrix} - \begin{bmatrix} \Delta X_{c.g.}/12 \\ \Delta Y_{c.g.}/12 \\ \Delta Z_{c.g.}/12 \end{bmatrix} \quad (1)$$

where the positions of the baseline rotor c.g. relative to the baseline helicopter c.g. are given by:

$$\begin{Bmatrix} \ell_{F_x} \\ d_{F_x} \\ h_{F_x} \end{Bmatrix} = \begin{Bmatrix} 20.43 \text{ ft} \\ 0.0 \text{ ft} \\ 7.49 \text{ ft} \end{Bmatrix}, \quad \begin{Bmatrix} \ell_{R_x} \\ d_{R_x} \\ h_{R_x} \end{Bmatrix} = \begin{Bmatrix} -18.46 \text{ ft} \\ 0.0 \text{ ft} \\ 12.16 \text{ ft} \end{Bmatrix}$$

The vector

$$\begin{matrix} \text{DXCG} \\ \text{DYCG} \\ \text{DZCG} \end{matrix} \begin{Bmatrix} \Delta X_{c.g.} \\ \Delta Y_{c.g.} \\ \Delta Z_{c.g.} \end{Bmatrix}$$

is the position in inches of the c.g. of the actual helicopter relative to the baseline specifications. Baseline helicopter c.g. positions are

$$\begin{Bmatrix} X_{c.g.} \\ Y_{c.g.} \\ Z_{c.g.} \end{Bmatrix} = \begin{Bmatrix} 331 \text{ in.} \\ 0.0 \text{ in.} \\ 11.2 \text{ in.} \end{Bmatrix}$$

and the sign conventions are as given in figure 4.

To compute forces and moments at the rotor hub, helicopter body-axis velocities (from subroutine SMART, rigid-body dynamics model) are transformed from the body reference frame to the rotor SNPW reference frame. Representation of the body axis velocities at the rotor hubs is given in equation (2).

$$\begin{matrix} \text{UFR1,URR1} \\ \text{VFR1,VRR1} \\ \text{WFR1,WRR1} \end{matrix} \begin{Bmatrix} u_{F_1}, u_{R_1} \\ v_{F_1}, v_{R_1} \\ w_{F_1}, w_{R_1} \end{Bmatrix} = \begin{Bmatrix} u_B \\ v_B \\ w_B \end{Bmatrix} + \begin{bmatrix} 0 & -h_{F,R} & -d_{F,R} \\ h_{F,R} & 0 & \ell_{F,R} \\ d_{F,R} & -\ell_{F,R} & 0 \end{bmatrix} \begin{Bmatrix} p_B \\ q_B \\ r_B \end{Bmatrix} \quad (2)$$

Body-axis velocities (at the rotor hub) are transformed (eq. (3)) from the body to the SNP reference frame through shaft incidence angles  $i_{F,R}$  (fig. 5).

$$\begin{matrix} \text{UFR2,URR2} \\ \text{VFR2,VRR2} \\ \text{WFR2,WRR2} \end{matrix} \begin{Bmatrix} u_{F_2}, u_{R_2} \\ v_{F_2}, v_{R_2} \\ w_{F_2}, w_{R_2} \end{Bmatrix} = \begin{bmatrix} \cos i_{F,R} & 0 & \sin i_{F,R} \\ 0 & 1 & 0 \\ -\sin i_{F,R} & 0 & \cos i_{F,R} \end{bmatrix} \begin{Bmatrix} u_{F_1}, u_{R_1} \\ v_{F_1}, v_{R_1} \\ w_{F_1}, w_{R_1} \end{Bmatrix} \quad (3)$$

The rotor SNP may be considered an intermediate reference frame between the helicopter body and SNPW reference frames.

ORIGINAL PAGE  
OF POOR QUALITY

Rotor sideslip angle is defined by equation (4),

$$\begin{matrix} \text{BETA FR} \\ \text{BETA PR} \end{matrix} \beta'_{F,R} = \arctan \frac{v_{F,R_2}}{u_{F,R_2}} \quad (4)$$

and SNP translational velocities are effectively resolved (eqs. (5) and (6)) through  $\beta'_{F,R}$  into the SNPW reference frame, as shown in figure 6. Rotor-hub forces and moments are eventually computed in this frame, as indicated in the figure.

$$\begin{matrix} \text{UFR} \\ \text{URR} \end{matrix} u_{F,R} = \sqrt{u_{F,R_2}^2 + v_{F,R_2}^2} \quad (5)$$

$$\begin{matrix} \text{WFR} \\ \text{WRR} \end{matrix} w_{F,R} = w_{F,R_2} \quad (6)$$

Next, helicopter-body angular velocities (from SMART) are transformed (eqs. (7) and (8)) to the SNPW reference frame as shown in figure 6.

$$\begin{matrix} \text{PFR} \\ \text{QFR} \\ \text{RFR} \end{matrix} \begin{bmatrix} p_F \\ q_F \\ r_F \end{bmatrix} = \begin{bmatrix} \cos \beta'_F \cos i_F & \sin \beta'_F & \cos \beta'_F \sin i_F \\ -\sin \beta'_F \cos i_F & \cos \beta'_F & \sin \beta'_F \sin i_F \\ -\sin i_F & 0 & \cos i_F \end{bmatrix} \begin{bmatrix} p_B \\ q_B \\ r_B \end{bmatrix} \quad (7)$$

$$\begin{matrix} \text{PRR} \\ \text{QRR} \\ \text{RRR} \end{matrix} \begin{bmatrix} p_R \\ q_R \\ r_R \end{bmatrix} = \begin{bmatrix} -\cos \beta'_R \cos i_R & -\sin \beta'_R & -\cos \beta'_R \sin i_R \\ -\sin \beta'_R \cos i_R & \cos \beta'_R & -\sin \beta'_R \sin i_R \\ \sin i_R & 0 & -\cos i_R \end{bmatrix} \begin{bmatrix} p_B \\ q_B \\ r_B \end{bmatrix} \quad (8)$$

Rotor angular velocity is corrected for helicopter yaw rate in equation (9):

$$\begin{matrix} \text{OMEG FR} \\ \text{OMEG RR} \end{matrix} \Omega_{F,R} = \Omega'_{F,R} - r_{F,R} \quad (9)$$

and rotor tip speed is calculated based on this rpm in equation (10):

$$\begin{matrix} \text{VTIP FR} \\ \text{VTIP RR} \end{matrix} V_{\text{Tip } F,R} = R_{B,F,R} \Omega_{F,R} \quad (10)$$

Advance ratio and the free stream component of inflow ratio are calculated in equations (11) and (12):



$$\begin{array}{l} \text{AMUFR} \\ \text{AMURR} \end{array} \quad u_{F,R} = \frac{u_{F,R}}{R_{B_{F,R}} (\Omega'_{F,R} - r_{F,R})} \quad (11)$$

$$\begin{array}{l} \text{ALMPFR} \\ \text{ALMPRR} \end{array} \quad \lambda'_{F,R} = \frac{w_{F,R}}{R_{B_{F,R}} (\Omega'_{F,R} - r_{F,R})} \quad (12)$$

Prior to their usage in computations (i.e., for flapping coefficients and rotor forces and moments), the pilot's control inputs are transformed to the SNPW reference frame and corrected for control phasing angle ( $\phi_p$ ) and pitch-flap coupling ( $\delta_3$ ). Thus, it is unnecessary to make these corrections during the actual computation of these quantities (as noted in the flapping assumptions which follow). Longitudinal and lateral cyclic pitch in the SNPW reference frame (from subroutine CONTROL) are transformed to the SNPW reference frame in equations (13) and (14).

$$\begin{array}{l} \text{AICFR1} \\ \text{BICFR1} \end{array} \begin{bmatrix} A'_{1CF_1} \\ B'_{1CF_2} \end{bmatrix} = \begin{bmatrix} \cos \beta'_F & -\sin \beta'_F \\ \sin \beta'_F & \cos \beta'_F \end{bmatrix} \begin{bmatrix} A'_{1CF} \\ B'_{1CF} \end{bmatrix} \quad (13)$$

$$\begin{array}{l} \text{AICRR1} \\ \text{BICRR1} \end{array} \begin{bmatrix} A'_{1CR_1} \\ B'_{1CR_1} \end{bmatrix} = \begin{bmatrix} \cos \beta'_R & \sin \beta'_R \\ -\sin \beta'_R & \cos \beta'_R \end{bmatrix} \begin{bmatrix} A'_{1CR} \\ B'_{1CR} \end{bmatrix} \quad (14)$$

Although the pitch-flap coupling and control phasing angles are zero in the current configuration of the ARC CH-47B, the capability for these variations has been included in the simulation model. The purpose of the control phasing angle,  $\phi_p$ , is to offset the lead of the blade relative to the pitch hinge, which was introduced by pitch-flap ( $\delta_3$ ) coupling (fig. 7, taken from ref. 10). In equations (15) and (16), rotor cyclic pitch positions are transformed through control phasing angle,  $\phi_p$  (fig. 8).

$$\begin{array}{l} \text{AICFR2} \\ \text{BICFR2} \end{array} \begin{bmatrix} A'_{1CF_2} \\ B'_{1CF_2} \end{bmatrix} = \begin{bmatrix} \cos \phi_{p_F} & -\sin \phi_{p_F} \\ \sin \phi_{p_F} & \cos \phi_{p_F} \end{bmatrix} \begin{bmatrix} A'_{1CF_1} \\ B'_{1CF_1} \end{bmatrix} \quad (15)$$

$$\begin{array}{l} \text{AICRR2} \\ \text{BICRR2} \end{array} \begin{bmatrix} A'_{1CF_2} \\ B'_{1CF_2} \end{bmatrix} = \begin{bmatrix} \cos \phi_{p_R} & -\sin \phi_{p_R} \\ \sin \phi_{p_R} & \cos \phi_{p_R} \end{bmatrix} \begin{bmatrix} A'_{1CR_1} \\ B'_{1CR_1} \end{bmatrix} \quad (16)$$

In equation (17), rotor cyclic and collective positions are corrected for  $\delta_3$  (ref. 11).

ORIGINAL  
OF POOR QUALITY

$$\begin{matrix} \text{AICFR, AICRR} \\ \text{BICFR, BICRR} \\ \text{THOFR, THORR} \end{matrix} \begin{bmatrix} A_{1C_{F,R}} \\ B_{1C_{F,R}} \\ \theta_{0F,R} \end{bmatrix} = \begin{bmatrix} A'_{1C_{F,R_2}} \\ B'_{1C_{F,R_2}} \\ \theta'_{0F,R} \end{bmatrix} + K_{\beta_{F,R}} \begin{bmatrix} a_{1F,R} \\ b_{1F,R} \\ a_{0F,R} \end{bmatrix} \quad (17)$$

where  $K_{\beta_{F,R}} = -\tan(\delta_{3F,R})$ .

Rotor degrees of freedom are limited to feathering and the computation of steady state flapping and coning coefficients. No in-plane (lead-lag) degree of freedom has been considered. Flapping and coning coefficients are computed by solving a 3x3 linear system of algebraic equations, and are developed based upon the following simplifying assumptions (ref. 1):

1. Only the first harmonic terms are used.
2. There is a uniform inflow.
3. No reverse flow is considered.
4. Identical forms for the front and rear rotors are used.
5. There are no pitch-flap coupling effects (the control inputs are corrected in this regard).
6. There is a zero tip-loss factor.
7. There is a negligible hinge offset.
8. Rigid blades are used.
9. There are no compressibility effects.
10. There is a constant rotor airfoil-section lift-curve slope.
11. The rotor airfoil-section drag varies only with rotor angle of attack.

Steady-state flapping and coning angles are found by solving equation (18) with Cramer's Rule. (The derivation of these equations is given in appendix A.)

$$\begin{bmatrix} A_{F,R} & B_{F,R} & C_{F,R} \\ D_{F,R} & E_{F,R} & F_{F,R} \\ G_{F,R} & H_{F,R} & I_{F,R} \end{bmatrix} \begin{bmatrix} a_{0F,R} \\ a_{1F,R} \\ b_{1F,R} \end{bmatrix} = \begin{bmatrix} J_{F,R} \\ K_{F,R} \\ L_{F,R} \end{bmatrix} \quad (18)$$

where:

$$A_{F,R} = \frac{12I_{F,R}}{\rho a_{F,R} c_{F,R} R^4} - \frac{3}{2} K_{\beta_{F,R}} (1 + \mu_{F,R}^2)$$

$$B_{F,R} = 0$$

$$C_{F,R} = 2\mu_{F,R} K_{\beta_{F,R}}$$

$$D_{F,R} = -\frac{2}{3} K_{\beta_{F,R}} \mu_{F,R}$$

ORIGINAL PAGE  
OF POOR QUALITY

$$E_{F,R} = \frac{1}{4} - \frac{\mu_{F,R}^2}{8}$$

$$F_{F,R} = K_{\beta_{F,R}} \left( \frac{1}{4} + \frac{3}{8} \mu_{F,R}^2 \right)$$

$$G_{F,R} = -\frac{4}{3} \frac{\mu_{F,R}^2}{\left( 1 + \frac{\mu_{F,R}^2}{2} \right)}$$

$$H_{F,R} = -K_{\beta_{F,R}}$$

$$I_{F,R} = 1.0$$

$$J_{F,R} = \frac{3}{2} \theta'_{0F,R} (1 + \mu_{F,R}^2) + 2\lambda_{F,R} - 2\mu_{F,R} B'_{1C_{F,R_2}} + \theta_{tw_{F,R}} (1.2 + \mu_{F,R}^2)$$

$$K_{F,R} = \frac{2}{3} \mu_{F,R} \theta'_{0F,R} + \frac{1}{2} \lambda_{F,R} \mu_{F,R} + \frac{1}{2} \theta_{tw_{F,R}} \mu_{F,R} - B'_{1C_{F,R_2}} \left( \frac{1}{4} + \frac{3}{8} \mu_{F,R}^2 \right) \\ - \frac{4I_{F,R} q_{F,R}}{\rho a_{F,R} c_{F,R} R_{B_{F,R}}^4 \Omega_{F,R}} \left( 1 - \frac{\mu_{F,R}^4}{4} \right)$$

$$L_{F,R} = A'_{1C_{F,R_2}} - \frac{16I_{F,R} p_{F,R}}{\rho a_{F,R} c_{F,R} R_{B_{F,R}}^4 \Omega_{F,R}} \left( 1 - \frac{\mu_{F,R}^2}{2} \right)$$

Using Wheatley-Bailey theory (refs. 5-7), thrust, torque, side force, and drag at the rotor hubs are computed. Expressions for thrust and torque follow the theory as developed for a tandem rotor helicopter using the SNPW reference frame. Expressions for rotor side force and drag were greatly simplified by BV during their development because the simplified forms provided a better match with flight test data than did the full theoretical expressions.

Mean rotor thrust is computed with equation (19).

$$\begin{aligned} \text{CTFR1} \quad \frac{2C_{T_{F,R}}}{a_{F,R} \sigma_{F,R}} &= \frac{1}{2} \left\{ \lambda_{F,R} + \frac{2}{3} \theta_{0_{F,R}} + \frac{1}{2} \theta_{tw_{F,R}} \right. \\ \text{CTRR1} \quad &\left. + \mu_{F,R} \left[ \mu_{F,R} \left( \theta_{0_{F,R}} + \frac{1}{2} \theta_{tw_{F,R}} \right) - B_{1C_{F,R}} \right] \right\} \end{aligned} \quad (19)$$

In coefficient form, thrust is modified owing to limits on its maximum allowable value, for rotor stall, and due to ground effect. Since the maximum allowable normalized thrust coefficient,  $2C_T/a\sigma$ , is 1.0, a limit is imposed if the computed value is greater than 1.0. As a function of advanced ratio, normalized thrust coefficient is modified as shown in figure 9 for the effects of rotor stall. This is an empirical correction which was derived by BV to provide a better match of the model's dynamic response with wind-tunnel test data and is selected (along with a correction to rotor torque) with flag NSTALL in the simulation model. Thrust coefficient is computed as shown in equation (20)

$$\begin{aligned} \text{CTFR} \quad C_{T_{F,R}} &= \left( \frac{2C_{T_{F,R}}}{a_{F,R} \sigma_{F,R}} \right) \frac{a_{F,R} \sigma_{F,R}}{2} \\ \text{CTFR} \end{aligned} \quad (20)$$

and if longitudinal velocity is less than 40 knots (and if the ground-effect correction is selected with flag NGREFF), thrust is modified for ground effect as a function of altitude and airspeed. Thrust is calculated in equation (21)

$$T_{F,R} = C_{T_{F,R}} \rho \pi R_{B_{F,R}}^4 \Omega_{F,R}^2 \left( 1 + K_{g.e.,F,R} T_{i.g.e.,F,R} \right) \quad (21)$$

where

$$K_{ge_{F,R}} = 1 - \frac{U_{F,R}}{U_{ge}} \quad (U_{g.e.} = 40 \text{ knots})$$

and  $T_{i.g.e.}$  is determined from figure 10 as a function of the rotor height to diameter ratio  $(h/D)_{\text{rotor}}$ .

Mean aerodynamic torque required is found from equation (22)

$$\begin{aligned} \text{CQFR1} \quad \frac{2C_{Q_{F,R}}}{a_{F,R} \sigma_{F,R}} &= \mu_{F,R} \left\{ 0.25 \mu_{F,R} \left[ 4.65 \frac{\delta_{F,R}}{a_{F,R}} - a_{0F,R}^2 + 0.25 \left( B_{1C_{F,R}} a_{1F,R} - 3a_{1F,R}^2 \right. \right. \right. \\ \text{CQRR1} \quad &+ A_{1C_{F,R}} b_{1F,R} - b_{1F,R}^2 \left. \left. \right] \right\} + \frac{\lambda_{F,R}}{2} \left( \frac{B_{1C_{F,R}}}{2} - a_{1F,R} \right) \\ &+ \frac{a_{0F,R}}{3} \left( b_{1F,R} - \frac{A_{1C_{F,R}}}{2} \right) \left\} + \frac{1}{2} \left( \frac{\delta_{F,R}}{2a_{F,R}} - \lambda_{F,R}^2 \right) - \lambda_{F,R} \left( \frac{\theta_{0F,R}}{3} + \frac{\theta_{tw_{F,R}}}{4} \right) \\ &+ \frac{1}{8} \left( A_{1C_{F,R}} b_{1F,R} - B_{1C_{F,R}} a_{1F,R} - a_{1F,R}^2 - b_{1F,R}^2 \right) \end{aligned} \quad (22)$$

As a function of rotor thrust and advance ratio, the torque coefficient is modified for rotor stall (flag NSTALL) as shown in figure 11. Also, an empirical correction is made to the torque coefficient to attain a better match with flight-test data. This correction, the effects of which are shown in figure 12, is calculated as a function of advance ratio and thrust coefficient (flag NTRQCK). Including the two corrections, the aerodynamic torque coefficient is:

$$\begin{aligned} \text{CQFR} \quad C_{Q_{F,R}} &= \left( \frac{2C_{Q_{F,R}}}{a_{F,R} \sigma_{F,R}} \right) \frac{a_{F,R} \sigma_{F,R}}{2} + \Delta C_{Q_{F,R,R.S.}} + \Delta C_{Q_{F,R}} \\ \text{CQRR} \end{aligned} \quad (23)$$

and the rotor torque required is

$$\begin{aligned} \text{QAERFR} \quad Q_{AER_{F,R}} &= C_{Q_{F,R}} \rho \pi R_B^5 \Omega^2 \\ \text{QAERRR} \end{aligned} \quad (24)$$

Rotor sideforce is calculated with equations (25) - (27).

$$\begin{aligned} \text{CYFR1} \quad \frac{2C_{Y_{F,R}}}{a_{F,R} \sigma_{F,R}} &= \frac{2C_{T_{F,R}}}{a_{F,R} \sigma_{F,R}} b_{1F,R} + \mu_{F,R} \left\{ a_{1F,R} \left[ \frac{1}{4} \left( b_{1F,R} - A_{1C_{F,R}} \right) - \mu_{F,R} a_{0F,R} \right] \right. \\ \text{CYRR1} \quad &+ \frac{1}{2} a_{0F,R} \left( \mu_{F,R} B_{1C_{F,R}} - 1.5 \theta_{0F,R} - 3\lambda_{F,R} - \theta_{tw_{F,R}} \right) \left. \right\} \\ &+ \frac{1}{4} \lambda_{F,R} \left( b_{1F,R} - A_{1C_{F,R}} \right) + \frac{1}{6} a_{0F,R} \left( B_{1C_{F,R}} + a_{1F,R} \right) \end{aligned} \quad (25)$$

$$\begin{aligned} \text{CYFR} \quad C_{Y_{F,R}} &= \left( \frac{2C_{Y_{F,R}}}{a_{F,R} \sigma_{F,R}} \right) \frac{a_{F,R} \sigma_{F,R}}{2} \\ \text{CYRR} \end{aligned} \quad (26)$$

$$\begin{array}{l} \text{YFR} \\ \text{YRR} \end{array} \quad Y_{F,R} = C_{Y_{F,R}} \rho \pi R_{B_{F,R}}^4 \Omega_{F,R}^2 \quad (27)$$

A quadratic form is assumed for blade-profile drag (eq. (28)) and the normalized-drag (H-force) coefficient is calculated as in equation (29).

$$\begin{array}{l} \text{DELFR} \\ \text{DELRR} \end{array} \quad \delta_{F,R} = \delta_{0F,R} + 9\delta_{1F,R} C_{T_{F,R}}^2 \quad (28)$$

$$\begin{array}{l} \text{CHFR1} \\ \text{CHRR1} \end{array} \quad \frac{2C_{H_{F,R}}}{a_{F,R} \sigma_{F,R}} = C_{T_{F,R}} a_{1F,R} + \frac{\delta_{F,R} \nu_{F,R}}{2a_{F,R}} \quad (29)$$

Equations (30) and (31) show the calculations for rotor drag coefficient and H-force, respectively.

$$\begin{array}{l} \text{CHFR} \\ \text{CHRR} \end{array} \quad C_{H_{F,R}} = \left( \frac{2C_{H_{F,R}}}{a_{F,R} \sigma_{F,R}} \right) \frac{a_{F,R} \sigma_{F,R}}{2} \quad (30)$$

$$\begin{array}{l} \text{HFR} \\ \text{HRR} \end{array} \quad H_{F,R} = C_{H_{F,R}} \rho \pi R_{B_{F,R}}^4 \Omega_{F,R}^2 \quad (31)$$

Rolling and pitching moments at the rotor hub resulting from aerodynamic forces are found as a function of steady-state flapping angles (eqs. (32) and (33)).

$$\begin{array}{l} \text{AMHBFR} \\ \text{AMHBRR} \end{array} \quad M_{\text{hub}_{F,R}} = \frac{1}{2} e_{F,R} b_{F,R} M_{W_{F,R}} \Omega_{F,R}^2 a_{1F,R} \quad (32)$$

$$\begin{array}{l} \text{ALHBFR} \\ \text{ALHBRR} \end{array} \quad L_{\text{hub}_{F,R}} = \frac{1}{2} e_{F,R} b_{F,R} M_{W_{F,R}} \Omega_{F,R}^2 b_{1F,R} \quad (33)$$

Inflow ratio dynamics, which are modeled using the ARC local linearization program LOLIN (ref. 12), are first order and depend upon thrust, advance ratio, and an empirically derived rotor-on-rotor interference algorithm.

$$\dot{\lambda}_F = -\frac{1}{\tau_{\lambda_F}} \left\{ \lambda_F - \frac{w_F}{\Omega_F R_{B_F}} + \frac{C_{T_F}}{2 \sqrt{\mu_F^2 + \lambda_F^2}} + \frac{D_{F_{RF}} C_{T_R}}{2 \sqrt{\mu_R^2 + \lambda_R^2}} \right\} \quad (34)$$

$$\dot{\lambda}_R = -\frac{1}{\tau_{\lambda_R}} \left\{ \lambda_R - \frac{w_R}{\Omega_R R_{B_R}} + \frac{C_{T_R}}{2 \sqrt{\mu_R^2 + \lambda_R^2}} + \frac{D_{F_{FR}} C_{T_F}}{2 \sqrt{\mu_F^2 + \lambda_F^2}} \right\} \quad (35)$$

ORIGINAL FORM  
OF POOR QUALITY

Referring to equations (34) and (35), rotor-on-rotor interference parameters  $D_{FR}$  (rear on forward) and  $D_{FR}$  (forward on rear) are calculated as shown in equation (36)

$$\begin{matrix} BDFFR \\ BDFRF \end{matrix} D_{FR(RF)} = d'_{FR(RF)} (1 - |\sin \beta_{FUS}|) + C_{F_2} |\sin \beta_{FUS}| \quad (36)$$

where  $d'_{FR}$  and  $d'_{RF}$  are found, depending upon whether the helicopter is in forward or rearward flight, in figures 13 and 14 and  $C_{F_2}$  is found in figure 15. A more detailed description of the LOLIN approach to solving equations (34) and (35) and an explanation of the differences between this approach and the one used originally by BV, is given in appendix B.

Finally, rotor forces and moments at each rotor hub are transformed to the helicopter c.g. These forces and moments form a portion of the total forces and moments acting on the rigid body (helicopter) and are integrated in SMART to give the translational and rotational states.

In equations (37) and (38), forces at each rotor hub are transformed from the SNPW to the helicopter body reference frame.

$$\begin{matrix} XAERFR \\ YAERFR \\ ZAERFR \end{matrix} \begin{bmatrix} X_{AER_F} \\ Y_{AER_F} \\ Z_{AER_F} \end{bmatrix} = \begin{bmatrix} -\cos \beta'_F \cos i_F & -\sin \beta'_F \cos i_F & \sin i_F \\ -\sin \beta'_F & \cos \beta'_F & 0 \\ -\cos \beta'_F \sin i_F & -\sin \beta'_F \sin i_F & -\cos i_F \end{bmatrix} \begin{bmatrix} H_F \\ Y_F \\ T_F \end{bmatrix} \quad (37)$$

$$\begin{matrix} XAERRR \\ YAERRR \\ ZAERRR \end{matrix} \begin{bmatrix} X_{AER_R} \\ Y_{AER_R} \\ Z_{AER_R} \end{bmatrix} = \begin{bmatrix} -\cos \beta'_R \cos i_R & \sin \beta'_R \cos i_R & \sin i_R \\ -\sin \beta'_R & -\cos \beta'_R & 0 \\ -\cos \beta'_R \sin i_R & \sin \beta'_R \sin i_R & -\cos i_R \end{bmatrix} \begin{bmatrix} H_R \\ Y_R \\ T_R \end{bmatrix} \quad (38)$$

Total moments at the helicopter c.g. due to the rotors have contributions from two sources: (1) moments at the helicopter c.g. resulting from forces at the rotor hub and (2) moments at the hub transformed to the c.g. Equation (39) shows the computation of the first contribution, equations (40) and (41) show the computation of the second contribution, and equation (42) gives the summation of moments from each of the two sources.

$$\begin{matrix} ALFR1, ALRR1 \\ AMFR1, AMRR1 \\ ANFR1, ANRR1 \end{matrix} \begin{bmatrix} I'_{AER_{F,R}} \\ M'_{AER_{F,R}} \\ N'_{AER_{F,R}} \end{bmatrix} = \begin{bmatrix} 0 & h_{F,R} & d_{F,R} \\ -h_{F,R} & 0 & -\ell_{F,R} \\ -d_{F,R} & \ell_{F,R} & 0 \end{bmatrix} \begin{bmatrix} X_{AER_{F,R}} \\ Y_{AER_{F,R}} \\ Z_{AER_{F,R}} \end{bmatrix} \quad (39)$$

$$\begin{aligned} \text{ALFR2} \begin{bmatrix} L''_{\text{AER}_F} \\ M''_{\text{AER}_F} \\ N''_{\text{AER}_F} \end{bmatrix} &= \begin{bmatrix} \cos \beta'_F \cos i_F & -\sin \beta'_F \cos i_F & -\sin i_F \\ \sin \beta'_F & \cos \beta'_F & 0 \\ \cos \beta'_F \sin i_F & -\sin \beta'_F \sin i_F & \cos i_F \end{bmatrix} \begin{bmatrix} L_{\text{hub}_F} \\ M_{\text{hub}_F} \\ Q_{\text{GOV}_F} \end{bmatrix} \end{aligned} \quad (40)$$

$$\begin{aligned} \text{ALRR2} \begin{bmatrix} L''_{\text{AER}_R} \\ M''_{\text{AER}_R} \\ N''_{\text{AER}_R} \end{bmatrix} &= \begin{bmatrix} -\cos \beta'_R \cos i_R & -\sin \beta'_R \cos i_R & \sin i_R \\ -\sin \beta'_R & \cos \beta'_R & 0 \\ -\cos \beta'_R \sin i_R & -\sin \beta'_R \sin i_R & -\cos i_R \end{bmatrix} \begin{bmatrix} L_{\text{hub}_R} \\ M_{\text{hub}_R} \\ Q_{\text{GOV}_R} \end{bmatrix} \end{aligned} \quad (41)$$

$$\begin{aligned} \text{ALARFR, ALARRR} \begin{bmatrix} L_{\text{AER}_{F,R}} \\ M_{\text{AER}_{F,R}} \\ N_{\text{AER}_{F,R}} \end{bmatrix} &= \begin{bmatrix} L'_{\text{AER}_{F,R}} \\ M'_{\text{AER}_{F,R}} \\ N'_{\text{AER}_{F,R}} \end{bmatrix} + \begin{bmatrix} L''_{\text{AER}_{F,R}} \\ M''_{\text{AER}_{F,R}} \\ N''_{\text{AER}_{F,R}} \end{bmatrix} \end{aligned} \quad (42)$$

Total rotor forces and moments,

$$\begin{Bmatrix} \text{XAERFR, XAERRR} \\ \text{YAERFR, YAERRR} \\ \text{ZAERFR, ZAERRR} \end{Bmatrix} \text{ and } \begin{Bmatrix} \text{ALARFR, ALARRR} \\ \text{AMARFR, AMARRR} \\ \text{ANARFR, ANARRR} \end{Bmatrix}$$

are passed to the AERO subroutine for summation with the fuselage quantities calculated therein; aerodynamic forces and moments (rotor + fuselage) are transferred to SMART as inputs

$$\begin{Bmatrix} \text{FAX} \\ \text{FAY} \\ \text{FAZ} \end{Bmatrix} \text{ and } \begin{Bmatrix} \text{TAL} \\ \text{TAM} \\ \text{TAN} \end{Bmatrix}$$

Table 1 is a list of the ROTOR subroutine variables together with constants and conversion factors. Included is each variable, its FORTRAN mnemonic, units, common location, if applicable, and physical description. Table 2 is a list of the variables transferred between ROTOR and other subroutines.

#### Fuselage Aerodynamics

Tabular data from rotor-off wind-tunnel tests provides the basis for fuselage aerodynamic forces and moments. These are represented in the helicopter body reference frame and are normalized by fuselage dynamic pressure. The data are obtained from the function tables by linear interpolation on fuselage angle of attack and sideslip angle (figs. 16-21).



# ORIGINAL OF POOR QUALITY

To calculate fuselage angle of attack, rotor downwash velocity at the fuselage is computed with an empirical expression, and is used to modify vertical velocity (eq. (43)).

$$\text{WBPR } w'_B = w_B - \frac{(\lambda'_F - \lambda_F) \Omega_F R_{BF}}{1 + D_{FR}} \quad (43)$$

Using the vertical velocity at the fuselage,  $w'_B$ , fuselage angle of attack is calculated from equation (44).

$$\text{ALPHFS } \alpha_{FUS} = \arctan\left(\frac{w'_B}{u_B}\right) \quad (44)$$

Fuselage sideslip angle is computed in equation (45), which is somewhat simplified from the helicopter sideslip angle computed in SMART.

$$\text{BETA FS } \beta_{FUS} = \arctan\left(\frac{v_B}{u_B}\right) \quad (45)$$

Fuselage dynamic pressure, used to normalize force and moment entries in the function tables, is found using equation (46).

$$\text{SQFS } q_{FUS} = \frac{1}{2} \rho (u_B^2 + v_B^2 + w_B'^2) \quad (46)$$

From the function tables, the resulting forces and moments are:  $(D/q)_{FUS}$ ,  $(Y/q)_{FUS}$ ,  $(L/q)_{FUS}$ ,  $(\mathcal{L}/q)_{FUS}$ ,  $(M/q)_{FUS}$ ,  $(N/q)_{FUS}$ . These quantities are then corrected for differences in the equivalent "flat-plate area" between the actual helicopter and the model used in the wind-tunnel tests from which the data were obtained. This correction accounts for additional sources of drag (i.e., rotor hubs, rotor blades, landing gear) that were not included in the wind-tunnel model.

Correction terms to be applied to the fuselage forces are calculated as shown in equations (47)-(49), where  $\Delta fe$  is the difference in flat-plate area; fuselage forces are calculated in equations (50)-(52).

$$\Delta\left(\frac{D}{q}\right)_{FUS} = \frac{\Delta fe}{[1 + (\tan \alpha_{FUS})^2 (\tan \beta_{FUS})^2]^{1/2}} \quad (47)$$

$$\Delta\left(\frac{Y}{q}\right)_{FUS} = \frac{\Delta fe \tan \beta_{FUS}}{[1 + (\tan \alpha_{FUS})^2 (\tan \beta_{FUS})^2]^{1/2}} \quad (48)$$

$$\Delta\left(\frac{L}{q}\right)_{FUS} = \frac{\Delta fe \tan \alpha_{FUS}}{[1 + (\tan \alpha_{FUS})^2 (\tan \beta_{FUS})^2]^{1/2}} \quad (49)$$

$$\text{XAERFS } X_{FUS} = -q_{FUS} \left[ \left(\frac{D}{q}\right)_{FUS} + \Delta\left(\frac{D}{q}\right)_{FUS} \right] \quad (50)$$

$$\text{YAERFS } Y_{\text{FUS}} = q_{\text{FUS}} \left[ \left( \frac{Y}{q} \right)_{\text{FUS}} - \Delta \left( \frac{Y}{q} \right)_{\text{FUS}} \right] \quad (51)$$

$$\text{ZAERFS } Z_{\text{FUS}} = -q_{\text{FUS}} \left[ \left( \frac{L}{q} \right)_{\text{FUS}} + \Delta \left( \frac{L}{q} \right)_{\text{FUS}} \right] \quad (52)$$

To make the corrections necessary for differences in c.g. position between the actual helicopter and the wind-tunnel model, this moment arm is computed as in equation (53).

$$\begin{array}{l} \text{SLCFS} \\ \text{SDCFS} \\ \text{SHCFS} \end{array} \begin{bmatrix} \ell_{c_{\text{FUS}}} \\ d_{c_{\text{FUS}}} \\ h_{c_{\text{FUS}}} \end{bmatrix} = \begin{bmatrix} \ell_{c_x} \\ d_{c_x} \\ h_{c_x} \end{bmatrix} - \begin{bmatrix} \Delta X_{c.g.}/12 \\ \Delta Y_{c.g.}/12 \\ \Delta Z_{c.g.}/12 \end{bmatrix} \quad (53)$$

$$\begin{bmatrix} \ell_{c_x} \\ d_{c_x} \\ h_{c_x} \end{bmatrix} \text{ is the baseline model c.g. offset (fig. 22), which has the constant numerical value of } \begin{bmatrix} -1.47 \text{ ft} \\ 0 \text{ ft} \\ 1.31 \text{ ft} \end{bmatrix} \cdot \begin{bmatrix} X_{c.g.} \\ Y_{c.g.} \\ Z_{c.g.} \end{bmatrix} \text{ is}$$

the position (in inches) of the c.g. of the actual helicopter relative to its baseline (fig. 4).

Using equation (54), fuselage moments are adjusted for this difference in c.g. position,

$$\begin{array}{l} \text{ALARFS} \\ \text{AMARFS} \\ \text{ANARFS} \end{array} \begin{bmatrix} L_{\text{FUS}} \\ M_{\text{FUS}} \\ N_{\text{FUS}} \end{bmatrix} = \begin{bmatrix} (L/q)_{\text{FUS}} \\ (M/q)_{\text{FUS}} \\ (N/q)_{\text{FUS}} \end{bmatrix} q_{\text{FUS}} + \begin{bmatrix} 0 & h_{c_{\text{FUS}}} & d_{c_{\text{FUS}}} \\ -h_{c_{\text{FUS}}} & 0 & -\ell_{c_{\text{FUS}}} \\ -d_{c_{\text{FUS}}} & \ell_{c_{\text{FUS}}} & 0 \end{bmatrix} \begin{bmatrix} X_{\text{FUS}} \\ Y_{\text{FUS}} \\ Z_{\text{FUS}} \end{bmatrix} \quad (54)$$

If the helicopter is in rearward flight, the signs on  $X_{\text{FUS}}$ ,  $M_{\text{FUS}}$ , and  $N_{\text{FUS}}$  are reversed to account for the aerodynamic differences at this flight condition.

Total aerodynamic forces and moments include rotor and fuselage contributions, which are summed at the end of the subroutine (eqs. (55) and (56)) and passed to SMART.

$$\begin{array}{l} \text{FAX} \\ \text{FAY} \\ \text{FAZ} \end{array} \begin{bmatrix} X_{\text{AERO}} \\ Y_{\text{AERO}} \\ Z_{\text{AERO}} \end{bmatrix} = \begin{bmatrix} X_{\text{FUS}} \\ Y_{\text{FUS}} \\ Z_{\text{FUS}} \end{bmatrix} + \begin{bmatrix} X_{\text{AER}_F} \\ Y_{\text{AER}_F} \\ Z_{\text{AER}_F} \end{bmatrix} + \begin{bmatrix} X_{\text{AER}_R} \\ Y_{\text{AER}_R} \\ Z_{\text{AER}_R} \end{bmatrix} \quad (55)$$

$$\begin{matrix} \text{TAL} \\ \text{TAM} \\ \text{TAN} \end{matrix} \begin{bmatrix} L_{\text{AERO}} \\ M_{\text{AERO}} \\ N_{\text{AERO}} \end{bmatrix} = \begin{bmatrix} L_{\text{FUS}} \\ M_{\text{FUS}} \\ N_{\text{FUS}} \end{bmatrix} + \begin{bmatrix} L_{\text{AER}_F} \\ M_{\text{AER}_F} \\ N_{\text{AER}_F} \end{bmatrix} + \begin{bmatrix} L_{\text{AER}_R} \\ M_{\text{AER}_R} \\ N_{\text{AER}_R} \end{bmatrix} \quad (56)$$

Table 3 gives the definition of the variables, constants, and conversion factors of the AERO subroutine. Table 4 lists input/output variables to and from other subroutines, together with required input data.

### Engine and Governor

Power is supplied to the rotor system by two Lycoming T-55-L7C turbine engines mounted on the aft pylon. Although the representations are identical mathematically, each engine is modeled separately. The block diagram in figure 23 illustrates the modeling method for the left engine, including the governor and forward rotor-shaft dynamics. Nonlinear functions are shown in more detail in figures 24-30.

As shown in figure 23, trimming of the engine by zeroing  $\dot{\Omega}$ , is done while in initial condition (I.C.) mode by setting flag ISTEADY after the rigid-body states have been trimmed. Pilot inputs, shown on the left side of the diagram, include: positions of the collective stick ( $\delta_c$  is fed forward into the engine to compensate for rpm droop);  $N_1$  lever (compressor speed); and beep trim switches (torque may be adjusted on the left engine individually, or engine torque and rotor rpm may be adjusted on both engines simultaneously). Changes in beep trimmer and collective positions modify the fuel control actuator ( $N_2$ ) command. The fuel control mechanism is modeled as a first-order system, with friction in the response represented by a deadband and by hysteresis. Unlimited commanded power is calculated, as shown in figure 31, as the difference between equivalent rotor rpm ( $N_R$ ) and the fuel control actuator position ( $N_{R_c}$ ). The term  $N_{R_\phi}$  provides the intercept of the unlimited commanded power curve, and the slope of the curve ( $M$ ) is an empirically derived constant between engine fuel flow and engine power. Feedback of  $N_R(\Omega)$  in the unlimited, commanded power calculation represents the governing loop of the engine, where engine power is modified to regulate variations in rotor rpm.

As shown in figures 23 and 31, the topping power level of the engine is a function of  $N_R(\Omega)$  and the compressor speed ( $N_1$ ). Three positions, STOP, GROUND, and FLY are available on the  $N_1$  lever; actuator motion between the positions is at a constant rate of 0.8 in./sec. Unlimited commanded power is then topped as a function of rotor rpm and compressor speed.

Gas generator dynamics are modeled as a first-order lag with a time constant and internal limiter, both of which are variable. The gas generator dynamics time constant is a function of power output, modified as a function of power error. The variable internal limiter adjusts for the engine, which powers down six times faster than it powers up, and is a function of power output.

The engine governor and rotor shaft dynamics, modeled as a third-order system (fig. 23), regulate rotor rpm. Inputs to the governor and shaft dynamics model are power available from each engine and power required for the accessories (hydraulic systems, transmission losses, etc.). As shown in the figure, this system is driven by the difference between resistive torque (damping plus spring torque) and rotor torque

required. Rotor acceleration is the difference between shaft resistive torque and engine torque available. Engine outputs: rotor rpm (OMEGA), spring torque

$$\begin{Bmatrix} QGOVF \\ QGOVR \end{Bmatrix}$$

and rotor rpm uncorrected for helicopter yaw rate

$$\begin{Bmatrix} OMEGPF \\ OMEGPR \end{Bmatrix}$$

are passed to the ROTOR subroutine.

Table 5 is a list of variables computed in the ENGINE subroutine, together with constants and conversion factors, and table 6 has ENGINE subroutine input/output variables, and logical flags.

### Mechanical Controls

The purpose of the CONTROL subroutine is to represent the mechanical hardware between the cockpit controls and the rotor swashplate. A block diagram of the subroutine logic is shown in figure 32. Mechanical control system inputs are lateral cyclic ( $\delta_{Ap}$ ), collective ( $\delta_{Cp}$ ), longitudinal stick ( $\delta_{Bp}$ ), and directional ( $\delta_{Rp}$ ) cockpit control positions. The SAS and ECS actuator inputs from the respective subroutines, and selected with the flags shown in the figure, augment the appropriate cockpit control positions. Longitudinal cyclic position is also augmented by the differential-collective-pitch-trim (DCPT) actuator which (although this capability has been disconnected in the ARC helicopter) may be selected in the simulation model by setting flag IDCPT. The purpose of the DCPT actuator is to artificially provide a stable longitudinal stick position gradient with airspeed (fig. 33). To accomplish this, as a function of airspeed, the DCPT actuator automatically introduces a positive pitching moment (fig. 34), requiring the pilot to move the longitudinal stick forward to maintain trim (ref. 13).

After control-stop limiting (downstream of cockpit control-position limiting, which is not included in the diagram), control positions are converted from inches to degrees of equivalent swashplate, resulting in  $\Theta_{AF,R}$ ,  $\Theta_{CF,R}$ ,  $\Theta_{BF,R}$ , and  $\Theta_{RF,R}$ .

First-stage control mixing (longitudinal and vertical, lateral and directional) is followed by cumulative lateral stop limiting (of the authority of differential lateral and combined lateral inputs). Results of (vertical and lateral) second-stage mixing,  $\Theta_{FSP}$ ,  $\Theta_{FPP}$ ,  $\Theta_{RSP}$ , AND  $\Theta_{RPP}$  are limited at the swashplate prior to driving the swiveling and pivoting upper-boost actuators. (In order that the swashplates move smoothly and not bind up, each is driven by a combination of swiveling and pivoting motions. Swashplate displacement is the sum of the two inputs.) The actuation dynamics are modeled as first-order lags, the outputs of which,  $\Theta_{0F,R}$  and  $A_{1CF,R}$ , may be interpreted to be collective and lateral cyclic pitch angles represented in helicopter body axes, respectively.

As described in reference 4, longitudinal cyclic pitch angle is scheduled with equivalent airspeed (fig. 34); actuation dynamics are modeled as a first-order lag.

Mechanical control-system outputs are rotor hub collective and cyclic positions

$$\begin{Bmatrix} \text{AICFRC, AICRRC} \\ \text{BICFRC, BICRRC} \\ \text{THOFRC, THORRC} \end{Bmatrix}$$

which are passed to the ROTOR subroutine. Table 7 is a summary of the variables used in the CONTROL subroutine; table 8 gives subroutine input/output variables and logical flags.

### Stability Augmentation System

The basic augmentation of the CH-47B helicopter is modeled in the SAS subroutine. Rate damping only is implemented in longitudinal and lateral axes (figs. 35 and 36); the directional axis has turn coordination and  $N_z$  stabilization in addition to rate damping (fig. 37). Figures 38 and 39 show the directional SAS nonlinearities in detail.

The longitudinal SAS consists of pitch-rate feedback through cascaded first-order lag, lead-lag, and washout filters. The lateral SAS is comprised of a single first-order lag applied to roll rate. In the  $N_z$  stabilization portion of the directional SAS, sideslip angle is calculated using the pressure difference between the static ports located on the nose of the aircraft. In an appendix to reference 4 it was determined that this pressure difference may be represented as in equation (57)

$$\Delta p_{\text{static}} = (1.1) \left( \frac{9}{4} \right) \sin(2\gamma) \sin(2\beta) q \quad (57)$$

where  $\gamma$  = the angle between longitudinal axis and the static port line ( $52^\circ$ ) and  $q$  = the dynamic pressure ( $= (1/2)\rho V_{eq}^2$ ). The portion of the yaw SAS rudder input calculated to zero sideslip angle is given in equation (58) where  $K_{\Delta p_{\delta R}}$  is a velocity-dependent gain whose purpose is to wash out this rudder input at high speeds (fig. 38).

$$\text{DRBYAW } \delta_{R\beta} \Big|_{\text{equivalent pedal}} = (\Delta p \text{ in. H}_2\text{O}) \left( K_{\Delta p_{\delta R}} \frac{\text{in. pedal}}{\text{in. H}_2\text{O}} \right) \quad (58)$$

Directional SAS yaw damping uses simple filtering with, at  $V_{eq} = 40$  knots, a change from a first-order lag in cascade with a lead-lag to a first-order lag in cascade with a washout filter applied to yaw rate. Turn coordination is implemented with a first-order lag on helicopter roll rate. Computation of the SAS filtering outputs uses subroutine FACT/UPDATE, designed to solve ordinary differential equations (ref. 14).

Augmentation in any or all of the three axes may be selected with switches located in the CONTROL subroutine. Flags RSASQ, RSASP, and RSASR select the longitudinal, lateral, and directional SAS inputs, respectively.

SAS effectiveness may be demonstrated using dynamic response and stability-derivative data. Figures 40-42 show SAS off and on responses for each of the longitudinal, lateral, and directional axes in hover. Figures 43-45 and 46-48 give similar results for  $V_{eq} = 75$  and 130 knots, respectively. More complete static and dynamic

model data may be found in volume II of this report, which gives the validation results. Included therein are static trim and stability derivative data as well as a summary of dynamic check results.

Table 9 is a list of the SAS subroutine variables together with constants and conversion factors. Included is each variable, its FORTRAN mnemonic, its units, its common location if applicable, and its physical description. Table 10 is a list of the variables transferred between SAS and other subroutines.

### Electronic Control System

Using the ECS of the CH-47B, a researcher may either implement an experimental control system or, by designing explicit model-following laws, exercise the helicopter's variable-stability capability. The ECS subroutine is a model of this system; subroutine inputs are the research pilot's cockpit control positions and the outputs are ECS signals sent to the mechanical controls subroutine, CONTROL. No specific ECS is documented in this report. It is anticipated that a particular ECS design will be developed along with an individual experiment, and will be documented at that time. However, during model validation, some simple procedures were developed which aid in properly linking the ECS to the rest of the model. A discussion of these follows.

Prior to engaging the ECS (with flag IECSCON in subroutine CONTROL), the helicopter is trimmed using the basic airframe and mechanical control system. In this case, the SAS must be turned off before trimming, since SAS inputs alter the cockpit control positions for trim.

When the ECS is engaged the helicopter is flown by the research pilot; therefore, in the simulation the safety pilot's inputs to the mechanical control system are disconnected as the ECS is turned on (see the CONTROL schematic, fig. 32). To avoid destroying the trimmed condition of the helicopter when the safety pilot's controls are disconnected, each trim cockpit control position is used as a bias which is added to the appropriate ECS input (which is zero at trim, by definition); this is shown in equations (59)-(62).

$$DLATTOT = DLATECS + DATOTIC \quad (59)$$

$$DLONTOT = DLONECS + DBTOTIC \quad (60)$$

$$DYAWTOT = DYAW ECS + DRTOTIC \quad (61)$$

$$DCOLTOT = DCOLECS + DCTOTIC \quad (62)$$

where

$$\begin{Bmatrix} DATOTIC \\ DBTOTIC \\ DRTOTIC \\ DCTOTIC \end{Bmatrix} = \begin{Bmatrix} DLATP \\ DLONP \\ DYAWP \\ DCOLP \end{Bmatrix} \bigg|_{\text{trim}}$$

Table 11 gives the ECS subroutine input/output variable definition

## Slung Load

Subroutine SLING models a baseline, externally suspended load in three degrees of freedom. This is accomplished by introducing three new state variables, each defined as a relative displacement of the load and helicopter body reference frames. Additionally, terms which represent the effect of the slung load motion on the helicopter response are computed and passed to subroutine SMART. Simulation of the slung-load dynamics is optional and may be selected with flag ISLING.

Figure 49 (taken from ref. 1) illustrates the geometry of the slung load, its attachment, and position relative to the helicopter. The baseline load data, which are included in the simulation model, is a "MIL-VAN" weighing 7500 lb. It is suspended on cables from tandem attachment points on the fuselage equally spaced about the helicopter c.g. It has been assumed that these attachment points may transmit no moments between the load and the helicopter. Referring to the figure:  $\mu_L$ ,  $\lambda_L$ , and  $\nu_L$  are defined to be the longitudinal and lateral cable sway angles and the lateral differential cable angle, respectively.

To compute slung-load aerodynamic quantities, velocities in the helicopter body reference frame at the slung-load c.g. are computed via equations (63)-(65).

$$\text{USL } u_{SL} = u_B + (L_L + R_L)q_B + L_L \dot{\mu}_L \quad (63)$$

$$\text{VSL } v_{SL} = v_B - (L_L + R_L)p_B - L_L \dot{\lambda}_L \quad (64)$$

$$\text{WSL } w_{SL} = w_B \quad (65)$$

Slung-load dynamic pressure, sideslip angle, and angle of attack, respectively, are computed in equations (66)-(68).

$$\text{SQSL } q_{SL} = \frac{1}{2} \rho (u_{SL}^2 + v_{SL}^2 + w_{SL}^2)^{1/2} \quad (66)$$

$$\text{BETSL } \beta_{SL} = \arctan\left(\frac{v_{SL}}{u_{SL}}\right) - \nu_L \quad (67)$$

$$\text{ALFSL } \alpha_{SL} = \arctan\left(\frac{w_{SL}}{u_{SL}}\right) + \theta_{SL} \quad (68)$$

Slung-load drag, sideforce, and yawing moment, respectively, are found from figures 50-52 as a function of load angle of attack and sideslip angle. These data, normalized in the simulation model by load dynamic pressure, are taken from wind-tunnel tests. Prior to their use in the cable angle calculations, the load aerodynamic quantities are resolved into the helicopter body reference frame, as in equations (69)-(71).

$$\text{XAERSL } X_{AER_L} = -q_{SL} \left[ \left(\frac{D}{q}\right)_{SL} \cos \nu_L + \left(\frac{Y}{q}\right)_{SL} \sin \nu_L \right] \quad (69)$$

ORIGINAL PAGE  
OF POOR QUALITY

$$YAERL \quad Y_{AERL} = q_{SL} \left[ \left( \frac{Y}{q} \right)_{SL} \cos v_L - \left( \frac{D}{q} \right)_{SL} \sin v_L \right] \quad (70)$$

$$ANARSL \quad N_{AERL} = q_{SL} \left( \frac{N}{q} \right)_{SL} \quad (71)$$

Using  $X_{AERL}$ ,  $Y_{AERL}$ , and  $N_{AERL}$  as inputs, suspension-cable angular accelerations are computed with the nonlinear second-order differential equations (72)-(74), from reference 1.

$$\begin{aligned} AMULDD \quad \ddot{u}_L = & \frac{X_{AERL}}{m_L L_L} - \frac{\dot{u}_B}{L_L} - \left( \frac{L_L + R_L}{L_L} \right) \dot{q}_B + \left( \frac{J_L}{m_L L_L^2} - \frac{L_L + R_L}{L_L} \right) r_p \\ & - r_B \dot{\lambda}_L + \frac{r_B v_B}{L_L} - \bar{K}_L \frac{q}{L_L} (\sin \theta + \sin \mu_L) - K_{\dot{u}} \dot{u} \end{aligned} \quad (72)$$

where

$$\bar{K}_L = \frac{[(m_L g)^2 + X_{AERL}^2]^{1/2}}{m_L g}$$

$$\begin{aligned} ALMLDD \quad \ddot{\lambda}_L = & \frac{-Y_{AERL}}{m_L L_L} + \frac{\dot{v}_B}{L_L} - \left( \frac{L_L + R_L}{L_L} \right) \dot{p}_B - \left( \frac{J_L}{m_L L_L^2} - \frac{L_L + R_L}{L_L} \right) r_B q_B - \frac{J_L}{m_L L_L} q_B \dot{v}_L \\ & + r_B \dot{\mu}_L + \frac{r_B u_B}{L_L} - \frac{q}{L_L} (\sin \phi + \sin \lambda_L) - K_{\dot{\lambda}} \dot{\lambda}_L \end{aligned} \quad (73)$$

$$ANULDD \quad \ddot{v}_L = \frac{N_{AERL}}{J_L} - \dot{r}_B - \frac{m_L g a_L^2}{4 J_L L_L} \cos \theta \cos \phi v_L - K_{\dot{v}} \dot{v}_L \quad (74)$$

(During model validation, the value of  $K_{\dot{v}}$  was changed from the original value of +1.8 to -0.03 to match BV dynamic-response data.)

Integration results in cable angular velocities as in equations (75)-(77):

$$AMULD \quad \dot{u}_L = \int \ddot{u}_L dt \quad (75)$$

$$ALMLD \quad \dot{\lambda}_L = \int \ddot{\lambda}_L dt \quad (76)$$

$$ANULD \quad \dot{v}_L = \int \ddot{v}_L dt \quad (77)$$



and cable positions as in equations (78)-(80):

$$\text{AMUL } \mu_L = \int \dot{\mu}_L dt \quad (78)$$

$$\text{ALML } \lambda_L = \int \dot{\lambda}_L dt \quad (79)$$

$$\text{ANUL } v_L = \int \dot{v}_L dt \quad (80)$$

At a straight and level flight condition, values of  $\mu_L$ ,  $\lambda_L$ , and  $v_L$  may be found by solving equations (72), (73), and (74) at steady state. Resulting trim values are given in equations (81)-(83).

$$\text{AMULIC } \mu_{L.I.C.} = \sin^{-1} \left[ -\sin \theta + \frac{X_{AER_L}}{\bar{K}_L g m_L} \right] \quad (81)$$

$$\text{ALMLIC } \lambda_{L.I.C.} = -\phi \quad (82)$$

$$\text{ANULIC } v_{L.I.C.} = 0 \quad (83)$$

where I.C. represents the initial flight condition. By selecting flag ISLTRM, initial values of the slung-load states are computed at the same time that the helicopter is being trimmed.

In the original BV simulation model, the helicopter and slung load were modeled together as a coupled nine degree-of-freedom system. However, since subroutine SMART was designed to handle only six degrees of freedom, the ARC model is somewhat modified from the original. Equations (84)-(89) are the nine degree-of-freedom helicopter equations of motion in the helicopter body reference frame (ref. 1), where the underlined terms are those which arise specifically from the slung load.

$$\dot{u}_B = \frac{X_{AERO}}{M_H} - q_B w_B - g \sin \theta + r_B v_B - \frac{m_L}{M_H} (q_B w_B - \bar{K}_L g \sin \mu_L) - \frac{J_L}{L_L M_H} r_B p_B \quad (84)$$

$$\dot{v}_B = \frac{Y_{AERO}}{M_H} + g \sin \phi \cos \theta + p_B w_B - r_B u_B + \frac{m_L}{M_H} p_B w_B - \frac{J_L}{L_L M_H} (r_B q_B + q_B \dot{v}_L) - \frac{m_L}{M_H} g \sin \lambda_L \quad (85)$$

$$\begin{aligned} \dot{w}_B = & \frac{Z_{AERO}}{(m_L + M_H)} + g \cos \phi \cos \theta + q_B u_B - p_B v_B + \frac{m_L (L_L + R_L)}{(m_L + M_H)} (q_B^2 + p_B^2) \\ & + \frac{M_L L_L}{(m_L + M_H)} (p_B \dot{\lambda}_L + q_B \dot{\mu}_L) \end{aligned} \quad (86)$$

ORIGINAL  
OF POOR QUALITY

$$\dot{q}_B = \frac{M_{AERO}}{I_{yy}} + \frac{I_{xz}}{I_{yy}} (r_B^2 - p_B^2) + \left( \frac{I_{zz} - I_{xx}}{I_{yy}} \right) r_B p_B - \frac{R_L J_L}{L_L I_{yy}} r_B p_B - \frac{m_L g R_L}{I_{yy}} \bar{k}_L \mu_L \quad (87)$$

$$\dot{p}_B = \left\{ L_{AERO} I_{zz} + N_{AERO} I_{xz} + p_B q_B I_{xz} (I_{xx} - I_{yy} + I_{zz}) + r_B q_B [I_{zz} (I_{yy} - I_{zz}) - I_{xz}^2] \right. \\ \left. + \left( \frac{R_L J_L I_{zz}}{L_L} \right) (r_B q_B + q_B \dot{v}_L) + \frac{m_L g a_L^2}{4 L_L} I_{xz} \cos \phi \cos \Theta v_L + m_L g R_L I_{zz} \lambda_L \right\} / (I_{xx} I_{zz} - I_{xz}^2) \quad (88)$$

$$\dot{r}_B = \left\{ N_{AERO} I_{xx} + L_{AERO} I_{xz} + p_B q_B (I_{xx}^2 - I_{xx} I_{yy} + I_{xz}^2) + r_B q_B [I_{xz} (I_{yy} - I_{xx} - I_{zz})] \right. \\ \left. + \frac{m_L g a_L^2}{4 L_L} I_{xx} \cos \Theta \cos \phi v_L + \frac{R_L J_L I_{xz}}{L_L} (r_B q_B + q_B \dot{v}_L) + m_L g R_L I_{xz} \lambda_L \right\} / (I_{xx} I_{zz} - I_{xz}^2) \quad (89)$$

The underlined portions of the above equations are designated as the slung-load contributions to the helicopter body reference frame accelerations and are given in equations (90)-(95).

$$UBDS \quad \dot{u}_{BS} = \frac{-m_L}{M_H} (q_B w_B - \bar{k}_L g \sin \mu_L) - \frac{J_L}{L_L M_H} r_B p_B \quad (90)$$

$$VBDS \quad \dot{v}_{BS} = \frac{-m_L}{M_H} p_B w_B - \frac{J_L}{L_L M_H} (r_B q_B + q_B \dot{v}_L) - \frac{m_L}{M_H} g \sin \lambda_L \quad (91)$$

$$WBDS \quad \dot{w}_{BS} = \frac{m_L (L_L + R_L)}{(m_L + M_H)} (q_B^2 + p_B^2) + \frac{m_L L_L}{(m_L + M_H)} (p_B \dot{\lambda}_L + q_B \dot{\mu}_L) \quad (92)$$

$$QBDS \quad \dot{q}_{BS} = \frac{-R_L J_L}{L_L I_{yy}} r_B p_B + \frac{m_L g R_L}{I_{yy}} \bar{k}_L \mu_L \quad (93)$$

$$PBDS \quad \dot{p}_{BS} = \left\{ \left( \frac{R_L J_L I_{zz}}{L_L} \right) (q_B r_B + q_B \dot{v}_L) + \frac{m_L g a_L^2}{4 L_L} I_{xz} \cos \phi \cos \Theta v_L \right. \\ \left. + m_L g R_L I_{zz} \lambda_L \right\} / (I_{xx} I_{zz} - I_{xz}^2) \quad (94)$$

$$FBDS \quad \dot{r}_{BS} = \left\{ \frac{m_L g a_L^2}{4 L_L} I_{xx} \cos \Theta \cos \phi v_L + \frac{R_L J_L I_{xz}}{L_L} (r_B q_B + q_B \dot{v}_L) \right. \\ \left. + m_L g R_L I_{xz} \lambda_L \right\} / (I_{xx} I_{zz} - I_{xz}^2) \quad (95)$$

These contributions are added directly to the helicopter body reference frame acceleration calculations in SMART. By executing SMART immediately prior to SLING, the states are calculated in the same order as in the original BV model.

Table 12 gives the SLING subroutine variable definition; table 13 is a list of subroutine input/output variables and logical flags.

### OPERATIONAL CONSIDERATIONS

Real-time piloted simulation using a simulator cab and visual display requires the constant input information described in table 14.

Additionally, in order that a pilot may land the helicopter model, a simple gear model has been devised. The landing gear subroutine is not actually executed; rather, subroutine BLAND has been modified so that the ground is contacted artificially (i.e., the gear reaction force is prescribed to be equal to the aircraft weight) and no reactive moments are calculated).

### CONCLUSIONS

A mathematical simulation model of the ARC CH-47B helicopter has been purchased from the Boeing Vertol Company and implemented on the ARC Sigma IX computer. Volume I of this report includes engineering explanations of each model subroutine; also given are the appropriate assumptions and simplifications necessary to ensure the validity of a particular experiment.

Volume II of this report gives a comparison among ARC and BV model dynamic response data and flight test data, together with ARC static-trim and stability-derivative data. Successful validation of the ARC model has been completed against BV model data. As with all mathematical models of physical systems, however, this model is not a perfect replication of the CH-47B helicopter. This is particularly true with a quasi-steady rotor dynamics model, the type implemented herein. To represent specific aspects of the helicopter response more closely and to meet the needs of a particular simulation experiment, it may be desirable to modify the model described in this report.

# APPENDIX A: FLAPPING AND CONING EQUATIONS

Using Wheatley-Bailey theory (refs. 6 and 7), flapping and coning angles are computed in the shaft-normal-plane-wind reference frame. Due to pitch-flap coupling ( $\delta_3$ ), the solution for coning and flapping angles ( $a_0, a_1, b_1$ ) is coupled with the definition of swashplate cyclic and collective pitch angles ( $A_{1c}, B_{1c}, \theta_0$ ), as shown in equations (A1)-(A7). Additionally, coning angle is a function of rotor thrust, defined in equation (A1).

$$\begin{array}{l} \text{AOFR} \\ \text{AORR} \end{array} \quad a_0 = \left( \frac{\rho a c R_B^4}{12 I_{F,R}} \right) \left[ 4 \left( \frac{2 C_T}{a \sigma} \right) + \frac{\theta_0}{6} + \frac{\theta_{tw}}{5} + \frac{\mu^2 \theta_0}{2} \right] \quad (\text{A1})$$

$$\begin{array}{l} \text{A1FR} \\ \text{A1RR} \end{array} \quad a_1 = \frac{4}{1 - (\mu^2/2)} \left[ \mu \left( \frac{\lambda}{2} + \frac{2\theta_0}{3} + \frac{\theta_{tw}}{2} - \frac{3\mu B_{1c}}{8} \right) - \frac{B_{1c}}{4} \right] - \frac{16 q_{F,R} [1 + (\mu^2/2)]}{(\rho a c R_B^4 \Omega) / I_{F,R}} \quad (\text{A2})$$

$$\begin{array}{l} \text{B1FR} \\ \text{B2RR} \end{array} \quad b_1 = \frac{4\mu a_0}{3[1 + (\mu^2/2)]} + A_{1c} - \frac{16 p_{F,R} [1 - (\mu^2/2)]}{(\rho a c R_B^4 \Omega) / I_{F,R}} \quad (\text{A3})$$

where

$$\begin{array}{l} \text{A1CFR} \\ \text{A1CRR} \end{array} \quad A_{1c} = A'_{1c_2} + K_\beta a_1 \quad (\text{A4})$$

$$\begin{array}{l} \text{B1CFR} \\ \text{B1CRR} \end{array} \quad B_{1c} = B'_{1c_2} + K_\beta b_1 \quad (\text{A5})$$

$$\begin{array}{l} \text{THOFR} \\ \text{THORR} \end{array} \quad \theta_0 = \theta'_0 + K_\beta a_0 \quad (\text{A6})$$

$$\begin{array}{l} \text{CTFR1} \\ \text{CTRR1} \end{array} \quad \frac{2C_T}{a\sigma} = \frac{\lambda}{2} + \frac{\theta_0}{3} + \frac{\theta_{tw}}{4} + \mu \left[ \mu \left( \frac{\theta_0}{2} + \frac{\theta_{tw}}{4} \right) - \frac{B_{1c}}{2} \right] \quad (\text{A7})$$

The purpose of this appendix is to provide the algebraic steps necessary to decouple these equations, eventually resulting in the model equation (18). Following is the step by step decoupling of the equations, reproduced from reference 4.

1. Substituting for  $(2C_T/a\sigma)$  in the  $a_0$  equation:

$$a_0 = \left( \frac{\rho a c R_B^4}{12 I_{F,R}} \right) \left( 4 \left\{ \frac{\lambda}{2} + \frac{\theta_0}{3} + \frac{\theta_{tw}}{4} + \mu \left[ \mu \left( \frac{\theta_0}{2} + \frac{\theta_{tw}}{4} \right) - \frac{B_{1c}}{2} \right] \right\} + \frac{\theta_0}{6} + \frac{\theta_{tw}}{5} - \frac{\mu^2 \theta_0}{2} \right) \quad (\text{A8})$$

$$a_0 = \left( \frac{\rho a c R_B^4}{12 I_{F,R}} \right) \left( 2\lambda + \frac{4\theta_0}{3} + \theta_{tw} + 2\mu^2 \theta_0 + \mu^2 \theta_{tw} - 2\mu B_{1c} + \frac{\theta_0}{6} + \frac{\theta_{tw}}{5} - \mu^2 \frac{\theta_0}{2} \right) \quad (\text{A9})$$

$$a_0 = \left( \frac{\rho a c R_B^4}{12 I_{F,R}} \right) \left[ \theta_0 \left( \frac{4}{3} + 2\mu^2 + \frac{1}{6} - \frac{\mu^2}{2} \right) - 2\mu B_{1c} + 2\lambda + \theta_{tw} \left( \frac{6}{5} + \mu^2 \right) \right] \quad (\text{A10})$$

2. Substituting for  $\phi_0$  and  $B_{1c}$ :

$$\left(\frac{12I_{F,R}}{\rho ac R_B^4}\right) a_0 = (\phi'_0 + K_\beta a_0) \left(\frac{3}{2} + \frac{3}{2} \mu^2\right) - 2\mu (B'_{1c_2} + K_\beta b_1) + 2\lambda + \phi_{tw} \left(\frac{6}{5} + \mu^2\right) \quad (A11)$$

$$\begin{aligned} a_0 \underbrace{\left[ \frac{12I_{F,R}}{\rho ac R_B^4} - K_\beta \left(\frac{3}{2} + \frac{3}{2} \mu^2\right) \right]}_A &+ \underbrace{a_1(0.0)}_B + \underbrace{b_1(2\mu K_\beta)}_C \\ &= \underbrace{\phi'_0 \left(\frac{3}{2} + \frac{3}{2} \mu^2\right) - 2\mu B'_{1c_2} + 2\lambda + \phi_{tw} \left(\frac{6}{5} + \mu^2\right)}_J \end{aligned} \quad (A12)$$

3. After defining coefficients as indicated above, the equation has the form:

$$Aa_0 + Ba_1 + Cb_1 = J \quad (A13)$$

4. Rearranging the  $a_1$  equation:

$$\left(\frac{1}{4} - \frac{\mu^2}{8}\right) a_1 = \frac{\mu\lambda}{2} + \frac{2\mu\phi_0}{3} + \frac{\mu\phi_{tw}}{2} - \frac{3\mu^2 B_{1c}}{8} - \frac{B_{1c}}{4} - \frac{16q_{F,R}[1 + (\mu^2/2)][(1/4) - (\mu^2/8)]}{(\rho ac R_B^4 \Omega)/I_{F,R}} \quad (A14)$$

5. Substituting for  $\phi_0$  and  $B_{1c}$ :

$$\begin{aligned} \left(\frac{1}{4} - \frac{\mu^2}{8}\right) a_1 &= (\phi'_0 + K_\beta a_0) \frac{2\mu}{3} - (B'_{1c_2} + K_\beta b_1) \left(\frac{1}{4} + \frac{3\mu^2}{8}\right) \\ &+ \frac{\mu\lambda}{2} + \frac{\mu\phi_{tw}}{2} - \frac{16q_{F,R}[1 + (\mu^2/2)][(1/4) - (\mu^2/8)]}{(\rho ac R_B^4 \Omega)/I_{F,R}} \end{aligned} \quad (A15)$$

$$\begin{aligned} a_0 \underbrace{\left(-\frac{2}{3} K_\beta \mu\right)}_D &+ a_1 \underbrace{\left(\frac{1}{4} - \frac{\mu^2}{8}\right)}_E + b_1 \underbrace{\left[K_\beta \left(\frac{1}{4} + \frac{3\mu^2}{8}\right)\right]}_F \\ &= \underbrace{\frac{2\mu\phi'_0}{3} - B'_{1c_2} \left(\frac{1}{4} + \frac{3\mu^2}{8}\right) + \frac{\mu\lambda}{2} + \frac{\mu\phi_{tw}}{2} - \frac{16q_{F,R}[1 + (\mu^2/2)][(1/4) - (\mu^2/8)]}{(\rho ac R_B^4 \Omega)/I_{F,R}}}_K \end{aligned} \quad (A16)$$

6. The definition of the above coefficients results in the form of equation (A17):

$$Da_0 + Ea_1 + Fb_1 = K \quad (A17)$$

7. Substituting for  $A_{1c}$  in the  $b_1$  equation:

$$b_1 = \frac{4\mu a_0}{3[1 + (\mu^2/2)]} + A'_{1c_2} + K_\beta a_1 - \frac{16p_{F,R}[1 - (\mu^2/2)]}{(\rho ac R_B^4 \Omega)/I_{F,R}} \quad (A18)$$

$$a_0 \underbrace{\frac{-4\mu}{3[1 + (\mu^2/2)]}}_G + a_1 \underbrace{(-K_\beta)}_H + b_1 \underbrace{(1.0)}_I = A'_{1c_2} - \underbrace{\frac{16p_{F,R}[1 - (\mu^2/2)]}{(\rho ac R_B^4 \Omega)/I_{F,R}}}_L \quad (A19)$$

8. After the above definitions, the equation has the form:

$$Ga_0 + Ha_1 + Ib_1 = L \quad (A20)$$

As discussed in the text, equations (A13), (A17), and (A20), which are the same as the text matrix equation (18), are solved for  $a_0$ ,  $a_1$ , and  $b_1$ .

# APPENDIX B: INFLOW DYNAMICS SOLUTION

In the original version of the model (developed by Boeing Vertol Company) from which this model was adapted, the inflow ratio was modeled by the equation (B1) expression, including a first-order lag (ref. 1). Past cycle values of  $C_{T,F,R}$ ,  $\lambda_{F,R}$ , and  $\mu_{F,R}$  were used, so no iteration on the current value of  $\mu_{F,R}$  was performed using this implementation.

$$\begin{matrix} \text{ALAMFR} \\ \text{ALAMRR} \end{matrix} \lambda_{F,R} = \lambda'_{F,R} - \left[ \frac{C_{T,F,R}}{2(\mu_{F,R}^2 + \lambda_{F,R}^2)^{1/2}} + \frac{D_{F,RF(FR)} C_{T,R,F}}{2(\mu_{R,F}^2 + \lambda_{R,F}^2)^{1/2}} \right] \left[ \frac{1}{\lambda_{F,R} s + 1} \right] \quad (B1)$$

where

$$\lambda'_{F,R} = \frac{w_{F,R}}{R_{B,F,R} (\Omega'_{F,R} - r_{F,R})} = \frac{w_{F,R}}{R_{B,F,R} \Omega_{F,R}}$$

as defined in model equation (12).

A more exact real-time solution was obtained by Boris Voh, who represented the above as a differential equation and solved it using a local linearization method implemented as subroutine LOLIN (ref. 12). Following is the solution method, using the forward rotor equation as an example:

$$\lambda_F = \frac{w_F}{R_{B,F} \Omega_F} - \left[ \frac{C_{T,F}}{2(\mu_F^2 + \lambda_F^2)^{1/2}} + \frac{D_{F,RF} C_{T,R}}{2(\mu_R^2 + \lambda_R^2)^{1/2}} \right] \left[ \frac{1}{\tau_{\lambda_F} s + 1} \right] \quad (B2)$$

$$\lambda_F (\tau_{\lambda_F} s + 1) = \frac{w_F}{R_{B,F} \Omega_F} (\tau_{\lambda_F} s + 1) - \left[ \frac{C_{T,F}}{2(\mu_F^2 + \lambda_F^2)^{1/2}} + \frac{D_{F,RF} C_{T,R}}{2(\mu_R^2 + \lambda_R^2)^{1/2}} \right] \quad (B3)$$

$$\tau_{\lambda_F} \dot{\lambda}_F + \lambda_F = \frac{\tau_{\lambda_F}}{R_{B,F} \Omega_F} \dot{w}_F + \frac{w_F}{R_{B,F} \Omega_F} - \frac{C_{T,F}}{2(\mu_F^2 + \lambda_F^2)^{1/2}} - \frac{D_{F,RF} C_{T,R}}{2(\mu_R^2 + \lambda_R^2)^{1/2}} \quad (B4)$$

$$\dot{\lambda}_F = \frac{\dot{w}_F}{R_{B,F} \Omega_F} - \frac{1}{\tau_{\lambda_F}} \left[ \lambda_F - \frac{w_F}{R_{B,F} \Omega_F} + \frac{C_{T,F}}{2(\mu_F^2 + \lambda_F^2)^{1/2}} + \frac{D_{F,RF} C_{T,R}}{2(\mu_R^2 + \lambda_R^2)^{1/2}} \right] \quad (B5)$$

Following are the definitions necessary for the application of LOLIN to this problem:

ORIGIN  
OF POOR

<u>Description</u>	<u>LOLIN definition</u>	<u>Engineering definition</u>
Nonlinear function	FN	$\begin{bmatrix} \dot{\lambda}_F \\ \dot{\lambda}_R \end{bmatrix}$
Partial derivative of nonlinear function with respect to time	FT	$\begin{bmatrix} \ddot{\lambda}_F \\ \ddot{\lambda}_R \end{bmatrix}$
Jacobian of system	FS	$\begin{bmatrix} \frac{\partial \dot{\lambda}_F}{\partial \lambda_F} & \frac{\partial \dot{\lambda}_F}{\partial \lambda_R} \\ \frac{\partial \dot{\lambda}_R}{\partial \lambda_F} & \frac{\partial \dot{\lambda}_R}{\partial \lambda_R} \end{bmatrix}$
System state vector	SI	$\begin{bmatrix} \lambda_F \\ \lambda_R \end{bmatrix}$

where

$$\begin{bmatrix} \dot{\lambda}_F \\ \dot{\lambda}_R \end{bmatrix}$$

is defined above in equation (B5), the time derivative of the function,

$$\begin{bmatrix} \ddot{\lambda}_F \\ \ddot{\lambda}_R \end{bmatrix} = \begin{bmatrix} 0 \\ 0 \end{bmatrix}$$

and the four elements of the Jacobian may be calculated as in equations (B6)-(B9):

$$\frac{\partial \dot{\lambda}_F}{\partial \lambda_F} = -\frac{1}{\tau_{\lambda_F}} \left[ 1 + \frac{a_F \sigma_F}{8(\mu_F^2 + \lambda_F^2)^{1/2}} - \frac{C_{TF} \lambda_F}{2(\mu_F^2 + \lambda_F^2)^{3/2}} \right] \quad (B6)$$

$$\frac{\partial \dot{\lambda}_F}{\partial \lambda_R} = -\frac{1}{\tau_{\lambda_F}} \left[ \frac{C_{TR} (\partial D_{FRF} / \partial \lambda_R)}{2(\mu_R^2 + \lambda_R^2)^{1/2}} + \frac{a \partial D_{FRF}}{8(\mu_R^2 + \lambda_R^2)^{1/2}} - \frac{D_{FRF} C_{TR} \lambda_R}{2(\mu_R^2 + \lambda_R^2)^{3/2}} \right] \quad (B7)$$

where

$$\frac{\partial D_{FRF}}{\partial \lambda_R} = \frac{(1 - |\sin \beta_{FUS}|) \Delta d'_{FRF}}{\Delta |-(\lambda_R / \mu_R) - 0.25| \mu_R}$$



$$\frac{\partial \dot{\lambda}_R}{\partial \lambda_F} = -\frac{1}{\tau_{\lambda_R}} \left[ \frac{C_{TF} \partial D_{FR} / \partial \lambda_F}{2(\mu_F^2 + \lambda_F^2)^{1/2}} + \frac{a \sigma D_{FR}}{8(\mu_F^2 + \lambda_F^2)^{1/2}} - \frac{D_{FR} C_{TF} \lambda_F}{2(\mu_F^2 + \lambda_F^2)^{3/2}} \right] \quad (B8)$$

where

$$\frac{\partial D_{FR}}{\partial \lambda_F} = \frac{[1 - |\sin \beta_{FUS}|] \Delta d_{FR}}{\Delta |-(\lambda_F / \mu_R) - 0.25| \mu_F}$$

$$\frac{\partial \dot{\lambda}_R}{\partial \lambda_R} = -\frac{1}{\tau_{\lambda_R}} \left[ 1 + \frac{a_R \sigma_R}{8(\mu_R^2 + \lambda_R^2)^{1/2}} - \frac{C_{TR} \lambda_R}{2(\mu_R^2 + \lambda_R^2)^{3/2}} \right] \quad (B9)$$

Using LOLIN, equations (B1) may be solved with a Newton-Raphson numerical technique in equations (B10) and B11).

$$\text{ALAMFR } \lambda_{F_{n+1}} = \lambda_{F_n} + \frac{\frac{\partial \dot{\lambda}_F}{\partial \lambda_R} \dot{\lambda}_R - \frac{\partial \dot{\lambda}_R}{\partial \lambda_F} \dot{\lambda}_F}{\det \begin{bmatrix} \frac{\partial \dot{\lambda}_F}{\partial \lambda_F} & \frac{\partial \dot{\lambda}_F}{\partial \lambda_R} \\ \frac{\partial \dot{\lambda}_R}{\partial \lambda_F} & \frac{\partial \dot{\lambda}_R}{\partial \lambda_R} \end{bmatrix}} \bigg|_n \quad (B10)$$

$$\text{ALAMRR } \lambda_{R_{n+1}} = \lambda_{R_n} + \frac{\frac{\partial \dot{\lambda}_R}{\partial \lambda_F} \dot{\lambda}_F - \frac{\partial \dot{\lambda}_F}{\partial \lambda_R} \dot{\lambda}_R}{\det \begin{bmatrix} \frac{\partial \dot{\lambda}_F}{\partial \lambda_F} & \frac{\partial \dot{\lambda}_F}{\partial \lambda_R} \\ \frac{\partial \dot{\lambda}_R}{\partial \lambda_F} & \frac{\partial \dot{\lambda}_R}{\partial \lambda_R} \end{bmatrix}} \bigg|_n \quad (B11)$$

ORIGINAL PAGE 1  
OF POOR QUALITY

## REFERENCES

1. Cogan, C.; Gajkowski, B. J.; and Garnett, Jr., T. S.: Full Flight Envelope Math Model for 347/HLH Control System Analysis - Control Document. Boeing Company, Vertol Division, report 501-10148-1, 1972.
2. Yamakawa, G.; and Miller, L. G.: Airworthiness and Qualification Test, Phase D, CH-47B. USAASTA #66-23, 1970.
3. Albion, N.; Leet, J. R.; and Mollenkof, A.: Ground Based Flight Simulation of CH-47C Helicopter. Boeing Company, Vertol Division, report D8-2418-1, 1969.
4. Hackett, W. E.; Garnett, T. S.; and Borek, B. V.: Mathematical Model of the CH-47B Helicopter Capable of Real Time Simulation of the Full Flight Envelope. NASA CR-166458, 1983.
5. Hennessy, J. P.: Charts and Equations for the Rapid Calculation of Rotor Thrust and Flapping Coefficients. Boeing Company, Vertol Division, report 15-A-13, 1949.
6. Wheatley, J. B.: An Aerodynamic Analysis of the Autogiro Rotor with a Comparison Between Calculated and Experimental Results. NASA TR-487, 1934.
7. Bailey, F. J., Jr.: A Simplified Theoretical Method of Determining the Characteristics of a Lifting Rotor in Forward Flight. NACA TR-716, 1941.
8. McFarland, R. E.: A Standard Kinematic Model for Flight Simulation at Ames. NASA CSCR-2, 1973.
9. Sinacori, J. B.; Stapleford, Robert L.; Jewell, Wayne F.; and Lehman, John M.: Researcher's Guide to the NASA Ames Flight Simulator for Advanced Aircraft (FSAA). NASA CR-2875, 1977.
10. Radford, R. C.: The Longitudinal Stability of the CH-47A Helicopter with the Forward Rotor Delta-Three - Results of Flight Test Program. Boeing Company, Vertol Division, report 114-AD-006, 1967.
11. Bramwell, A. R. S.: Helicopter Dynamics. John Wiley and Sons, Inc., New York, 1976.
12. Voh, B.: "LOLIN/LOLIN2," NASA Ames Program Specification (NAPS), no. 215, 1982.
13. Davis, J. M.: Stability and Control Analysis, CH-47B/CH-47C. Boeing Company, Vertol Division, report 114-AD-603, 1966.
14. McFarland, R. E.; and Rockkind, A. B.: FACT/UPDATE, NASA Ames Program Specification (NAPS), no. 194, 1977.

TABLE 1A.- ROTOR SUBROUTINE VARIABLE DEFINITION

Simulation mnemonic	Engineering variable	Units	Common location (if applicable)	Physical description
AICFR	$A_{ICF}$	rad ↓	CH(218)	Forward rotor lateral cyclic pitch, SNP wind reference frame, transformed through control phasing angle ( $\phi_p$ ) and corrected for $\delta_3$ hinging ( $K_\beta$ )
AICFRI	$A'_{ICF1}$			Forward rotor lateral cyclic pitch, SNP wind reference frame
AICFR2	$A'_{ICF2}$			Forward rotor lateral cyclic pitch, SNP wind reference frame, transformed through control phasing angle ( $\phi_p$ )
AICRR	$A_{ICR}$		CH(280)	Rear rotor lateral cyclic pitch, SNP wind reference frame, transformed through control phasing angle ( $\phi_p$ ) and corrected for $\delta_3$ hinging ( $K_\beta$ )
AICRRI	$A'_{ICR1}$			Rear rotor lateral cyclic pitch, SNP wind reference frame
AICRR2	$A'_{ICR2}$			Rear rotor lateral cyclic pitch, SNP wind reference frame, transformed through control phasing angle ( $\phi_p$ )
ALAMFR	$\lambda_F$	---	CH(107)	Forward rotor inflow ratio
ALAMRR	$\lambda_R$	---	CH(108)	Rear rotor inflow ratio
ALARFR	$L_{AERF}$	ft-lb ↓	CH(52)	Total rolling moment due to forward rotor, helicopter body reference frame
ALARRR	$L_{AERR}$		CH(53)	Total rolling moment due to rear rotor, helicopter body reference frame
ALBDFR	$L_{hubF}$		CH(293)	Forward rotor hub rolling moment, body reference frame
ALBDRR	$L_{hubR}$		CH(294)	Rear rotor hub rolling moment, body reference frame
ALFRI	$L'_{AERF}$			Forward rotor rolling moment due to aerodynamic forces, helicopter body reference frame
ALFR2	$L''_{AERF}$			Forward rotor rolling moment due to hub moments, helicopter body reference frame

TABLE 1A.- CONTINUED.

Simulation mnemonic	Engineering variable	Units	Common location (if applicable)	Physical description
ALHBFR	$L_{hubF}$	ft-lb	CH(29)	Forward rotor hub rolling moment, SNP wind reference frame
ALHBRR	$L_{hubR}$	ft-lb	CH(28)	Rear rotor hub rolling moment, SNP wind reference frame
ALMPFR	$\lambda_F'$	---		Forward rotor free-stream component of inflow ratio
ALMPRR	$\lambda_R'$	---		Rear rotor free-stream component of inflow ratio
ALMSQF	$\lambda_F^2$	---	CH(4)	
ALMSQR	$\lambda_R^2$	---	CH(3)	
ALRR1	$L_{AERF}$	ft-lb		Rear rotor rolling moment due to aerodynamic forces, helicopter body reference frame
ALRR2	$L_{AERR}$			Rear rotor rolling moment due to hub moments, helicopter body reference frame
AMARFR	$M_{AERF}$		CH(54)	Total pitching moment due to forward rotor, helicopter body reference frame
AMARRR	$M_{AERR}$		CH(55)	Total pitching moment due to rear rotor, helicopter body reference frame
AMBDFR	$M_{hubF}$		CH(295)	Forward rotor hub pitching moment, body reference frame
AMBDRR	$M_{hubR}$		CH(296)	Rear rotor hub pitching moment, body reference frame
AMFR1	$M'_{AERF}$			Forward rotor pitching moment due to aerodynamic forces, helicopter body reference frame
AMFR2	$M'_{AERR}$			Forward rotor pitching moment due to hub moments, helicopter body reference frame
AMHBFR	$M_{hubF}$		CH(45)	Forward rotor hub pitching moment, SNP wind reference frame
AMHBRR	$M_{hubR}$		CH(44)	Rear rotor hub pitching moment, SNP wind reference frame

TABLE 1A.- CONTINUED.

Simulation mnemonic	Engineering variable	Units	Common location (if applicable)	Physical description
AMRR1	$M_{AER}^{'}$	ft-lb		Forward rotor pitching moment due to aerodynamic forces helicopter body reference frame
AMRR2	$M_{AER}^{''}$	ft-lb		Rear rotor pitching moment due to hub moments, helicopter body reference frame
AMUFR	$\mu_F$	---	CH(98)	Forward rotor advance ratio
AMURR	$\mu_R$	---	CH(99)	Rear rotor advance ratio
AMUSQF	$\mu_F^2$	---	CH(12)	
AMUSQR	$\mu_R^2$	---	CH(11)	
ANARFR	$N_{AERF}$	ft-lb	CH(56)	Total yawing moment due to forward rotor, helicopter body reference frame
ANARRR	$N_{AERR}$		CH(57)	Total yawing moment due to rear rotor, helicopter body reference frame
ANFR1	$N_{AERF}^{'}$			Forward rotor yawing moment due to aerodynamic forces, helicopter body reference frame
ANFR2	$N_{AERF}^{''}$			Forward rotor yawing moment due to hub moments, helicopter body reference frame
ANRR1	$N_{AERR}^{'}$			Rear rotor yawing moment due to aerodynamic forces, helicopter body reference frame
ANRR2	$N_{AERR}^{''}$			Rear rotor yawing moment due to hub moments, helicopter body reference frame
AOFR	$a_{0F}$	rad	CH(270)	Forward rotor mean coning angle
AOFRSQ	$a_{0F}^2$	rad <sup>2</sup>		
AORR	$a_{0R}$	rad	CH(271)	Rear rotor mean coning angle
AORRSQ	$a_{0R}^2$	rad <sup>2</sup>		

TABLE 1A.- CONTINUED.

Simulation mnemonic	Engineering variable	Units	Common location (if applicable)	Physical description
ALBDFR	$a_{1F}$	rad	CH(285)	Forward rotor longitudinal flapping angle, body reference frame
ALFR	$a_{1F}$	rad	CH(226)	Forward rotor longitudinal flapping angle, SNP wind reference frame
ALFRSQ	$a_{1F}^2$	rad <sup>2</sup>		
ALBDRR	$a_{1R}$	rad	CH(286)	Rear rotor longitudinal flapping angle, body reference frame
ALRR	$a_{1R}$	rad	CH(94)	Rear rotor longitudinal flapping angle, SNP wind reference frame
ALRRSQ	$a_{1R}^2$	rad <sup>2</sup>		
BDFFR	$D_{FFR}$	---	CH(232)	Forward-on-rear rotor interference term corrected for sideslip angle
BDFRF	$D_{FRF}$	---	CH(231)	Rear-on-forward rotor interference term corrected for sideslip angle
BETAFR	$\beta'_F$	rad	CH(88)	Forward rotor sideslip angle
BETARR	$\beta'_R$	rad	CH(89)	Rear rotor sideslip angle
BETC	$1 -  \sin \delta_{FUS} $	---		Term used in inflow ratio calculation
BICFR	$B_{1CF}$	rad	CH(220)	Forward rotor longitudinal cyclic pitch, SNP wind reference frame, transformed through control-phasing angle ( $\phi_p$ ) and corrected for $\delta_3$ hinging ( $K_2$ )
BICFR1	$B'_{1CF_1}$	rad		Forward rotor longitudinal cyclic pitch, SNP wind reference frame
BICFR2	$B'_{1CF_2}$	rad		Forward rotor longitudinal cyclic pitch, SNP wind reference frame, transformed through control phasing angle ( $\phi_p$ )

TABLE 1A.- CONTINUED.

Simulation mnemonic	Engineering variable	Units	Common location (if applicable)	Physical description
BICRR	$B_{1CR}$	rad	CH(281)	Rear rotor longitudinal cyclic pitch, SNP wind reference frame, transformed through control phasing angle ( $\phi_p$ ) and corrected for $\delta_3$ hinging ( $K_g$ )
BICRR1	$B'_{1CR1}$	rad		Rear rotor longitudinal cyclic pitch, SNP wind reference frame
BICRR2	$B'_{1CR2}$	rad		Rear rotor longitudinal cyclic pitch, SNP wind reference frame, transformed through control phasing angle ( $\phi_p$ )
BKGEFR	$K_{gef}$	---		Forward rotor ground effect correction term
BKGERR	$K_{ger}$	---		Rear rotor ground effect correction term
B1BDFR	$b_{1F}$	rad	CH(287)	Forward rotor lateral flapping angle, body reference frame
B1FR	$b_{1F}$	rad	CH(227)	Forward rotor lateral flapping angle, SNP wind reference frame
B1FRSQ	$b_{1F}^2$	rad <sup>2</sup>		
B1BDRR	$b_{1R}$	rad	CH(288)	Rear rotor lateral flapping angle, body reference frame
B1RR	$b_{1R}$	rad	CH(95)	Rear rotor lateral flapping angle, SNP wind reference frame
B1RRSQ	$b_{1R}^2$	rad <sup>2</sup>		
CBETFR	$\cos \beta'_F$	---		
CBETRR	$\cos \beta'_R$	---		
CFFR01	$\pi R_B^4$	ft <sup>4</sup>		
CFFR02	$a_F \sigma_F / 2$		CH(78)	
CFFR03	$9\delta F_1$			

TABLE 1A.- CONTINUED.

Simulation mnemonic	Engineering variable	Units	Common location (if applicable)	Physical description
CFRR05	$1/a_F$	1/ft	CH(79)	
CFRR06	$1/2a_F$			
CFRR65	$I_F / (a_F C_F B_F^4)$			
CFRR66	$2K_{\beta F}$			
CFRR67	$2K_{\beta F} / 3$			
CFRR68	$\theta_{t_F} / 2$			
CFRR69	$\theta_{t_F} / 4$			
CFRR70	$e_F b_F^M w_F / 2$			
CFRR01	$\pi R_{B_R}^4$			
CFRR02	$a_R \sigma_R / 2$			
CFRR03	$9^{\delta} R_1$			
CFRR05	$1/a_R$			
CFRR06	$1/2a_R$			
CFRR65	$I_R / (a_R C_R B_R^4)$			
CFRR66	$2K_{\beta R}$			
CFRR67	$2K_{\beta R} / 3$			
CFRR68	$\theta_{t_R} / 2$			
CFRR69	$\theta_{t_R} / 4$			



TABLE 1A.- CONTINUED.

Simulation mnemonic	Engineering variable	Units	Common location (if applicable)	Physical description
CFRR70	$e_{R} b_{R} M_{wR} / 2$			Forward rotor drag coefficient
CHFR	$C_{HF}$	---	CH(62)	Normalized forward rotor drag coefficient
CHFRL	$2C_{HF} / a\sigma$	---		Rear rotor drag coefficient
CHRR	$C_{HR}$	---	CH(63)	Normalized rear rotor drag coefficient
CHRR1	$2C_{HR} / a\sigma$	---		Cosine of forward rotor shaft incidence angle
COSIFR	$\cos i_F$	---	CH(47)	Cosine of rear rotor shaft incidence angle
COSIRR	$\cos i_R$	---	CH(49)	Cosine of forward rotor control phasing angle
CPHPFR	$\cos \phi_{PF}$	---	CH(35)	Cosine of rear rotor control phasing angle
CPHPRR	$\cos \phi_{PR}$	---	CH(34)	Forward rotor torque coefficient
CQFR	$C_{QF}$	---	CH(66)	Normalized forward rotor torque coefficient
CQFRL	$2C_{QF} / a\sigma$	---		Rear rotor torque coefficient
CQRR	$C_{QR}$	---	CH(67)	Normalized rear rotor torque coefficient
CQRR1	$2C_{QR} / a\sigma$	---		Coefficient used in rotor-on-rotor interference term calculation
CSFR02	$C_{F2}$	---		Forward rotor thrust coefficient
CTFR	$C_{TF}$	---	CH(31)	Normalized forward rotor thrust coefficient
CTFRL	$2C_{TF} / a\sigma$	---		Rear rotor thrust coefficient
CTRR	$C_{TR}$	---	CH(30)	Normalized rear rotor thrust coefficient
CTRR1	$2C_{TR} / a\sigma$	---		

TABLE 1A.- CONTINUED.

Simulation mnemonic	Engineering variable	Units	Common location (if applicable)	Physical description
CYFR	$C_{YF}$	---	CH(60)	Forward rotor side force coefficient
CYFRL	$2C_{YF}/a\sigma$	---		Normalized forward rotor side-force coefficient
CYRR	$C_{YR}$	---	CH(61)	Rear rotor side-force coefficient
CYRRL	$2C_{YR}/a\sigma$	---		Normalized rear rotor side-force coefficient
DCTF	$\partial C_{TF}/\partial \lambda_F$	---		Term used in inflow dynamics calculation
DCTR	$\partial C_{TR}/\partial \lambda_R$	---		Term used in inflow dynamics calculation
DDFFR	$\Delta D_{FFR}$			Term used in inflow dynamics calculation
DDFRF	$\Delta D_{FRF}$	---		Term used in inflow dynamics calculation
DEFS		---		Term used in inflow dynamics calculation
DEFSI		---		Term used in inflow dynamics calculation
DELCQ	$\Delta C_Q$	---		Empirical torque-correction term
DELCQF	$\Delta C_{QF}$	---		Forward rotor stall-correction term to torque
DELCQR	$\Delta C_{QR}$	---		Rear rotor stall-correction term to torque
DELFR	$\delta_F$	---	CH(9)	Profile drag contribution to forward rotor H-force
DELFR0	$\delta_{0F}$	---		Term used in forward rotor profile-drag calculation
DELFR1	$\delta_{1F}$	---		Term used in forward rotor profile-drag calculation
DELRR	$\delta_R$	---	CH(10)	Profile drag contribution to rear rotor H-force
DELRR1	$\delta_{1R}$	---		Term used in rear rotor profile-drag calculation

TABLE 1A.- CONTINUED.

Simulation mnemonic	Engineering variable	Units	Common location (if applicable)	Physical description
DFFR	$\dot{d}_{FFR}$	---		Forward-on-rear rotor interference parameter
DFRF	$\dot{d}_{FRF}$			Rear-on-forward rotor interference parameter
DLMFR	$d/dt(\lambda_F')$			Term used in inflow dynamics calculation
DLMRR	$d/dt(\lambda_R')$			Term used in inflow dynamics calculation
DXF	$\Delta  -(\lambda_F'/u_F) - 0.25 $			Term used in inflow dynamics calculation
DXR	$\Delta  -(\lambda_R'/u_R) - 0.25 $			Term used in inflow dynamics calculation
FFR	$\rho \pi R_F^2 \Omega_F^2$		CH(15)	(2 x 2) matrix used in inflow-ratio calculation
FRR	$\rho \pi R_R^2 \Omega_R^2$		CH(16)	(2 x 1) matrix used in inflow-ratio calculation
FS				Forward rotor drag (H-force), SNP reference frame
FT		lb	CH(25)	Forward rotor drag (H-force), body reference frame
HFR	$H_F$	lb	CH(289)	Height of rotor hub above ground
HFRBOD	$H_F$	ft		Height to diameter ratio, forward rotor
HROTOR	$h_{rotor}$	---		Height to diameter ratio, rear rotor
HROVDF	(h/D) rotor	---		Rear rotor drag (H-force), SNP reference frame
HROVDR	(h/D) rotor	---		Rear rotor drag (H-force) body reference frame
HRR	$H_R$	lb	CH(24)	Forward rotor RPM corrected for helicopter yaw rate
HRRBOD	$H_R$	lb	CH(290)	Rear rotor RPM corrected for helicopter yaw rate
OMEGFR	$\Omega_F' - r_F$	rad/sec	CH(201)	
OMEGRR	$\Omega_R' - r_R$	rad/sec	CH(202)	

TABLE 1A.- CONTINUED.

Simulation mnemonic	Engineering variable	Units	Common location (if applicable)	Physical description
OMSQFR	$(\dot{\Omega}_F' - r_F')^2$	rad <sup>2</sup> /sec <sup>2</sup>		
OMSQRR	$(\dot{\Omega}_R' - r_R')^2$	rad <sup>2</sup> /sec <sup>2</sup>		
PFR	$P_F$	rad/sec	CH(244)	Helicopter roll rate transformed to forward rotor SNP wind reference frame
PRR	$P_R$	rad/sec	CH(241)	Helicopter roll rate transformed to rear rotor SNP wind reference frame
QAERFR	$Q_{AERF}$	ft-lb	CH(64)	Forward rotor torque required
QAERRR	$Q_{AERR}$	ft-lb	CH(65)	Rear rotor torque required
QFR	$q_F$	rad/sec	CH(245)	Helicopter pitch rate transformed to forward rotor SNP wind reference frame
QRR	$q_R$	rad/sec	CH(242)	Helicopter pitch rate transformed to forward rotor SNP wind reference frame
RFR	$r_F$	rad/sec		Helicopter yaw rate transformed to forward rotor SNP wind reference frame
RRR	$r_R$	rad/sec		Helicopter yaw rate transformed to rear rotor SNP wind reference frame
SBETFR	$\sin \beta_F$	---		
SBETRR	$\sin \beta_R$			
SDFR	$d_F$	ft		Lateral distance from helicopter c.g. to $\zeta_L$ of forward rotor hub
SDRR	$d_R$	ft		Lateral distance from helicopter c.g. to $\zeta_L$ of rear rotor hub
SHFR	$h_F$	ft		Vertical distance from helicopter c.g. to $\zeta_L$ of forward rotor hub
SHRR	$h_R$	ft		Vertical distance from helicopter c.g. to $\zeta_L$ of forward rotor hub

TABLE 1A.- CONTINUED.

Simulation mnemonic	Engineering variable	Units	Common location (if applicable)	Physical description
SI				(2 x 1) matrix used in inflow dynamics calculation
SIGFR	$\sigma_F$	---	CH(222)	Forward rotor solidity ratio
SIGRR	$\sigma_R$	---	CH(223)	Rear rotor solidity ratio
SINIFR	$\sin i_F$		CH(46)	
SINIRR	$\sin i_R$		CH(48)	
SLFR	$\lambda_F$	ft		Longitudinal distance from helicopter c.g. to $\zeta$ of forward rotor hub
SLRR	$\lambda_R$	ft		Longitudinal distance from helicopter c.g. to $\zeta$ of rear rotor hub
SMLFI	$1/(\mu_F^2 + \lambda_F^2)$	---		Term used in inflow ratio calculation
SMLRI	$1/(\mu_R^2 + \lambda_R^2)$	---		Term used in inflow ratio calculation
SPHPFR	$\sin \phi_{PF}$	---	CH(33)	
SPHPRR	$\sin \phi_{PR}$	---	CH(32)	
TFR	$T_F$	lb	CH(23)	Forward rotor thrust
THOFR	$\theta_{0F}$	rad	CH(216)	Forward rotor collective pitch corrected for $\delta_3$ hinging ( $K_\beta$ )
THORR	$\theta_{0R}$	rad	CH(217)	Rear rotor collective pitch corrected for $\delta_3$ hinging ( $K_\beta$ )
TIGEFR	$T_{I.g.e.F}$			Altitude/airspeed dependent ground effect correction term, forward rotor
TIGERR	$T_{I.g.e.R}$			Altitude/airspeed dependent ground effect correction term, rear rotor

TABLE 1A.- CONTINUED.

Simulation mnemonic	Engineering variable	Units	Common location (if applicable)	Physical description
TLFI	$1/\tau_{\lambda_F}$	1/sec		
TLRI	$1/\tau_{\lambda_R}$	1/sec		
TMFR01	$\cos \beta'_F \cos i_F$	---		
TMFR02	$\cos \beta'_F \sin i_F$	---		
TMFR03	$\sin \beta'_F \cos i_F$	---		
TMFR04	$\sin \beta'_F \sin i_F$	---		
TMFR05	$1/R_{BF}(\Omega'_F - r_F)$	1/ft/sec		
TMFR08	$\delta_F/a_F$	---		
TMFR09	$\delta_F/2a_F$	---		
TMFR14	$\mu_F/2$	---	CH(159)	
TMFR15	$\lambda_F/2$	---	CH(160)	
TMFR16	$p_F/\Omega_F$	---	CH(161)	
TMFR19	$p_F/\Omega_F$	---	CH(164)	
TMFR23	$\alpha$	---	CH(168)	
TMFR32				Matrix element (1,1) in forward rotor flapping-coning linear system of equations

$$\alpha_{AF} = 12I_F/\rho a_F c_F R_{BF}^4 - \frac{3}{2} K_{BF}(1 + \mu_F^2)$$

TABLE 1A. - CONTINUED.

Simulation mnemonic	Engineering variable	Units	Common location (if applicable)	Physical description
TMFR33	$B_F = 0$			Matrix element (1,2) in forward rotor flapping-coning linear system of equations
TMFR34	$C_F = 2\mu_F K_{\beta F}$			Matrix element (1,3) in forward rotor flapping-coning linear system of equations
TMFR35	$E_F = \frac{1}{4} - \mu_F^2/8$			Matrix element (2,2) in forward rotor flapping-coning linear system of equations
TMFR36	$b$			Matrix element (3,1) in forward rotor flapping-coning linear system of equations
TMFR37	$H_F = -K_{\beta F}$			Matrix element (3,2) in forward rotor flapping-coning linear system of equations
TMFR39	$c$			Coning-equation constant term
TMFR40	$d$			Longitudinal flapping-equation constant term
TMFR41	$e$			Lateral flapping-equation constant term
TMFR42	$B_F E_F - C_F F_F$			Coning-flapping equations term
TMFR43	$B_F I_F - C_F H_F$			Coning-flapping equations term
TMFR44	$E_F I_F - F_F H_F$			Coning-flapping equations term

$$\dot{\phi}_{G_F} = -\frac{4}{3} \mu_F / (1 + \mu_F^2/2)$$

$$\dot{\phi}_{J_F} = \frac{3}{2} \theta_0' (1 + \mu_F^2) + 2\lambda_F - 2\mu_F B_1' c_{F2} + \theta_{tw_F} (1.2 + \mu_F^2)$$

$$\dot{\phi}_{K_F} = \frac{2}{3} \mu_F \theta_0' + \frac{1}{2} \mu_F \lambda_F + \frac{1}{2} \theta_{tw_F} \mu_F - B_1' c_{F2} \left( \frac{1}{4} + \frac{3}{8} \mu_F \right) - (4I_F q_F / \rho a c_F R_{B_F}^2 \Omega_F) (1 - \mu_F^4/4)$$

$$e_{L_F} = A_1' c_{F2} - (16I_{FP_F} / \rho a c_F R_{B_F}^4 \Omega_F) (1 - \mu_F^2/2)$$

TABLE 1A.- CONTINUED.

Simulation mnemonic	Engineering variable	Units	Common location (if applicable)	Physical description
TMFR45	$J_F G_F - L_F A_F$			Coning-flapping equations term
TMFR46				Inverse of determinant of flapping-coning system matrix
TMFR52	$1/3_F$			
TMFR56	$f$			Matrix element (2,3) in flapping-coning linear system of equations
TMFR57	$D_F = \frac{2}{3} K_{BF} \mu_F$			Matrix element (2,1) in flapping-coning linear system of equations
TMFR58	$I_F = 1.0$			Matrix element (3,3) in flapping-coning linear system of equations
TMFR59	$J_F D_F - K_F A_F$			Coning-flapping equations term
TMFR60	$L_F D_F - K_F G_F$			Coning-flapping equations term
TMFR62	$\frac{1}{2} \sqrt{\mu_F^2 + \lambda_F^2}$			
TMFR63	$I_F / (\rho a_F C_F R_{BF}^4)$		CH(175)	
TMFR64	$\frac{3}{2} (1 + \mu_F^2)$		CH(176)	
TMFR66	$\frac{1}{4} + \frac{3}{8} \mu_R^2$		CH(178)	
TMFR67	$\rho_F^2 e_F b_F M_F / 2$		CH(179)	

$$F_F = K_{3F} \left( \frac{1}{4} + \frac{3}{8} \mu_F^2 \right)$$



TABLE 1A.- CONTINUED.

Simulation mnemonic	Engineering variable	Units	Common location (if applicable)	Physical description
TMCN01	$1/(1 + D_{FR_F})$		CH(100)	
TMCN05	$\epsilon$		CH(104)	
TMCN06	$\tan^{-1}(\mu_F /  -\lambda_F )$	---	CH(105)	
TMRR01	$\cos \beta'_R \cos i_R$	---		
TMRR02	$\cos \beta'_R \sin i_R$	---		
TMRR03	$\sin \beta'_R \cos i_R$	---		
TMRR04	$\sin \beta'_R \sin i_R$	---		
TMRR05	$h$	1/ft/sec		
TMRR08	$\delta_R/a_R$	---		
TMRR09	$\delta_R/2a_R$	---		
TMRR14	$\mu_R^2/2$	---	CH(129)	
TMRR15	$\mu_R/2$		CH(130)	
TMRR16	$\lambda_R/2$		CH(131)	

$$\epsilon(\lambda'_F - \lambda_F)R_{BF}(\Omega'_F - r_F)$$

$$h_{1/R_{BR}}(\Omega'_R - r_R)$$

TABLE 1A.- CONTINUED.

Simulation mnemonic	Engineering variable	Units	Common location (if applicable)	Physical description
TMRR19	$q_r/\Omega_R$		CH(134)	Matrix element (1,1) in rear rotor flapping-coning linear system of equations Matrix element (1,2) in rear rotor flapping-coning linear system of equations Matrix element (1,3) in rear rotor flapping-coning linear system of equations Matrix element (2,2) in rear rotor flapping-coning linear system of equations Matrix element (3,1) in rear rotor flapping-coning linear system of equations Matrix element (3,2) in rear rotor flapping-coning linear system of equations Coning equation constant term Longitudinal flapping equation constant term Lateral flapping equation constant term
TMRR23	$p_r/\Omega_R$		CH(138)	
TMRR32	$i$			
TMRR33	$B_R = 0$			
TMRR34	$C_R = 2\mu_R K_{\beta R}$			
TMRR35	$E_R = 1/4 - \mu_F^2/8$			
TMRR36	$j$			
TMRR37	$H_R = -K_{\beta R}$			
TMRR39	$k$			
TMRR40	$l$			
TMRR41	$m$			

$$i_A = 12I_R/\rho a_R c_R R_{BR}^4 - \frac{3}{2} K_{\beta R} (1 + \mu_R^2)$$

$$j_{GR} = -\frac{4}{3} \mu_R/(1 + \mu_R^2/2)$$

$$k_{JR} = \frac{3}{2} \mu_{GR}' (1 + \mu_R^2) + 2\lambda_R - 2\mu_R B_{i_{CR_2}}' + \theta_{tw_R} (1.2 + \mu_R^2)$$

$$l_{KR} = \frac{2}{3} \mu_R \theta_{GR}' + \frac{1}{2} \mu_R \lambda_R + \frac{1}{2} \theta_{tw_R} \mu_R - B_{i_{CR_2}}' \left( \frac{1}{4} + \frac{3}{8} \mu_R^2 \right) - (4I_{RQR}/\rho a_R c_R R_{BR}^4 \Omega_R) (1 - \mu_R^4/4)$$

$$m_{LR} = A_{i_{CR_2}}' - (16I_{ROR})/(\rho a_R c_R R_{BR}^4 \Omega_R) (1 - \mu_R^2/2)$$

TABLE 1A.- CONTINUED.

Simulation mnemonic	Engineering variable	Units	Common location (if applicable)	Physical description
TMRR42	$B_R^{ER} - C_R^{ER}$			Coning-flapping equations term
TMRR43	$B_R^{IR} - C_R^{HR}$			Coning-flapping equations term
TMRR44	$E_R^{IR} - F_R^{HR}$			Coning-flapping equations term
TMRR45	$J_R^{GR} - L_R^{AR}$			Coning-flapping equations term
TMRR46				Inverse of determinant of flapping-coning system matrix
TMRR52	$1/\Omega_R$			
TMRR56	$n$			
TMRR57	$D_R = 2/3K_{BR}\mu_R$			Matrix element (2,3) in rear rotor flapping-coning linear system of equations
TMRR58	$I_R = 1.0$			Matrix element (2,1) in flapping-coning linear system of equations
TMRR59	$J_R^{DR} - K_R^{AR}$			Matrix element (3,3) in flapping-coning linear system of equations
TMRR60	$L_R^{DR} - K_R^{GR}$			Coning-flapping equations term
TMRR62	$\frac{1}{2} \sqrt{\mu_R^2 + \lambda_R^2}$			Coning-flapping equations term
TMRR63	$I_R / (\rho a_R c_R^4 B_R)$		CH(145)	Coning-flapping equations term
TMRR64	$\frac{3}{2} (1 + \mu_R^2)$		CH(146)	
TMRR66	$\frac{1}{4} + \frac{3}{8} \mu_R^2$		CH(148)	
TMRR67	$\Omega_R^2 e_R b_R M_{wR} / 2$		CH(149)	

$$n_{FR} = K_{BR} \left( \frac{1}{4} + \frac{3}{8} \mu_R^2 \right)$$

TABLE 1A.- CONTINUED.

Simulation mnemonic	Engineering variable	Units	Common location (if applicable)	Physical description	
TRR	$T_R$	lb	CH(22)	Rear rotor thrust	
UFR	$u_F$	ft/sec	CH(5)	Helicopter longitudinal velocity at forward rotor hub SNP wind reference frame	
UFRL	$u_{F1}$			Helicopter longitudinal velocity at forward rotor hub, body reference frame	
UFR2	$u_{F2}$			Helicopter longitudinal velocity at forward rotor hub, SNP reference frame	
URR	$u_R$			Helicopter longitudinal velocity at rear rotor hub, SNP wind reference frame	
URRL	$u_{R1}$			Helicopter longitudinal velocity at rear rotor hub, body reference frame	
URR2	$u_{R2}$			Helicopter longitudinal velocity at rear rotor hub, SNP reference frame	
VFRL	$v_{F1}$			Helicopter lateral velocity at forward rotor hub, body reference frame	
VFR2	$v_{F2}$			Helicopter lateral velocity at forward rotor hub, SNP reference frame	
VRR1	$v_{R1}$			Helicopter lateral velocity at rear rotor hub, body reference frame	
VRR2	$v_{R2}$			Helicopter lateral velocity at rear rotor hub, SNP reference frame	
VTIPFR	$R_{BF}(\Omega_F' - r_F)$		CH(211)	Forward rotor tip speed	
VTIPRR	$R_{BR}(\Omega_R' - r_R)$		CH(212)	Rear rotor tip speed	
WFR	$w_F$				Helicopter vertical velocity at forward rotor hub, SNP wind reference frame
WFRL	$w_{F1}$				Helicopter vertical velocity at forward rotor hub, body reference frame

TABLE 1A.- CONCLUDED.

Simulation mnemonic	Engineering variable	Units	Common location (if applicable)	Physical description
WFR2	$w_{F2}$	ft/sec		Helicopter vertical velocity at forward rotor hub, SNP reference frame
WRR	$w_R$	ft/sec		Helicopter vertical velocity at rear rotor hub, SNP wind reference frame
WRR1	$w_{R1}$	ft/sec		Helicopter vertical velocity at rear rotor hub, body reference frame
WRR2	$w_{R2}$	ft/sec		Helicopter vertical velocity at rear rotor hub, SNP reference frame
XAERFR	$x_{AERF}$	lb	CH(72)	Forward rotor hub longitudinal force transformed to helicopter body reference frame
XAERRR	$x_{AERR}$		CH(75)	Rear rotor hub longitudinal force transformed to helicopter body reference frame
YAERFR	$y_{AERF}$		CH(73)	Forward rotor hub lateral force, transformed to helicopter body reference frame
YAERRR	$y_{AERR}$		CH(76)	Rear rotor hub lateral force, transformed to helicopter body reference frame
YFR	$y_F$		CH(27)	Forward rotor side force, SNP reference frame
YFRBOD	$y_F$		CH(291)	Forward rotor side force, body reference frame
YRR	$y_R$		CH(26)	Rear rotor side force, SNP reference frame
YRRBOD	$y_R$		CH(292)	Rear rotor side force, body reference frame
ZAERFR	$z_F$		CH(74)	Forward rotor hub vertical force, transformed to helicopter body reference frame
ZAERRR	$z_R$		CH(77)	Rear rotor hub vertical force, transformed to helicopter body reference frame

TABLE 1B.- ROTOR CONSTANTS AND CONVERSION FACTORS

Simulation mnemonic	Engineering variable	Units	Common location (if applicable)	Nominal value	Physical description
AINFR	$i_F$	rad		0.15708	Forward rotor shaft incidence angle
AINRR	$i_R$	rad		0.06981	Rear rotor shaft incidence angle
BKBEF	$K_{\beta F}$	---		0	$-\tan \delta_{\beta F}$
BKBETR	$K_{\beta R}$	---		0	$-\tan \delta_{\beta R}$
BMWFR	$M_{wF}$	ft-lb		144.7	Moment of forward rotor blade about hub
BMWRR	$M_{wR}$	ft-lb		144.7	Moment of rear rotor blade about hub
CFGN01	1/3			1/3	Moment of rear rotor blade about hub
CFGN02	2/3			2/3	
CFGN03	4/3			4/3	
CFGN05	1/6			1/6	
CSRR09	$C_{S9}$			-0.00001	Constant term used in empirical torque correction
CSRR12	$C_{S12}$			0.01753	Constant term used in empirical torque correction
CSRR13	$C_{S13}$			0.01753	Constant term used in empirical torque correction
CSRR14	$C_{S14}$			0.01753	Constant term used in empirical torque correction
CSRR15	$C_{S15}$			0.01753	Constant term used in empirical torque correction
CSRR16	$C_{S16}$			-0.0062	Constant term used in empirical torque correction
CSRR17	$C_{S17}$			-0.0062	Constant term used in empirical torque correction
CSRR18	$C_{S18}$			-0.0062	Constant term used in empirical torque correction
CSRR19	$C_{S19}$			-0.0062	Constant term used in empirical torque correction

TABLE 1B.- CONTINUED.

Simulation mnemonic	Engineering variable	Units	Common location (if applicable)	Nominal value	Physical description
CTPFRMX	$2C_T/a\sigma _{\max}$			1.0	Maximum value of normalized thrust coefficient
DELFR0	$\epsilon_{0F}$	---		.00925	Term used in calculation of forward rotor profile drag
DELFR1	$\delta_{1F}$	---		.23	Term used in calculation of forward rotor profile drag
DELH1		ft		9.83	Distance from helicopter c.g. to rotor hub
DELRR0	$\epsilon_{0R}$	---		.00925	Term used in calculation of rear rotor profile drag
DELRR1	$\delta_{1R}$	---		.23	Term used in calculation of rear rotor profile drag
FIFR	$I_F$	slug-ft <sup>2</sup>		2700	Forward rotor moment of inertia about vertical axis
FIRR	$I_R$	slug-ft <sup>2</sup>		2700	Rear rotor moment of inertia about vertical axis
PHIPFR	$\phi_{PF}$	rad		0	Forward rotor pitch-flap coupling control phasing angle
PHIPRR	$\phi_{PR}$	rad		0	Rear rotor pitch-flap coupling control phasing angle
RBFR	$R_{BF}$	ft		30	Forward rotor radius
RBRR	$R_{BR}$	ft		30	Rear rotor radius
SAFR	$a_F$	---		5.3	Lift-curve slope of forward rotor blade section
SARR	$a_R$	---		5.3	Lift-curve slope of rear rotor blade section
SBFR	$b_F$	---		3.0	Number of blades/forward rotor hub
SBRR	$b_R$	---		3.0	Number of blades/rear rotor hub
SCFR	$c_F$	ft		2.1042	Forward rotor hub mean aerodynamic chord

TABLE 1B.- CONCLUDED.

Simulation mnemonic	Engineering variable	Units	Common location (if applicable)	Nominal value	Physical description
SCRR	$c_R$	ft		2.1042	Rear rotor hub mean aerodynamic chord
SDFRX	$d_{Fx}$			0	Lateral position of baseline helicopter c.g. relative to forward rotor hub $Q_L$
SDRRX	$d_{Rx}$			0	Lateral position of baseline helicopter c.g. relative to rear rotor hub $Q_L$
SEFR	$e_F$			0.667	Forward rotor flapping hinge offset
SERR	$e_R$			0.667	Rear rotor flapping hinge offset
SHFRX	$h_{Fx}$			7.49	Vertical position of baseline helicopter c.g. relative to forward rotor hub $Q_L$
SHRRX	$h_{Rx}$			12.16	Vertical position of baseline helicopter c.g. relative to rear rotor hub $Q_L$
SLFRX	$\lambda_{Fx}$			20.43	Longitudinal position of baseline helicopter c.g. relative to forward rotor hub $Q_L$
SLRRX	$\lambda_{Rx}$			-18.46	Longitudinal position of baseline helicopter c.g. relative to rear rotor hub $Q_L$
THTWFR	$\theta_{twF}$	rad		-.2094	Forward rotor blade twist at tip
THTWRR	$\theta_{twR}$	rad		-.2094	Rear rotor blade twist at tip
TLF	$\tau_{\lambda F}$	sec		1/3	Forward rotor inflow dynamics time constant
TLR	$\tau_{\lambda R}$	sec		1/3	Rear rotor inflow dynamics time constant
UGE	$U_{g.e.}$	ft/sec		67.56	Airspeed below which thrust is modified for ground effect



TABLE 2.- ROTOR SUBROUTINE VARIABLE DEFINITION.

Input variables			Output variables		
Variable	Common location	Subroutine of origin	Variable	Common location	Subroutine of destination
AICFRC	CH(39)	CONTROL	ALARFR	CH(52)	AERO
AICRRC	CH(38)	↓	ALARRR	CH(53)	↓
BICFRC	CH(37)	↓	AMARFR	CH(54)	↓
BICRRC	CH(36)	↓	AMARRR	CH(55)	↓
HCG	A(176)	SMART	ANARFR	CH(56)	↓
OMEGPF	CH(115)	ENGINE	ANARRR	CH(57)	↓
OMEGPR	CH(116)	ENGINE	QAERFR	CH(64)	ENGINE
PB	A(37)	SMART	QAERRR	CH(65)	ENGINE
QB	A(38)	SMART	TMGN01	CH(100)	AERO
QGOVFR	CH(257)	ENGINE	TMGN05	CH(104)	↓
QGOVRR	CH(258)	ENGINE	TMGN06	CH(105)	↓
RB	A(39)	SMART	XAERFR	CH(72)	↓
SBETFS	CH(50)	AERO	XAERRR	CH(75)	↓
THOFRC	CH(42)	CONTROL	YAERFR	CH(73)	↓
THORRC	CH(43)	CONTROL	YAERRR	CH(76)	↓
UB	A(58)	SMART	ZAERFR	CH(74)	↓
VB	A(59)	SMART	ZAERRR	CH(77)	↓
WB	A(60)	SMART			

Logical flags			Required input data		
Flag	Common location	Function	Variable	Common location	Description
NGREFF	ICH(7)	Ground effect correction of thrust off/on (0/1)	DXCG	CH(68)	Position of actual helicopter c.g. relative to its reference (fig. 30)
NSTALL	ICH(5)	Rotor stall modification of thrust and torque off/on (0/1)	DYCG	CH(69)	
NTRQCR	ICH(6)	Empirical correction of rotor torque off/on (0/1)	DZCG	CH(70)	

TABLE 3A.- AERO SUBROUTINE VARIABLE DEFINITION

Simulation mnemonic	Engineering variable	Units	Common location (if applicable)	Physical description
ALARFS	$\mathcal{L}_{FUS}$	ft-lb	CH(238)	Fuselage rolling moment, helicopter body reference frame
ALPHFD	$\alpha_{FUS}$	deg		Fuselage angle of attack
ALPHFS	$\alpha_{FUS}$	rad	CH(214)	Fuselage angle of attack
ALQFS	$\mathcal{L}_{FUS}/q_{FUS}$	ft <sup>3</sup>		Fuselage rolling moment normalized to fuselage dynamic pressure
ALTQFS	$\mathcal{L}_{FUS}/q_{FUS}$	ft <sup>2</sup>		Fuselage lift force
AMARFS	$M_{FUS}$	ft-lb	CH(239)	Fuselage pitching moment, helicopter body reference frame
AMQFS	$M_{FUS}/q_{FUS}$	ft <sup>3</sup>		Fuselage pitching moment normalized to fuselage dynamic pressure
ANARFS	$N_{FUS}$	ft-lb	CH(240)	Fuselage yawing moment, helicopter body reference frame
ANQFS	$N_{FUS}/q_{FUS}$	ft <sup>3</sup>		Fuselage yawing moment, normalized to fuselage dynamic pressure
BETAFD	$\beta_{FUS}$	deg		Fuselage sideslip angle
BETAFS	$\beta_{FUS}$	rad	CH(59)	Fuselage sideslip angle
DQFS	$D_{FUS}/q_{FUS}$	ft <sup>2</sup>		Fuselage drag force, normalized to fuselage dynamic pressure
FAX	$X_{AERO}$	lb	A(136)	Sum of longitudinal fuselage and rotor aerodynamics forces, helicopter body reference frame
FAY	$Y_{AERO}$	lb	A(137)	Sum of lateral fuselage and rotor aerodynamic forces, helicopter body reference frame
FAZ	$Z_{ZERO}$	lb	A(138)	Sum of vertical fuselage and rotor aerodynamic forces, helicopter body reference frame

TABLE 3A.- CONTINUED.

Simulation mnemonic	Engineering variable	Units	Common location (if applicable)	Physical description
SBETFS	$\sin \beta_{FUS}$	-	CH(50)	Lateral position of wind-tunnel model c.g. relative to actual helicopter c.g.
SDCFS	$d_{c_{FUS}}$	ft		Lateral position of wind-tunnel model c.g. relative to baseline helicopter c.g.
SDCFSX	$d_{c_x}$			Vertical position of wind tunnel model c.g. relative to actual helicopter c.g.
SHCFS	$h_{c_{FUS}}$			Vertical position of wind tunnel model c.g. relative to baseline helicopter c.g.
SHCFSX	$h_{c_x}$			Longitudinal position of wind tunnel model c.g. relative to actual helicopter c.g.
SLCFS	$\ell_{c_{FUS}}$			Longitudinal position of wind tunnel model c.g. relative to baseline helicopter c.g.
SLCFSX	$\ell_{c_x}$			Fuselage dynamic pressure
SQFS	$q_{FUS}$	lb/ft <sup>2</sup>	CH(110)	Sum of fuselage and rotor aerodynamic rolling moments, helicopter body reference frame
TAL	$L_{AERO}$	ft-lb	A(155)	Sum of fuselage and rotor aerodynamic pitching moments, helicopter body reference frame
TAM	$M_{AERO}$	ft-lb	A(156)	Conversion factor between TAS (kt) and CAS (ft/sec)
TANALF	$\tan \alpha_{FUS}$	-		
TANBTF	$\tan \beta_{FUS}$	-		
TEMA	$1.689 \rho/\rho_0$		CH(92)	

TABLE 3A.- CONTINUED.

Simulation mnemonic	Engineering variable	Units	Common location (if applicable)	Physical description
TFN	$N_{AERO}$	ft-lb	A(157)	Sum of fuselage and rotor aerodynamic yawing moments, helicopter body reference frame
TMFS01	$\alpha$	ft <sup>2</sup>		Term used in flat-plate area correction of fuselage forces
TMCN03	$\rho/\rho_o$			Ambient to standard sea level density ratio
TMCN04	$\frac{2}{\pi}  \beta_{FUS} $	-	CH(103)	
VCALB1	$V_{cal}$	ft/sec		Calibrated airspeed
VTOTAL	$V_{T_{FUS}}$	ft/sec		Fuselage total velocity
WBPR	$w'_B$	ft/sec		Vertical velocity at fuselage
WBPRSQ	$w'^2_B$	(ft/sec) <sup>2</sup>		
WIFS		ft/sec	CH(215)	Rotor downwash contribution to vertical velocity at fuselage
ZAERFS	$X_{FUS}$	lb	CH(228)	Fuselage longitudinal force, helicopter body reference frame
XQFPC	$\alpha$	ft <sup>2</sup>		Term used in flat-plate area correction of fuselage forces
YAERFS	$Y_{FUS}$	lb	CH(229)	Fuselage lateral force, helicopter body reference frame

$$\alpha_{\Delta fe/\sqrt{1 + \tan^2 \alpha_{FUS}^2} + \tan \beta_{FUS}^2}$$

TABLE 3A.- CONCLUDED.

Simulation mnemonic	Engineering variable	Units	Common location (if applicable)	Physical description
YQFPC	$\alpha$	ft <sup>2</sup>		Term used in flat plate area correction of fuselage forces
YQFS	$Y_{FUS}/q_{FUS}$	ft <sup>2</sup>		Fuselage sideforce normalized to dynamic pressure
ZAERFS	$Z_{FUS}$	lb	CH(230)	Fuselage vertical force, helicopter body axes
ZOFPS	$\epsilon$	ft <sup>2</sup>		Term used in flat plate area correction of fuselage forces

$$\Delta f_e \tan \beta_{FUS} / \sqrt{1 + \tan^2 \alpha_{FUS}} + \tan \beta_{FUS}^2$$

TABLE 3B.- AERO CONSTANTS AND CONVERSION FACTORS

Simulation mnemonic	Engineering variable	Units	Common location (if applicable)	Nominal value $2/\pi$	Physical description
CFGN10	$2/\pi$			22	Flat-plate area correction value
DELFE	$\Delta f_e$	ft <sup>2</sup>		$\pi$	
PI	$\pi$		CH(21)	$\pi/2$	
PIOV2	$\pi/2$	deg/rad	CH(20)	57.3	
R2D			A(359)		
SDCFSX	$d_{c_x}$	ft		0	Lateral position of wind tunnel model c.g. relative to baseline helicopter c.g.
SHCFSX	$\ell_{c_x}$	ft		1.308	Vertical position of wind tunnel model c.g. relative to baseline helicopter c.g.
SLCFSX	$h_{c_x}$	ft		-1.467	Longitudinal position of wind tunnel model c.g. relative to baseline helicopter c.g.

TABLE 4.- AERO SUBROUTINE TRANSFER VARIABLES, INPUT DATA AND LOGICAL FLAGS

Input variables			Output variables		
Variable	Common location	Subroutine of origin	Variable	Common location	Subroutine of destination
ALARFR	CH(52)	ROTOR	BETAFS	CH(59)	SAS
ALARRR	CH(53)	↓	FAX	A(136)	SMART
AMARFR	CH(54)		FAY	A(137)	
AMARRR	CH(55)		FAZ	A(138)	
ANARFR	CH(56)		TAL	A(155)	
ANARRR	CH(57)	↓	TAM	A(156)	↓
TEMA	CH(92)	SMART	TAN	A(157)	
TMGNO1	CH(100)	ROTOR			
TMGNO5	CH(104)	ROTOR			
UB	A(58)	SMART			
VB	A(59)	SMART			
WB	A(60)	SMART			
XAERFR	CH(72)	ROTOR			
XAERRR	CH(75)	↓			
YAERFR	CH(73)				
YAERRR	CH(76)				
ZAERFR	CH(74)				
ZAERRR	CH(77)	↓			

Required Input Data		
Variable	Common location	Description
DXCG	CH(68)	Position of actual helicopter c.g. relative to its reference (fig. 30).
DYCG	CH(69)	
DZCG	CH(70)	

TABLE 5A.- ENGINE SUBROUTINE VARIABLES

Simulation mnemonic	Engineering variable	Units	Common location (if applicable)	Physical description
ACTPSL		deg		Left engine fuel-control actuator position
ACTPSR		deg		Right engine fuel-control actuator position
ANIVLTG		V		Voltage of signal from N <sub>1</sub> lever (simulator cab)
BEEP		deg		Initial condition on beep trimmer motor
DELANIV		V		Difference between past and present N <sub>1</sub> lever signal voltage
DLVERRL	N <sub>2</sub> err(L)	deg		Fuel control system error signal, left engine
DLVERRR	N <sub>2</sub> err(R)	deg		Fuel control system error signal, right engine
DOMEGF	$\Delta\Omega_F$	rad/sec		Forward rotor governor (delta $\Omega$ ) error signal
DOMEGR	$\Delta\Omega_R$	rad/sec		Rear rotor governor (delta $\Omega$ ) error signal
ENGLVCML		deg		Left engine N <sub>2</sub> lever angle command
ENGLVCMR		deg		Right engine N <sub>2</sub> lever angle command
ENGLVIL		%		Percent N <sub>1</sub> lever angle, left engine
ENGLVIR		%		Percent N <sub>2</sub> lever angle, right engine
ENGNLN01	N <sub>2</sub> $\delta_c$	deg		N <sub>2</sub> lever angle through collective angle
ENG03L		deg		N <sub>2</sub> lever angle through beep trimmer, left engine
ENG03R		deg		N <sub>2</sub> lever angle through beep trimmer, right engine



TABLE 5A.- CONTINUED.

Simulation mnemonic	Engineering variable	Units	Common location (if applicable)	Physical description
ENG13L	$\alpha_2$ (L)	deg		N <sub>2</sub> lever angle, left engine
ENG13R	$\alpha_2$ (R)	deg		N <sub>2</sub> lever angle, right engine
ENG14L	$N_{R\phi}$ (L)	rad/sec		Power curve intercept, $N_{R\phi}$ , left engine
ENG14R	$N_{R\phi}$ (R)	rad/sec		Power curve intercept, $N_{R\phi}$ , right engine
ENG20L		-		N <sub>1</sub> lever-topping power-correction term, left engine
ENG20R		-		
ENG21L	$P_c$ (L)	HP		Left engine commanded power
ENG21R	$P_c$ (R)	HP		Right engine commanded power
ENG22L		-		Modifying term for gas-generator time constant, left engine
ENG22R		-		Modifying term for gas-generator time constant, right engine
ENG24L		HP/sec		Gas generator dynamics parameter, left engine
ENG24R		HP/sec		Gas generator dynamics parameter, right engine
ENG26L	$\tau'_{pwr}$ (L)	sec		Unmodified gas-generator dynamics time constant, left engine
ENG26R	$\tau'_{pwr}$ (R)	sec		Unmodified gas-generator dynamics time constant, right engine

TABLE 5A.- CONTINUED.


Simulation mnemonic	Engineering variable	Units	Common location (if applicable)	Physical description
ENG27L	$\delta C_{TOT} - \delta C_{BIAS}$	HP/sec		Variable limit in gas-generator dynamics loop, left engine
ENG27R		HP/sec		Variable limit in gas-generator dynamics loop, right engine
EN2		deg/sec		Result of trimming loop to zero $\dot{\Omega}$
ELARG		deg		
IFIRSTL				Left-engine fuel-control-system hysteresis flag
IFIRSTR				Right-engine fuel-control-system hysteresis flag
OMEGA	$\Omega$	rad/sec		Rotor angular velocity
OMEGDOT	$\dot{\Omega}$	rad/sec <sup>2</sup>		Rotor angular acceleration
OMEGPF	$\Omega'_F$	rad/sec	CH(115)	Governor forward rotor angular velocity
OMEGPR	$\Omega'_R$	rad/sec	CH(116)	Governor rear rotor angular velocity
PCTTP		HP		Uncorrected topping power
PERL	$P_{er(L)}$			Left engine power error
PERR	$P_{er(R)}$			Right engine power error
POWERL	$P_{(L)}$			Left engine power available
POWERR	$P_{(R)}$			Right engine power available
POWOMEGA		%		Percent topping power

TABLE 5A.- CONCLUDED.

Simulation mnemonic	Engineering variable	Units	Common location (if applicable)	Physical description
QGOVF		ft-lb	CH(257)	Forward rotor shaft spring torque
QGOVR		ft-lb	CH(258)	Rear rotor shaft spring torque
QGOVFL		ft-lb		Forward rotor resistive torque
QGOVRL		ft-lb		Rear rotor resistive torque
QGOVI		ft-lb		
TAUPWRL	$\tau_{PWR}(L)$	sec		Gas generator dynamics time constant, left engine
TAUPWRR	$\tau_{PWR}(R)$			Gas generator dynamics time constant, right engine
TIME	$t$			Actual clock time
TIMESL				Time out of fuel control actuator deadband, left engine
TIMESR				Time out of fuel control actuator deadband, right engine
TORQUEL	$Q_L$	ft-lb		Left engine torque available
TORQUER	$Q_R$	ft-lb		Right engine torque available
TPL		HP		Left engine topping power
TPR		HP		Right engine topping power

TABLE 5B.- ENGINE CONSTANTS AND CONVERSION FACTORS

Simulation mnemonic	Engineering variable	Units	Nominal value	Physical description
APR	$P_{acc}$	ft-lb/sec	99,000	Accessory power required
DCBIAS	$\delta_{cBias}$	deg	2.0	Empirical bias value on collective input
ECS			4.71	Slope of $N_2$ curve $\delta_c$
EC2			10.	Beep trimmer motor constant
EC3			10.	Fuel control motor constant
EC4		HP/rad/sec	955.	Slope of power curve
EC5	M	HP	2850.	Standard day, sea-level topping power
ENG03LL		deg	0.	Beep trimmer position lower limit
ENG03UL		deg	44.	Beep trimmer position upper limit
E13LL		deg	15.	Fuel-control lever angle lower limit
E13UL		deg	75.	Fuel-control lever angle upper limit
GOVK1		ft-lb/sec/HP	550	Conversion factor between HP and ft-lb sec
GOVK2		ft-lb-sec/rad	36,000	Shaft damping constant
GOVK3		ft-lb/rad	580,000	Shaft spring constant
OMEGREF	$\Omega_{ref}$	rad/sec	24.086	Nominal rotor angular velocity
OMEGRF1	$1/\Omega_{ref}$	1/rad/sec	1/24.086	Reciprocal of $\Omega_{ref}$
RL		in/sec	0.8	Constant rate of $N_1$ lever actuator motion

TABLE 5B.- CONCLUDED.

Simulation mnemonic	Engineering variable	Units	Nominal value	Physical description
XIBLDINV	$1/I_{\text{Blade}}$	1/slug-ft <sup>2</sup>	$1.05 \times 10^{-4}$	Reciprocal of the moment of inertia of rotor blades about shaft axis
XITURBI	$1/I_{\text{Turb}}$	1/slug-ft <sup>2</sup>	$-4.98 \times 10^{-4}$	Negative reciprocal of the moment of inertia of the engine turbine

TABLE 6.- ENGINE SUBROUTINE TRANSFER VARIABLES.

Input variables			Output variables		
Variable	Common location	Subroutine of origin	Variable	Common location	Subroutine of destination
DCOLTOT	CH(210)	CONTROL	OMEGPF	CH(115)	ROTOR
IBEEP1		Simulator cab	OMEGPR	CH(116)	ROTOR
IBEEP12		Simulator cab	QGOVFR	CH(257)	ROTOR
QAERFR	CH(64)	ROTOR	QGOVRR	CH(258)	ROTOR
QAERRR	CH(65)	ROTOR			

Logical flags		
Flag	Common location	Function
ISTEADY	ICH(4)	Zeros $\dot{\Omega}$ after rigid body states have been trimmed off/on (0/1)

TABLE 7A.- CONTROL SUBROUTINE VARIABLE DEFINITION

Simulation mnemonic	Engineering variable	Units	Common location (if applicable)	Physical description
DAICFRC	$A'_{1CF}$	rad	CH(39)	Forward rotor lateral cyclic pitch, body reference frame
AICRRRC	$A'_{1CR}$		CH(38)	Rear rotor lateral cyclic pitch, body reference frame
BICFRC	$B'_{1CF}$		CH(37)	Forward rotor longitudinal cyclic pitch, body reference frame
BICRRRC	$B'_{1CR}$		CH(36)	Rear rotor longitudinal cyclic pitch, body reference frame
CFPP	$1 - e^{-T/\tau_{FPP}}$			Forward rotor pivoting-actuator-dynamics parameter
CFSP	$1 - e^{-T/\tau_{FSP}}$			Forward rotor swiveling-actuator-dynamics parameter
CLCF	$1 - e^{-T/\tau_{LCF}}$			Forward rotor longitudinal cyclic actuator dynamics parameter
CLCR	$1 - e^{-T/\tau_{LCR}}$			Rear rotor longitudinal cyclic actuator dynamics parameter
CRPP	$1 - e^{-T/\tau_{RPP}}$			Rear rotor pivoting actuator dynamics parameter
CRSP	$1 - e^{-T/\tau_{RSP}}$			Rear rotor swiveling actuator dynamics parameter
DAICFRC	$A'_{1CF}$	deg		Forward rotor lateral cyclic pitch, body reference frame
DAICRRRC	$A'_{1CR}$	deg		Rear rotor lateral cyclic pitch, body reference frame

TABLE 7A.- CONTINUED.

Simulation mnemonic	Engineering variable	Units	Common location (if applicable)	Physical description
DBICFRC	$\delta'_{1cF}$	deg		Forward rotor longitudinal cyclic pitch, body reference frame
DBICFRCN	$\delta'_{1cR}$			Forward rotor longitudinal cyclic actuator input
DBICRRRC	$\delta'_{1cR}$			Rear rotor longitudinal cyclic pitch, body reference frame
DBICRRCN	$\delta'_{1cR}$			Rear rotor longitudinal cyclic pitch, actuator input
DCOLTOT	$\delta_{cTOT}$	in.	CH(210)	Collective control input (= pilot + ECS)
DCPT	$\delta_{B_{DCP}}$	in.		Differential collective pitch trim contribution to longitudinal cyclic input
DLATTOT	$\delta_{A_{TOT}}$	in.	CH(207)	Lateral cyclic control input (= pilot + SAS/ECS)
DLONTOT	$\delta_{B_{TOT}}$	in.	CH(208)	Longitudinal cyclic control input (= pilot + SAS/ECS + DCPT)
DTHOFRC	$\theta'_{0F}$	deg		Forward rotor collective pitch, body reference frame
DTHORRC	$\theta'_{0R}$			Rear rotor collective pitch, body reference frame
DYAWTOT	$\delta_{R_{TOT}}$		CH(209)	Directional control input (= pilot + SAS/ECS)
EXPFPF	$-T/\tau_{FPF}$			Forward rotor upper boost pivoting actuator dynamics parameter



TABLE 7A.- CONTINUED.

Simulation mnemonic	Engineering variable	Units	Common location (if applicable)	Physical description
EXPFSF	$-T/\tau_{FSP}$ e	deg		Forward rotor upper boost swiveling actuator dynamics parameter
EXPRPP	$-T/\tau_{RPP}$ e			Rear rotor upper boost pivoting actuator dynamics parameter
EXPRSP	$-T/\tau_{RSP}$ e			Rear rotor upper boost swiveling actuator dynamics parameter
EXPTLCF	$-T/\tau_{LCF}$ e			Forward rotor longitudinal cyclic actuator dynamics parameter
EXPTLCR	$-T/\tau_{LCR}$ e			Rear rotor longitudinal cyclic actuator dynamics parameter
THOFRC	$\theta'_{0F}$	rad	CH(42)	Forward rotor collective pitch, body reference frame
THORRC	$\theta'_{0R}$	rad	CH(43)	Rear rotor collective pitch, body reference frame
THTAF	$\theta_{AF}$	deg		Forward rotor lateral control input converted to equivalent swashplate deflection
THTAR	$\theta_{AR}$			Rear rotor lateral control input converted to equivalent swashplate deflection
THTBF	$\theta_{BF}$			Forward rotor longitudinal control input converted to equivalent swashplate deflection
THTBR	$\theta_{BR}$			Rear rotor longitudinal control input converted to equivalent swashplate deflection

TABLE 7A.- CONTINUED.

Simulation mnemonic	Engineering variable	Units	Common location (if applicable)	Physical description
THTCF	$\theta_{CF}$	deg		Forward rotor collective control input converted to equivalent swashplate deflection
THTCR	$\theta_{CR}$			Rear rotor collective control input converted to equivalent swashplate deflection
THTRF	$\theta_{RF}$			Forward rotor directional control input converted to equivalent swashplate deflection
THTRR	$\theta_{RR}$			Rear rotor directional control input converted to equivalent swashplate deflection
THTFPP	$\theta_{FPP}$			Unlimited input to forward rotor upper-boost pivoting actuator
THTFPPD	$\theta_{FP}$			Forward rotor pivoting actuator output
THTFSP	$\theta_{FSP}$			Unlimited input to forward rotor upper boost swiveling actuator
THTFSPD	$\theta_{FS}$			Forward rotor swiveling actuator output
THTLCF	$\theta_{LCF}$			First stage mixing box output (vertical/longitudinal), forward rotor
THTLCR	$\theta_{LCR}$			First stage mixing box output (vertical/longitudinal), rear rotor
THTRF	$\theta_{RF}$			Directional input converted to equivalent swashplate deflection, forward rotor
THTRPP	$\theta_{RPP}$			Unlimited input to rear rotor pivoting actuator
THTRPPD	$\theta_{RP}$			Rear rotor pivoting actuator output

TABLE 7A.- CONCLUDED.

Simulation mnemonics	Engineering variable	Units	Common location (if applicable)	Physical description
THTPR	$\theta_{RR}$	deg ↓		Directional input converted to equivalent swashplate deflection, rear rotor
THTRSP	$\theta_{RSP}$			Unlimited input to rear rotor upper boost swiveling actuator
THTECPD	$\theta_{RS}$			Rear rotor swiveling actuator output
THTRYF				Forward rotor cumulative lateral-stop limiter output
THTRYF1				First-stage mixing box (lateral/directional) output, forward rotor
THTRYR				Rear rotor cumulative lateral-stop limiter output
THTRYR1				First-stage mixing box (lateral/directional) output, rear rotor

TABLE 7B.- CONTROL CONSTANTS AND CONVERSION FACTORS

Simulation mnemonic	Engineering variable	Units	Common location (if applicable)	Nominal value	Physical description
ALCAF		deg/in.		1.91	Conversion factor between lateral cyclic position and equivalent swashplate deflection, forward rotor
ALCAR		deg/in.		1.91	Conversion factor between lateral cyclic position and equivalent swashplate deflection, rear rotor
ALCRF		deg/in.		3.18	Conversion factor between pedal position and equivalent swashplate deflection, forward rotor
ALCRR		deg/in.		3.18	Conversion factor between pedal position and equivalent swashplate deflection, rear rotor
BICSLP		deg/knot		.075	Slope of longitudinal cyclic schedule curve (forward and rear rotors)
BP1		knot		60	Breakpoint of longitudinal cyclic schedule curve (forward and rear rotors)
BP2		knot		120	Breakpoint of longitudinal cyclic schedule curve (forward and rear rotors)
C1					
C2					
DATOTIC	$\delta_{A_{TOT}}$   I.C.	in.			Lateral axis initialization value when ECS is on
DBTOTIC	$\delta_{B_{TOT}}$   I.C.				Longitudinal axis initialization value when ECS is on
DCOLLL				0	Collective position lower limit
DCOLLUL				9.12	Collective position upper limit

TABLE 7B.- CONTINUED.

Simulation mnemonic	Engineering variable	Units	Common location (if applicable)	Nominal value	Physical description
DCTOTIC	$\delta_{CTOT}$ I.C.	in.			Collective initialization value when ECS is on
DLATLL		↓		-4.18	Lateral cyclic position lower limit
DLATUL				+4.18	Lateral cyclic position upper limit
DLONLL				-6.5	Longitudinal cyclic position lower limit
DLONUL				+6.5	Longitudinal cyclic position upper limit
DRTOTIC	$\delta_{RTOT}$ I.C.				Directional axis initialization value when ECS is on
DYAWLL		rad/deg		-3.6	Pedal position lower limit
DYAWUL				+3.6	Pedal position upper limit
D2R				1/57.3	Conversion factor between degrees and radius
HALF				.5	
ONEPT2				1.2	
TFPP	$\tau_{FPP}$			TBD	Forward rotor pivoting actuator time constant
TFSP	$\tau_{FSP}$			TBD	Forward rotor swiveling actuator time constant
THTFPPLL		deg		-11.65	Forward rotor pivoting actuator lower limit
THTFPPUL		deg		46.35	Forward rotor pivoting actuator upper limit
THTFSPLL		deg		-11.65	Forward rotor swiveling actuator lower limit
THTFSPUL		deg		46.35	Forward rotor swiveling actuator upper limit

TABLE 7B.- CONTINUED.

Simulation mnemonic	Engineering variable	Units	Common location (if applicable)	Nominal value	Physical definition
THTOBF		deg/in.		.615	Conversion factor between longitudinal cyclic position and equivalent swashplate displacement, forward rotor
THTOBR		deg/in.		.615	Conversion factor between longitudinal cyclic position and equivalent swashplate displacement, rear rotor
THTOCF		deg/in.		1.86	Conversion factor between collective position and equivalent swashplate displacement, forward rotor.
THOCCR		deg/in.		1.86	Conversion factor between collective position and equivalent swashplate displacement, rear rotor
THTRPPLL		deg		-11.65	Rear rotor pivoting actuator lower limit
THTRRPUL				46.35	Rear rotor pivoting actuator upper limit
THTRSPLL				-11.65	Rear rotor swiveling actuator lower limit
THTRSPUL				46.35	Rear rotor swiveling actuator upper limit
THTRYFLL				-16.5	Forward rotor cumulative lateral stop lower limit
THTRYFUL				+16.5	Forward rotor cumulative lateral stop upper limit
THTRYRLL				-16.5	Rear rotor cumulative lateral stop lower limit
THTRYRUL				+16.5	Rear rotor cumulative lateral stop upper limit
THTTF	$\theta_{TF}$			7.85	Forward rotor root collective pitch with cockpit collective lever full down

TABLE 7B.- CONCLUDED.


Simulation mnemonic	Engineering variable	Units	Common location (if applicable)	Nominal value	Physical description
THTR	$\theta_{TR}$	deg		7.85	Rear rotor root collective pitch with cockpit collective level full down
TLCF	$\tau_{LCF}$	sec 		TBD	Forward rotor longitudinal cyclic actuator time constant
TLCR	$\tau_{LCR}$			TBD	Rear rotor longitudinal cyclic actuator time constant
TRPP	$\tau_{RPP}$			TBD	Rear rotor pivoting actuator time constant
TRSP	$\tau_{RSP}$			TBD	Rear rotor swiveling actuator time constant

TABLE 8.- CONTROL SUBROUTINE TRANSFER VARIABLES

Input variables			Output variables		
Variable	Common location	Subroutine of origin	Variable	Common location	Subroutine of destination
DCOLECS	CH(275)	ECS	AICFRC	CH(39)	ROTOR
DCOLP	CH(206)	Simulator cab	AICRRC	CH(38)	ROTOR
DLATECS	CH(272)	ECS	BICFRC	CH(37)	ROTOR
DLATP	CH(203)	Simulator cab	BICRRC	CH(36)	ROTOR
DLATSAS	CH(17)	SAS	THOFRC	CH(42)	ROTOR
DLONECS	CH(273)	ECS	THORRC	CH(43)	ROTOR
DLONP	CH(204)	Simulator cab			
DLONSAS	CH(18)	SAS			
DYAWACS	CH(274)	ECS			
DYAWP	CH(205)	Simulator cab			
DYAWSAS	CH(19)	SAS			
LAND	IA(29)	Simulator cab			
IANU	IA(30)	Simulator cab			
ILWD	IA(33)	Simulator cab			
IRWD	IA(34)	Simulator cab			
VEQ	A(75)	SMART			

Logical flags		
Flag	Common location	Function
IDCPT	ICH(3)	Differential collective pitch trim off/on (0/1)
IECSCON	ICH(2)	Electronic control system off/on (0/1)
IMHIS	---	Simulator cab off/on (0/1)
RSASP	CH(282)	Lateral SAS off/on (0/1)
RSASQ	CH(283)	Longitudinal SAS off/on (0/1)
RSASR	CH(284)	Directional SAS off/on (0/1)



TABLE 9A.- SAS SUBROUTINE VARIABLE DEFINITION

Simulation mnemonic	Engineering variable	Units	Common location (if applicable)	Physical description
AA				(4 by 1) matrix used in FACT/UPDATE calculation of SAS filtering algorithms
AY1				(2 by 1) matrix used in FACT/UPDATE calculation of SAS filtering algorithms
AY2				(2 by 1) matrix used in FACT/UPDATE calculation of SAS filtering algorithms
BB				(4 by 1) matrix used in FACT/UPDATE calculation of SAS filtering algorithms
BETAFSL	$\beta_{FUS}  _{lim}$	rad		Fuselage sideslip angle limited to $\pm\pi/2$ rad.
BY1				(2 by 1) matrix used in FACT/UPDATE calculation of SAS filtering algorithms
BY2				(2 by 1) matrix used in FACT/UPDATE calculation of SAS filtering algorithms
CC				(4 by 1) matrix used in FACT/UPDATE calculation of SAS filtering algorithms
CR1	$1 - e^{-T/\tau_{R1}}$	-		Directional SAS filtering parameter (rate damping)
CR5	$1 - e^{-T/\tau_{R5}}$	-		Static port dynamics parameter
CR6	$1 - e^{-T/\tau_{R6}}$			Directional SAS filtering parameter (turn coordination)
CY1				(2 by 1) matrix used in FACT/UPDATE calculation of SAS filtering algorithms

TABLE 9A.- CONTINUED.

Simulation mnemonic	Engineering variable	Units	Common location (if applicable)	Physical description
CY2				(2 by 1) matrix used in FACT/UPDA E calculation of SAS filtering algorithms
C5	$1 - e^{-T/\tau_5}$			Lateral SAS parameter
DBYAW	$\delta R_B$	in.		Sideslip SAS contribution to directional SAS actuator displacement
DD				(4 by 1) matrix used in FACT/UPDATE calculation of SAS filtering algorithms
DLATSAS	$\delta ASAS$		CH(17)	Lateral SAS actuator displacement
DLONSAS	$\delta BSAS$		CH(18)	Longitudinal SAS actuator displacement
DPYAW	$\delta R_p$			Turn coordination contribution to directional SAS actuator displacement
DRBYAW	$\delta R_B$   equiv. pedal			Sideslip SAS static port dynamics input
DRBYAW1	$\delta R_B$   unlimited			Sideslip SAS static port dynamics output
DRYAW	$\delta R_r$			Rate damping contribution to directional SAS actuator displacement
DRYAW1	$\delta R_r$   $V > 40$ knots			Rate damping contribution to directional SAS actuator displacement when $V_{eq} > 40$ knots
DRYAW2	$\delta R_r$   $V < 40$ knots			Rate damping contribution to directional SAS actuator displacement when $V_{eq} < 40$ knots

TABLE 9A.- CONTINUED

Simulation mnemonic	Engineering variable	Units	Common location (if applicable	Physical description
DYAWSAS	$\delta_{RSAS}$	in.	CH(19)	Directional SAS actuator displacement
DY1				(2 by 1) matrix used in FACT/UPDATE calculation of SAS filtering algorithms
DY2				(2 by 1) matrix used in FACT/UPDATE calculation of SAS filtering algorithms
EXPTRL	$-T/\tau_{R_1}$	-		Directional SAS filtering parameter (rate damping)
EXPTR5	$-T/\tau_{R_5}$	-		Directional SAS filtering parameter ( $N_g$ stabilization)
EXPTR6	$-T/\tau_{R_6}$	-		Directional SAS filtering parameter (turn coordination)
EXPT5	$-T/\tau_{R_5}$	-		Lateral SAS filtering parameter
GKDPDR	$K_{\Delta p \delta_R}$	$\frac{\text{in. pedal}}{\text{in. H}_2\text{O}}$		Velocity dependent sideslip SAS gain
PBG		in.		Helicopter roll rate converted to inches of equivalent lateral cyclic displacement
PB1				Helicopter roll rate converted to inches of equivalent pedal displacement
QBG				Helicopter pitch rate converted to inches of equivalent longitudinal cyclic displacement
RBG				Helicopter yaw rate converted to inches of equivalent pedal displacement

TABLE 9A.- CONCLUDED.

Simulation mnemonic	Engineering variable	Units	Common location (if applicable	Physical description
RBG1		in.		Directional SAS parameter
XY1				(2 by 1) matrix used in FACT/UPDATE calculation of SAS filtering algorithms
XY2				(2 by 1) matrix used in FACT/UPDATE calculation of SAS filtering algorithms

TABLE 9B.- SAS CONSTANTS AND CONVERSION FACTORS

Simulation mnemonic	Engineering variables	Units	Common location (if applicable)	Nominal value	Physical description
ALONLIM	$\left\{ 1.1 \left( \frac{9}{4} \right) \sin(2 \times 52^\circ) \right\}$	in.		$\pm 1.7$	Longitudinal SAS actuator limits
ALATLIM		in.		$\pm 1.0$	Lateral SAS actuator limits
ADISLIM		in.		$\pm 1.68$	Directional SAS actuator limits
CK				2.4015	Sideslip SAS constant
DPINH20		in. $H_2O$ lb/ft <sup>2</sup>		.1529	Conversion factor between dynamic pressure in lb/ft <sup>2</sup> and inches of water
GKFDR	$K_{p\delta_R}$	$\frac{\text{in.}}{\text{rad/sec}}$		5.77	Directional SAS conversion factor between roll rate and inches of equivalent pedal displacement
GKPDS	$K_{p\delta_A}$	$\frac{\text{in.}}{\text{rad/sec}}$		4.0	Lateral SAS conversion factor between roll rate and inches of equivalent lateral cyclic displacement
GKQDB	$K_{q\delta_R}$	$\frac{\text{in.}}{\text{rad/sec}}$		16.0	Longitudinal SAS conversion factor between pitch rate and inches of equivalent longitudinal cyclic displacement
GKRDR	$K_{r\delta_R}$	$\frac{\text{in.}}{\text{rad/sec}}$		9.4	Directional SAS conversion factor between yaw rate and inches of equivalent pedal displacement
HALF			CH(109)	.5	
PIOV2			CH(20)	$\pi/2$	
TRL	$\tau_{R1}$	sec.		.1	Directional SAS time constant (rate damping)

TABLE 9B.- CONCLUDED.

Simulation mnemonic	Engineering variables	Units	Common location (if applicable)	Nominal value	Physical description
TR2	$\tau_{R2}$	sec		3.2	Directional SAS time constant (rate damping)
TR3	$\tau_{R3}$			1.6	Directional SAS time constant (rate damping)
TR4	$\tau_{R4}$			3.2	Directional SAS time constant (rate damping)
TR5	$\tau_{R5}$			.25	Directional SAS static port dynamics time constant ( $N_\beta$ stabilization)
TR6	$\tau_{R6}$			3.2	Directional SAS time constant (turn coordination)
T1	$\tau_1$			.37	Longitudinal SAS time constant
T2	$\tau_2$			2.0	Longitudinal SAS time constant
T3	$\tau_3$			3.5	Longitudinal SAS time constant
T4	$\tau_4$			20.0	Longitudinal SAS time constant
T5	$\tau_5$			.05	Lateral SAS time constant

TABLE 10.- SAS SUBROUTINE TRANSFER VARIABLES

Input variables			Output variables		
Variable	Common location	Subroutine of origin	Variable	Common location	Subroutine of destination
BETAFS	CH(59)	AERO	DLATSAS	CH(17)	CONTROL
SQFS	CH(110)	AERO	DLONSAS	CH(18)	CONTROL
PB	A(37)	SMART	DYAWSAS	CH(19)	CONTROL
QB	A(38)	↓			
RB	A(39)				
VEQ	A(75)				
QBAR	A(178)				

TABLE 11.- ECS SUBROUTINE TRANSFER VARIABLES.

Input variables			Output variables		
Variable	Common location	Subroutine of origin	Variable	Common location	Subroutine of destination
DCOLP	CH(206)	Simulator cab	DCOLECS	CH(275)	CONTROL
DLATP	CH(203)	Simulator cab	DLATECS	CH(272)	CONTROL
DLONP	CH(204)	Simulator cab	DLONECS	CH(273)	CONTROL
DYAWP	CH(205)	Simulator cab	DYAW ECS	CH(274)	CONTROL

TABLE 12A.- SLING SUBROUTINE VARIABLE DEFINITION

Simulation mnemonic	Engineering variable	Units	Common location (if applicable)	Physical description
ALFSL	$\alpha_{SL}$	rad	CH(203)	Slung load angle of attack
ALFSLD	$\alpha_{SL}$	deg		
ALML	$\lambda_L$	rad	CH(259)	Slung load lateral cable sway angle
ALMLD	$\dot{\lambda}_L$	rad/sec		
ALMLDD	$\ddot{\lambda}_L$	rad/sec <sup>2</sup>		
ALMLIC	$\lambda_{LIC}$	rad		Initial value of load lateral cable sway angle
AMUL	$\mu_L$	rad	CH(260)	Slung load longitudinal cable sway angle
AMULD	$\dot{\mu}_L$	rad/sec		
AMULDD	$\ddot{\mu}_L$	rad/sec <sup>2</sup>		
AMULIC	$\mu_{LIC}$	rad		Initial value of load longitudinal cable sway angle
ANARSL	$N_{AER_L}$	ft-lb <sub>f</sub>	CH(256)	Yawing moment about slung load center of gravity, helicopter body reference frame
ANQSL	$\left(\frac{N}{q}\right)_{SL}$	ft <sup>3</sup>		Normalized slung load yawing moment
ANUL	$\nu_L$	rad	CH(261)	Slung load lateral differential cable angle
ANULD	$\dot{\nu}_L$	rad/sec		



TABLE 12A.- CONTINUED.

Simulation mnemonic	Engineering variable	Units	Common location (if applicable)	Physical description
ANULDD	$\ddot{\psi}_L$	rad/sec <sup>2</sup>		
ASL	$m_L/M_H$	-		Slung load to helicopter mass ratio
BBSL	$\frac{J_L}{(L_L M_H)}$	ft		
BBSLMH	$\frac{J_L}{L_L}$	slug-ft		
BCSLMT	$\frac{m_L (L_L + R_L)}{(m_L + M_H)}$	ft		
BDSL	$\frac{m_L I_L}{(m_L + M_H)}$	ft		
BFSL	$\frac{R_L J_L}{L_L I_{xx}}$	-		
BETSL	$\beta_{SL}$	rad	CH(262)	Slung load sideslip angle
BETSLD	$\beta_{SL}$	deg		
BFSL	$\frac{m_L g R_L}{I_{xx}}$	ft <sup>3</sup> /sec <sup>2</sup>		
BMSL	$\frac{m_L g a_L^2}{4 J_L L_L}$	ft <sup>2</sup> /sec <sup>2</sup>		

TABLE 12A.- CONTINUED.

Simulation mnemonic	Engineering variable	Units	Common location (if applicable)	Physical description
BNSL	$\frac{J_L}{m_L L^2}$	-		
BPSL	$\frac{L_L + R_L}{L_L}$	-		
BQSL	$\frac{J_L}{m_L L^2} - \frac{L_L + R_L}{L_L}$	-		
BSSL	$\frac{g}{L_L}$	1/sec <sup>2</sup>		
BXSL	$m_L L_L$	slug-ft		
BXSL	$i/m_L L_L$	1/slug-ft		
CFEM19	$\frac{R_L J_L}{L_L}$	slug-ft <sup>2</sup>		
COSLML	$\cos \lambda_L$	-		
COSMUL	$\cos \mu_L$	-		
COSNUL	$\cos \nu_L$	-		
DQSL	$\left(\frac{D}{q}\right)_{SL}$	ft <sup>2</sup>		Normalized slung load drag force, load body reference frame

TABLE 12A.- CONTINUED.

Simulation mnemonic	Engineering variable	Units	Common location (if applicable)	Physical description
PBDS	$\dot{p}_{B_S}$	rad/sec <sup>2</sup>		Contribution to helicopter roll acceleration from slung load
QBDS	$\dot{q}_{B_S}$	rad/sec <sup>2</sup>		Contribution to helicopter pitch acceleration from slung load
RBDS	$\dot{r}_{B_S}$	rad/sec <sup>2</sup>		Contribution to helicopter yaw acceleration from slung load
SINLML	$\sin \lambda_L$	-		
SINMUL	$\sin \mu_L$	-		
SINNUl	$\sin \nu_L$	-		
SLKBAR	$\bar{K}_L$	-	CH(264)	$\left[ \frac{(m_L g)^2 + (X_{AER_L})^2}{m_L g} \right]^{1/2}$
SMSL	$m_L$	slugs	CH(247)	Slung load mass
SQSL	$q_{c_L}$	lb <sub>f</sub> /ft <sup>2</sup>		Slung load dynamic pressure
TEMP1	$\frac{m_L g a_L^2 \cos \phi \cos \theta \nu_L}{4L_L}$	ft-lb <sub>f</sub>		
TEMP2	$I_{xx} I_{zz}$	(slug-ft <sup>2</sup> ) <sup>2</sup>	CH(248)	
UBDS	$\dot{u}_{B_S}$	ft/sec <sup>2</sup>	CH(248)	Contribution to helicopter longitudinal acceleration from slung load, helicopter body reference frame

TABLE 12A.- CONCLUDED.

Simulation mnemonic	Engineering variable	Units	Common location (if applicable)	Physical description
USL	$u_{SL}$	ft/sec		Longitudinal velocity at the slung load c.g., helicopter body reference frame
VBDS	$\dot{v}_{BS}$	ft/sec <sup>2</sup>	CH(249)	Contribution to helicopter lateral acceleration from slung load, helicopter body reference frame
VSL	$v_{SL}$	ft/sec		Lateral velocity at the slung load center of gravity, helicopter body reference frame
WBDS	$\dot{w}_{BS}$	ft/sec <sup>2</sup>	CH(250)	Contribution to helicopter vertical acceleration from slung load, helicopter body reference frame
WLRL	$m_L g R_L$	ft-lb <sub>f</sub>		
WSL	$w_{SL}$	ft/sec		Vertical velocity at the slung load center of gravity, helicopter body reference frame
XAERSL	$x_{AER_L}$	lb <sub>f</sub>	CH(254)	Slung load drag force, helicopter body reference frame
YAERSL	$y_{AER_L}$	lb <sub>f</sub>	CH(255)	Slung load side force, helicopter body reference frame
YQSL	$\left(\frac{Y}{q}\right)_{SL}$	ft <sup>2</sup>		Normalized slung load side force, load body reference frame

TABLE 12B.- SLING CONSTANTS AND CONVERSION FACTORS

Simulation mnemonic	Engineering variable	Units	Common location (if applicable)	Nominal value	Physical description
ALMLDIC	$\dot{\lambda}_{L_{IC}}$	rad/sec		0	Initial value of lateral cable angle rate
AMULDIC	$\dot{\mu}_{IC}$	rad/sec			Initial value of longitudinal cable angle rate
ANULDIC	$\dot{\nu}_{IC}$	rad/sec			Initial value of lateral differential cable angle rate
ANULIC	$\nu_{IC}$	rad			Initial value of lateral differential cable angle
BJSL	$J_L$	slug-ft <sup>2</sup>	CH(266)	7771.12	Moment of inertia of slung load about load vertical axis
BLSL	$L_L$	ft	CH(267)	20.	Average cable length below attachment point
BRSL	$P_L$	ft	CH(268)	8.	Vertical distance between hook attachment and aircraft c.g.
G	$g$	ft/sec <sup>2</sup>		32.17	Sea level acceleration of gravity
HALF		-	CH(109)	.5	
KLANDOT	$K_{\lambda}$			.1	Lateral cable angle damping constant
KNUDOT	$K_{\mu}$			0	Longitudinal cable angle damping constant
KNUDOT	$K_{\nu}$			.18	Lateral differential cable angle damping constant
R2D		deg/rad		57.3	
SASL	$a_L$	ft	CH(297)	20.	Cable separation distance
SMSLIC	$m_L$	slugs		233.14	Slung load mass

TABLE 12B.- CONCLUDED.

Simulation mnemonic	Engineering variable	Units	Common location (if applicable)	Nominal value	Physical description
THESL	$\theta_{SL}$	rad	CH(269)		Angle between load x-axis and helicopter x-axis
WGHTSL	$W_L$	lb <sub>f</sub>		7500.	Slung load weight

TABLE 13.- SLING SUBROUTINE TRANSFER VARIABLES, INPUT DATA AND LOGICAL FLAGS.

Input variables			Output variables		
Variable	Common location	Subroutine of origin	Variable	Common location	Subroutine of destination
CPHI	A(11)	SMART	PBDS	CH(251)	SMART
CTHT	A(13)		QBDS	CH(252)	
PB	A(37)		RBDS	CH(253)	
PBD	A(55)		UBDS	CH(248)	
PHIR	A(4)		VBDS	CH(249)	
QB	A(38)		WBDS	CH(250)	
QBD	A(56)				
RB	A(39)				
RBD	A(57)				
RHO2	CH(101)				
SPHI	A(10)				
STHT	A(12)				
UB	A(58)				
UBD	A(413)				
VB	A(59)				
VBD	A(414)				
WB	A(60)				
XIXX	A(116)				
XIXZ	A(119)				
XIYY	A(117)				
XIZZ	A(118)				
XMASS	A(130)				

Required Input Data		
Variable	Common location	Description
BJSL	CH(266)	Moment of inertia of slung load about load vertical axis
BLSL	CH(267)	Average cable length below attachment point
BRSL	CH(268)	Vertical distance between hook attachment point and aircraft c.g.
SASL	CH(297)	Cable separation distance
SMSLIC	CH(269)	Slung load mass
THESL		Angle between load x-axis and helicopter x-axis
WGHTSL		Slung load weight

Logical Flags		
Flag	Common location	Function
ISLING	ICH(1)	Slung load subroutine option off/on (0/1)
ISLTRM	ICH(8)	Slung load trim in straight level flight off/on (0/1)

TABLE 14.- REQUIRED INPUT DATA FOR OPERATIONAL SIMULATIONS

Variable	Common location	Units	Physical description
DXCG	CH(68)	in.	Position of actual helicopter c.g. relative to its reference (fig. 30)
DYCG	CH(69)	in.	
DZCG	CH(70)	in.	
WAITIC	A(242)	lb <sub>f</sub>	Helicopter weight
XIXXIC	A(243)	slug-ft <sup>2</sup>	Helicopter moments and product of inertia
XIYYIC	A(244)	slug-ft <sup>2</sup>	
XIZZIC	A(245)	slug-ft <sup>2</sup>	
XIXZIC	A(246)	slug-ft <sup>2</sup>	
XP	A(171)	ft	Position of pilot, in helicopter body axes, relative to c.g. of aircraft
YP	A(172)	ft	
ZP	A(173)	ft	



ORIGINAL PAGE IS  
OF POOR QUALITY

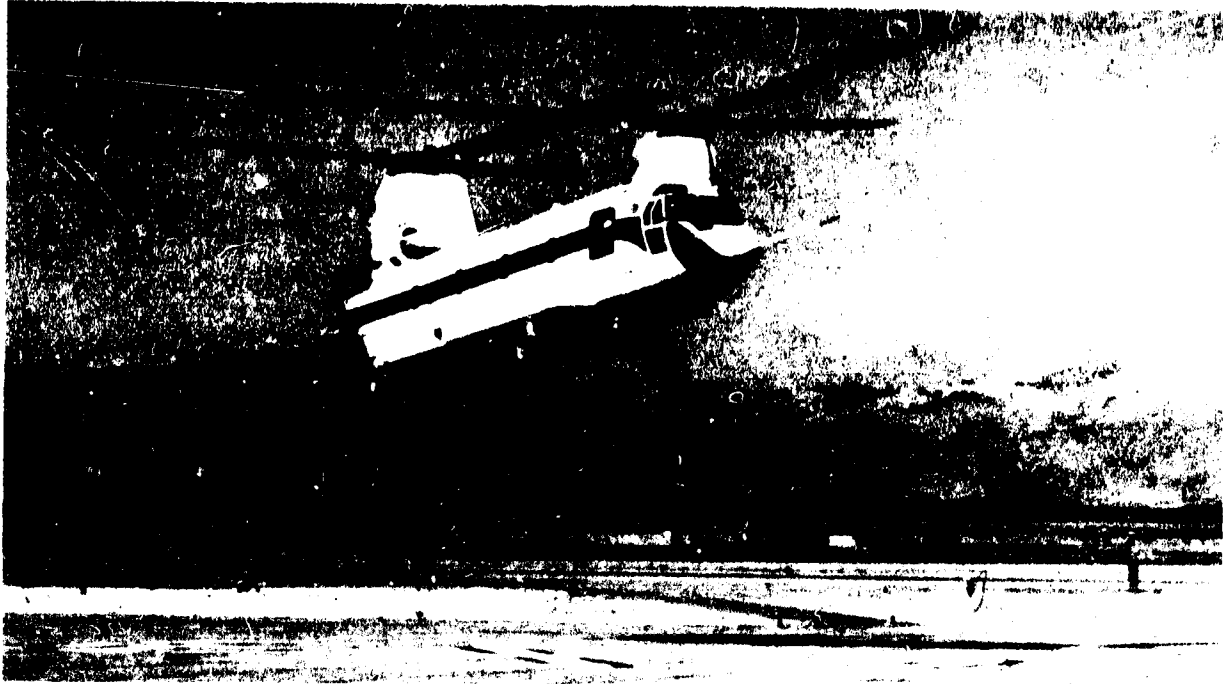


Figure 1.- CH-47B helicopter.

REMAINING PAGE BLANK NOT FILMED

ORIGINAL PAGE IS  
OF POOR QUALITY

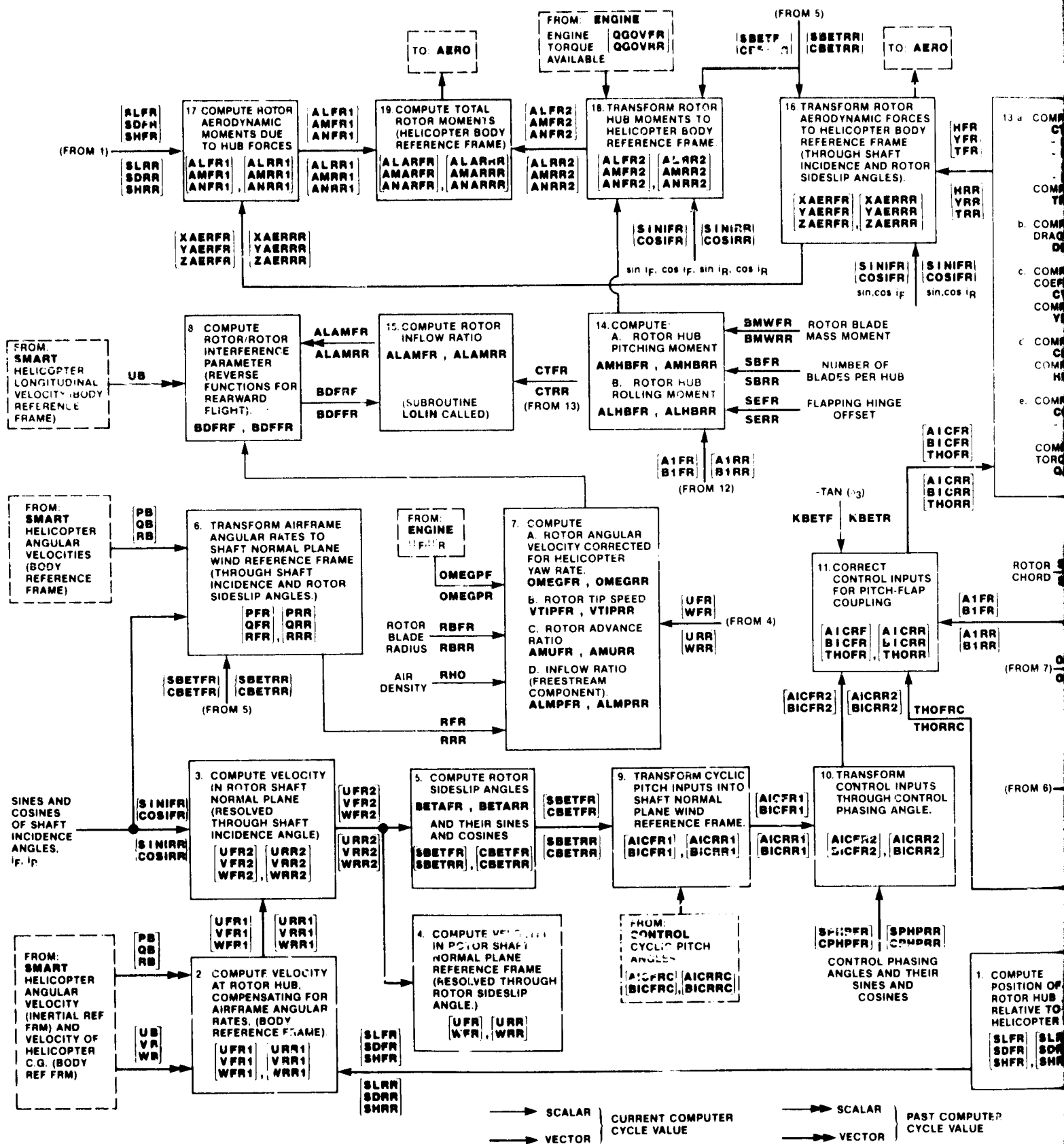


Figure 2.- Rotor signal flow diagram.



OF 1

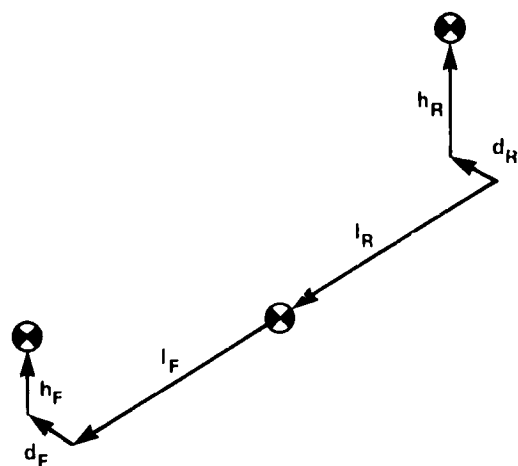


Figure 3.- Helicopter rotor center of gravity positions relative to rotorcraft center of gravity (ref. 1).

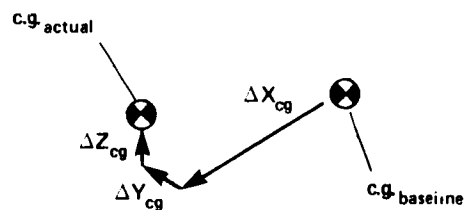


Figure 4.- Actual versus baseline helicopter center of gravity position.

PRECEDING PAGE BLANK NOT FILMED

ORIGINAL OF FIGURE 5  
OF POOR QUALITY

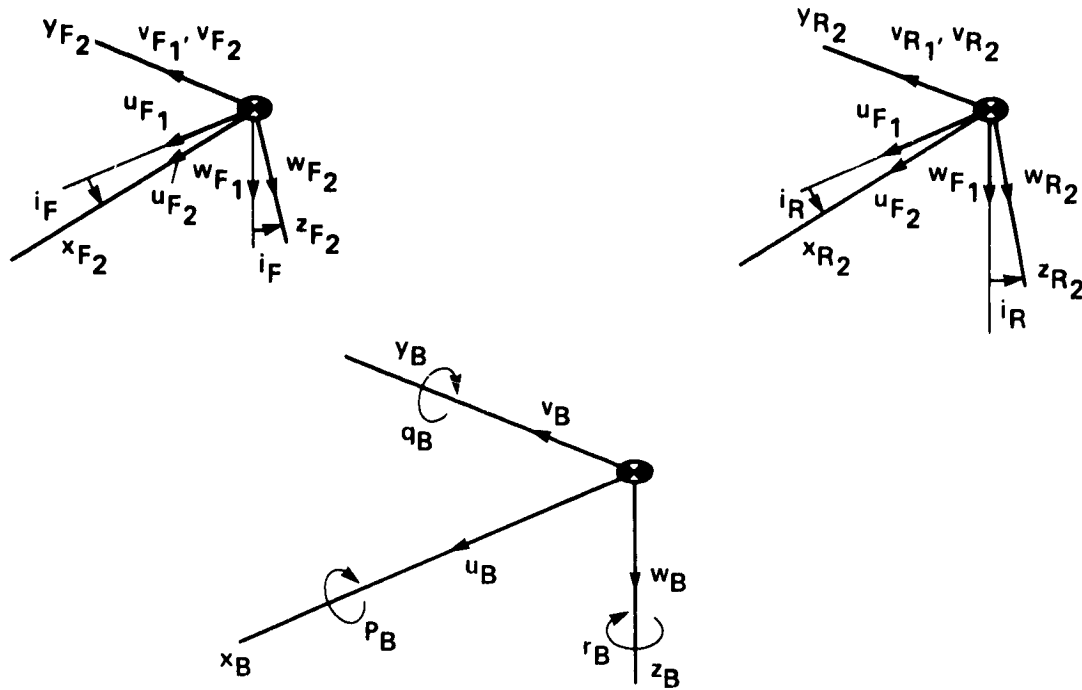


Figure 5.- Reference frame transformation through shaft incidence angles.

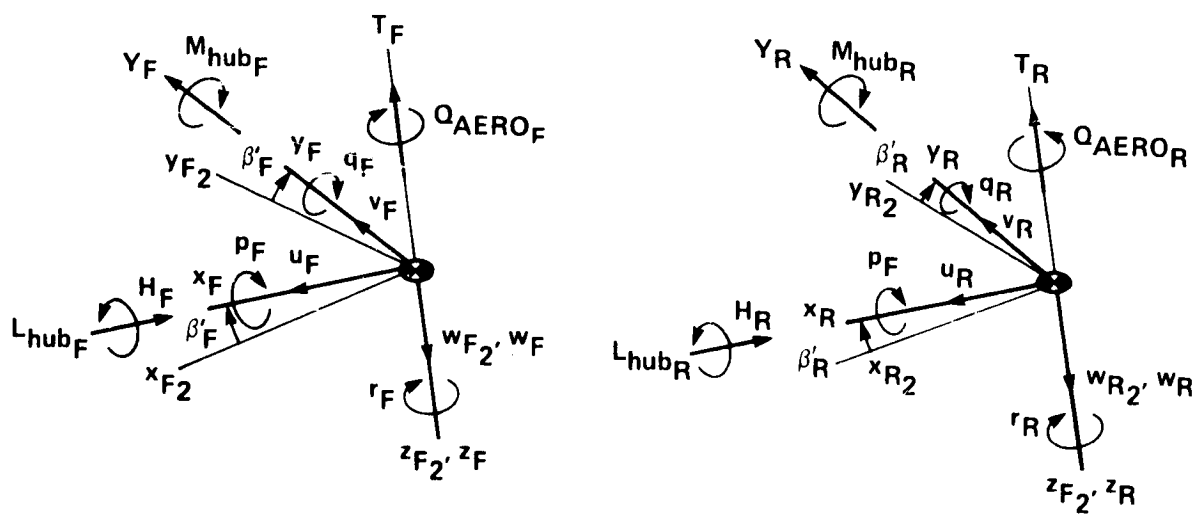


Figure 6.- Reference frame transformation through rotor sideslip angles.

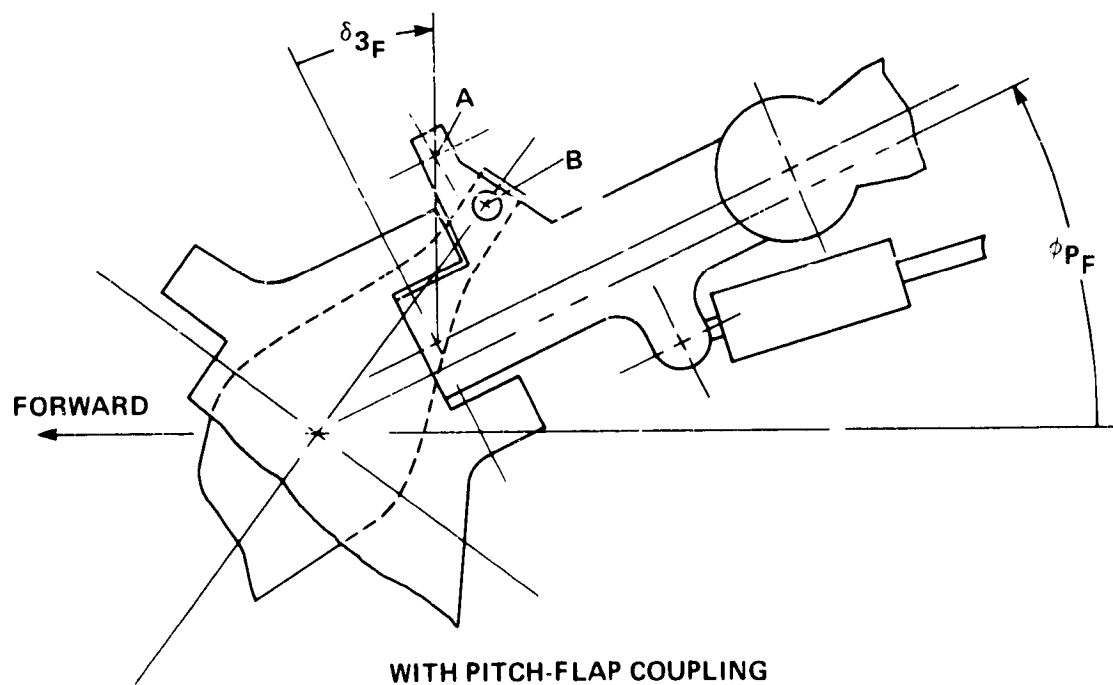
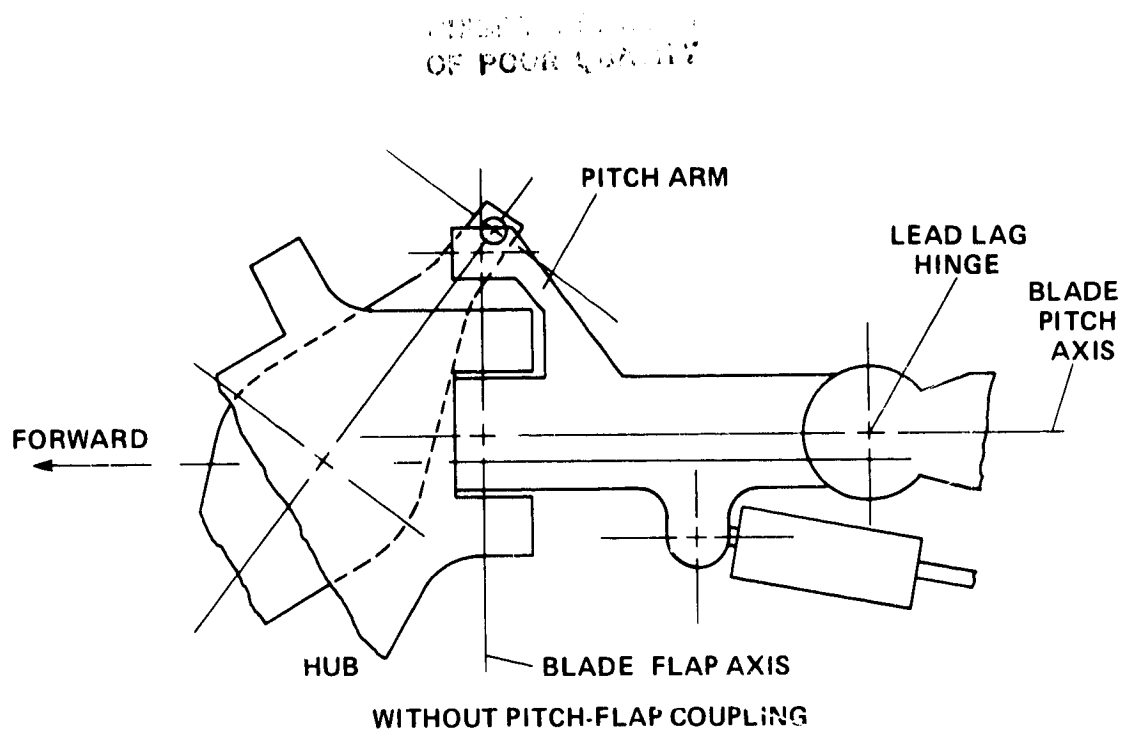


Figure 7.- Modification of rotor swashplate arrangement for pitch-flap coupling (ref. 11).

ORIGINAL  
OF POOR QUALITY

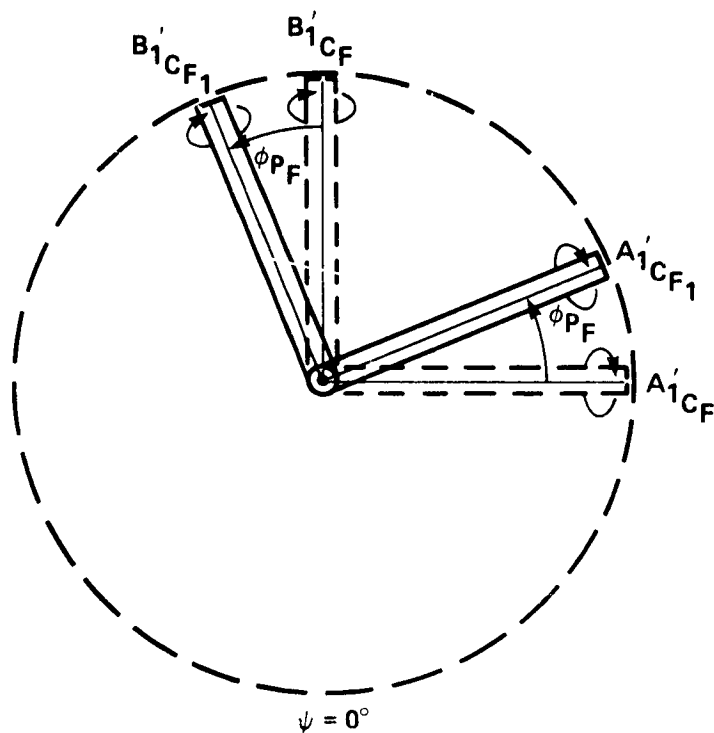
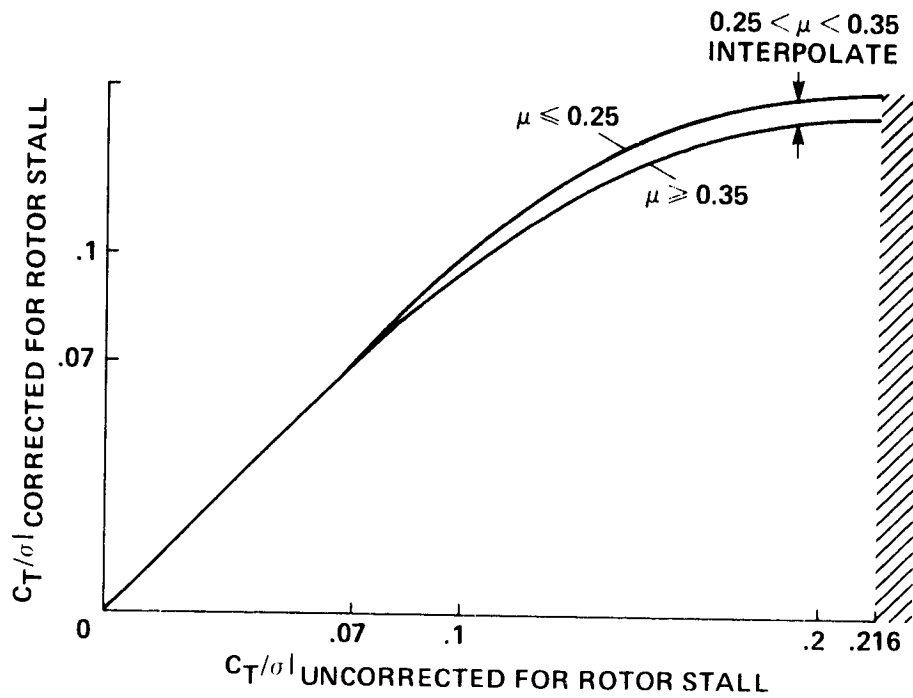


Figure 8.- Correction of cyclic pitch inputs for phasing angle,  $\phi_{p_F}$ .

# ORIGINAL OF POCOR 000000



$C_{T/\sigma} | \text{UNCORRECTED} \leq 0.216$

$$\mu \leq 0.25: C_{T/\sigma} | \text{CORRECTED} = -3.572 (C_{T/\sigma})^2 + 1.5494 (C_{T/\sigma}) - 0.02095$$

$$\mu \geq 0.35: C_{T/\sigma} | \text{CORRECTED} = -2.737 (C_{T/\sigma})^2 + 1.2884 (C_{T/\sigma}) - 0.006776$$

$0.25 < \mu < 0.35$ : INTERPOLATE BETWEEN VALUES

$$C_{T/\sigma} | \text{UNCORRECTED} > 0.216: C_{T/\sigma} | \text{CORRECTED} = C_{T/\sigma} | \text{UNCORRECTED}$$

Figure 9.- Rotor stall thrust coefficient correction (subroutine RSTALL).



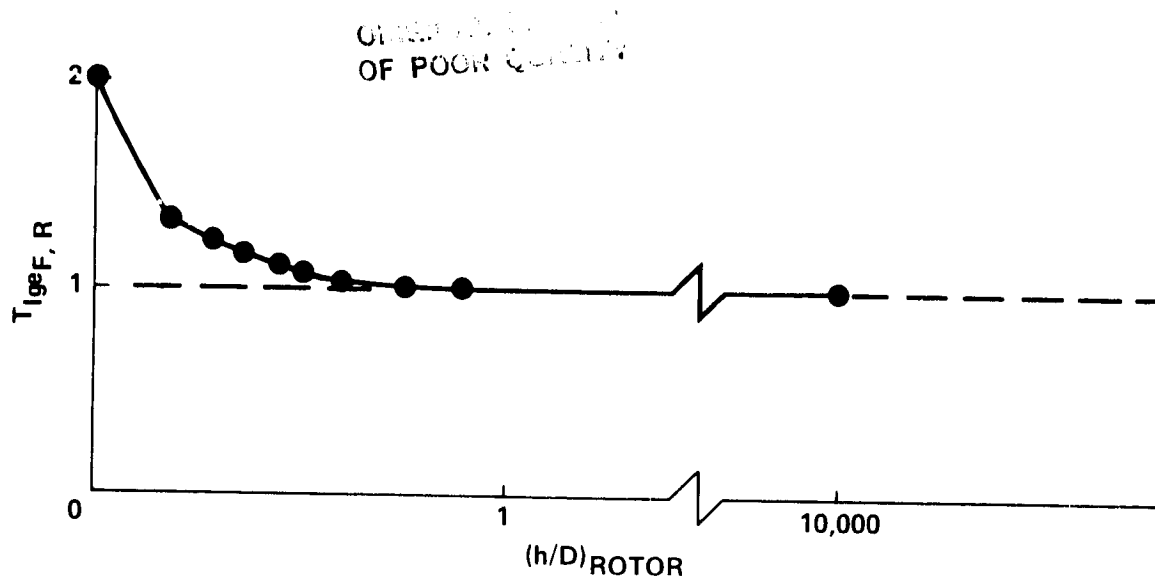


Figure 10.- Altitude dependent term for thrust modification due to ground effect.

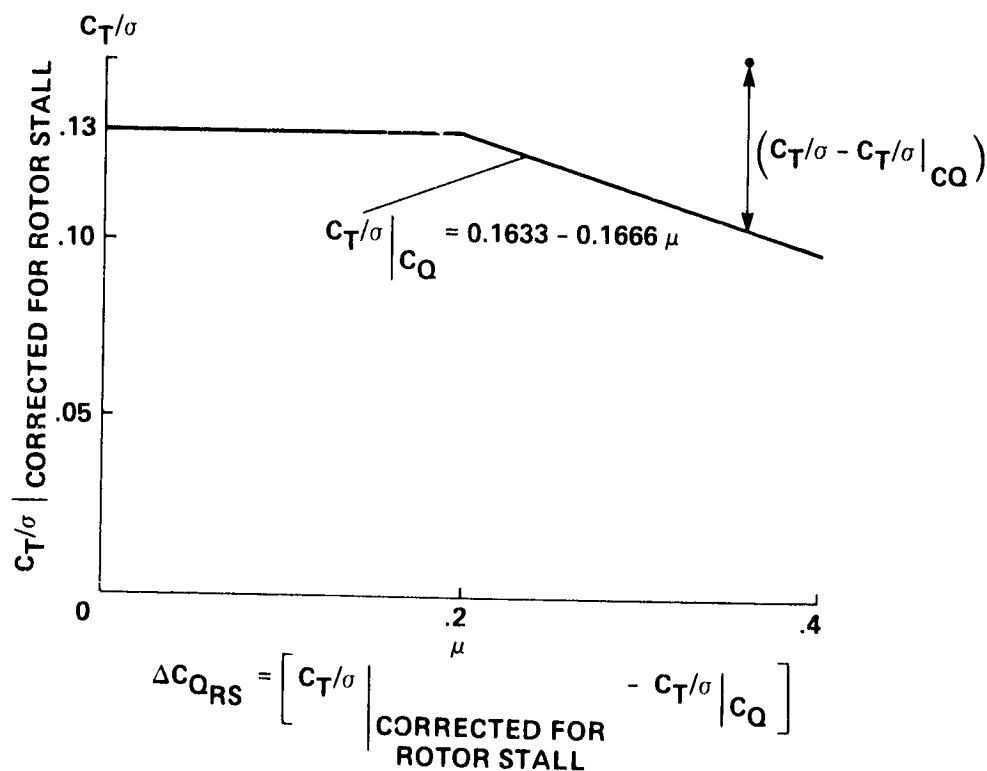
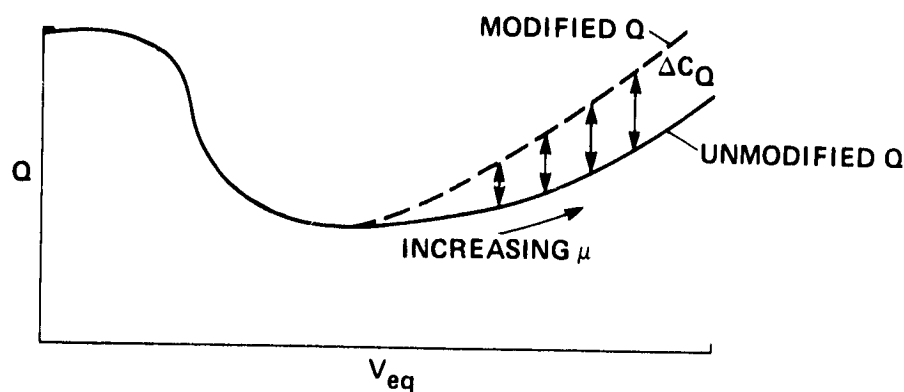


Figure 11.- Rotor stall torque coefficient correction (subroutine RSTALL).

# OF POOR QUALITY



WHERE  $\Delta C_{Q_{F,R}}$  IS COMPUTED AS FOLLOWS:

- IF  $\mu \leq 0.1$ :  $\Delta C_{Q_{F,R}} = 0.000833 (0.088 - \mu_{F,R}) + 0.01753 (C_{T_{F,R}} - 0.0062)$
- IF  $0.1 < \mu \leq 0.2$ :  $\Delta C_{Q_{F,R}} = 0.0002 (\mu_{F,R} - 0.1) - 0.00001 + 0.01753 (C_{T_{F,R}} - 0.0062)$
- IF  $0.2 < \mu \leq 0.3$ :  $\Delta C_{Q_{F,R}} = 0.00042 (\mu_{F,R} - 0.2) + 0.000006 + 0.01753 (C_{T_{F,R}} - 0.0062)$
- IF  $\mu > 0.3$ :  $\Delta C_{Q_{F,R}} = 0.0016 (\mu_{F,R} - 0.3) + 0.000048 + 0.01753 (C_{T_{F,R}} - 0.0062)$
- IF  $\Delta C_{Q_{F,R}} < -0.00001$ :  $\Delta C_{Q_{F,R}} = -0.00001$

Figure 12.- Empirical correction of rotor torque coefficient (in-line calculation).

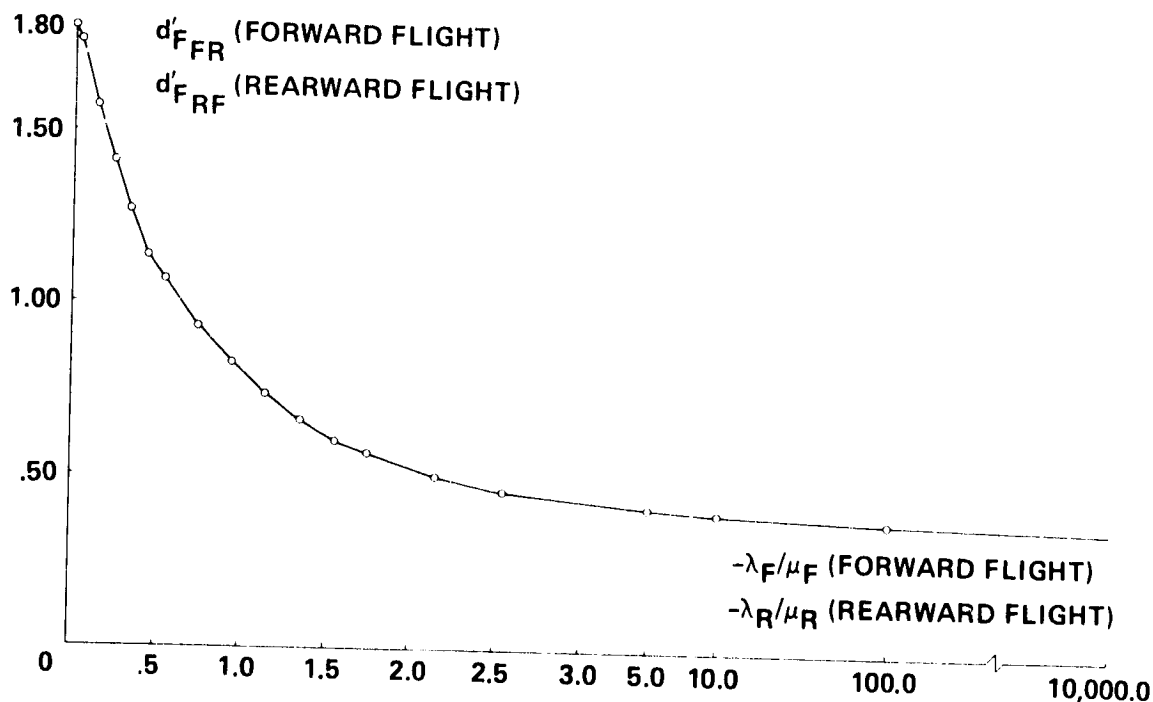


Figure 13.- Rotor-on-rotor interference terms:  $d'_{F_{FR}}$  (forward flight) and  $d'_{F_{RF}}$  (rearward flight).

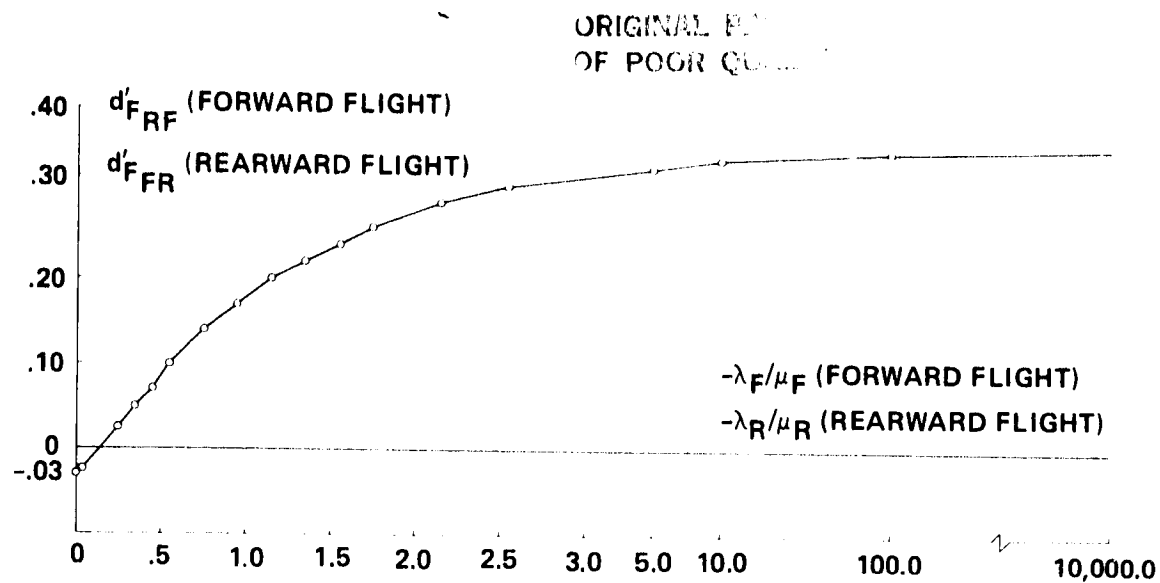


Figure 14.- Rotor-on-rotor interference terms:  $d'_{FRF}$  (forward flight) and  $d'_{FRR}$  (rearward flight).

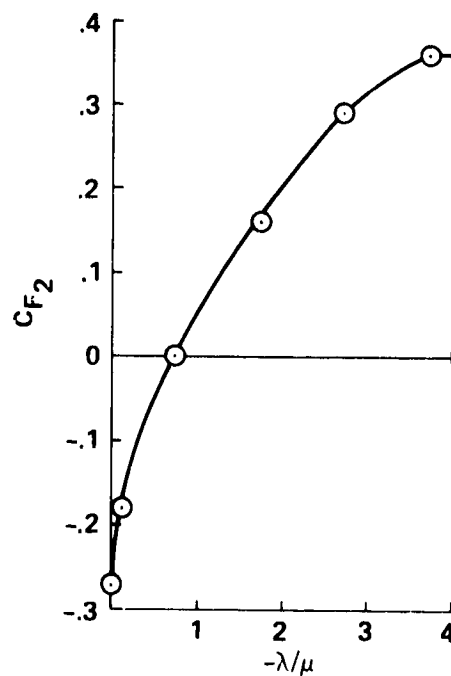


Figure 15.- Rotor on rotor interference term.

ORIGINAL PAGE IS  
OF POOR QUALITY.

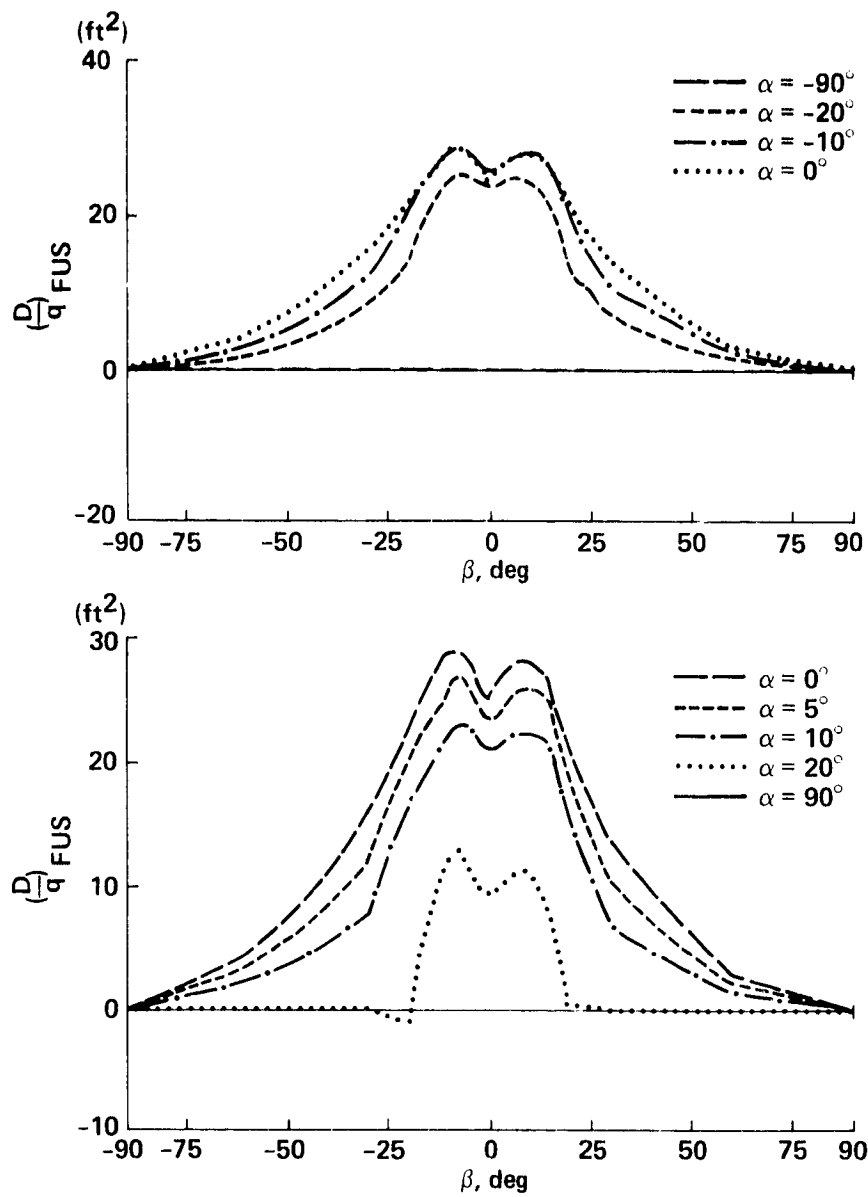


Figure 16.- Fuselage drag data (table: FDOQT).

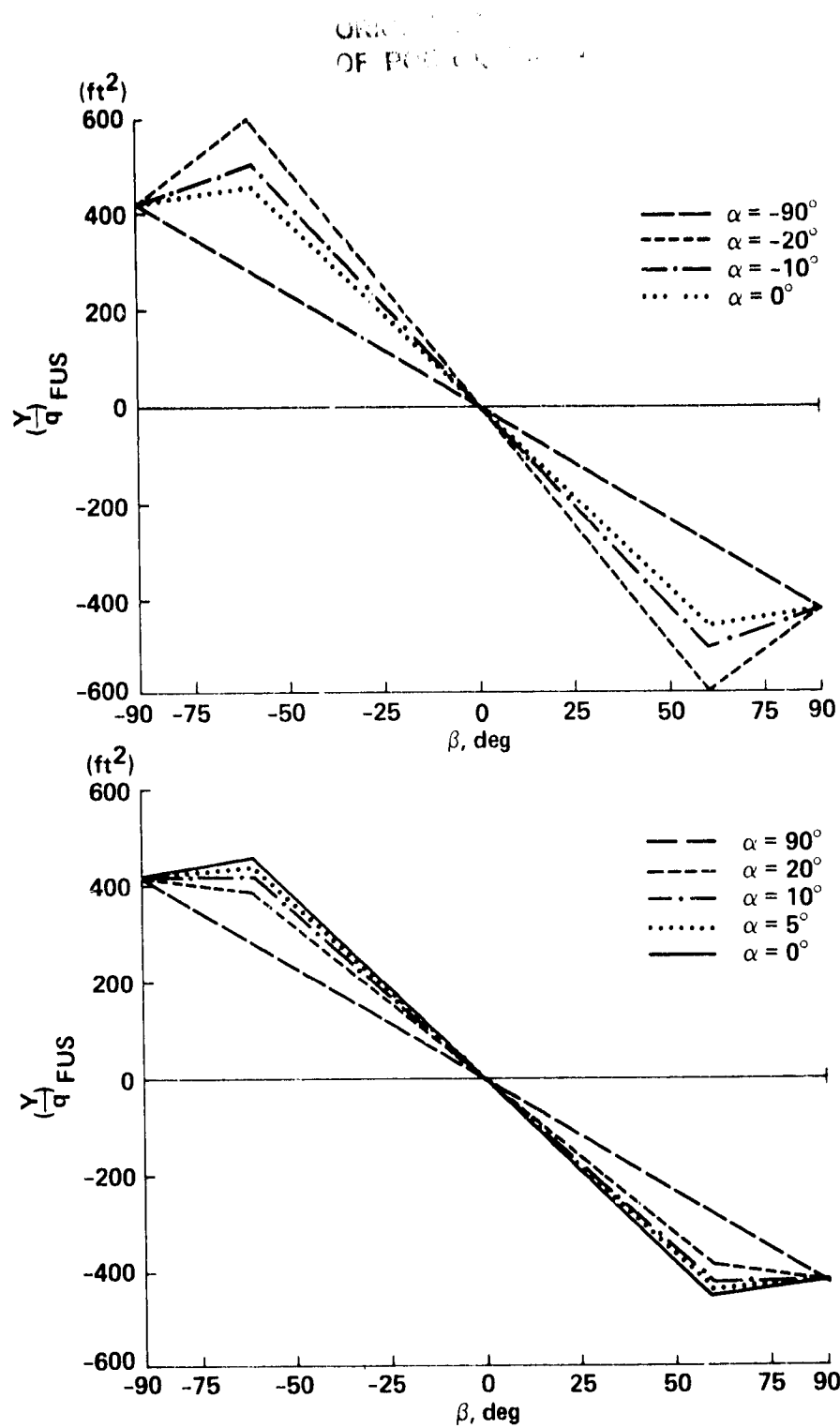


Figure 17.- Fuselage sideforce data (table: FYOQT).

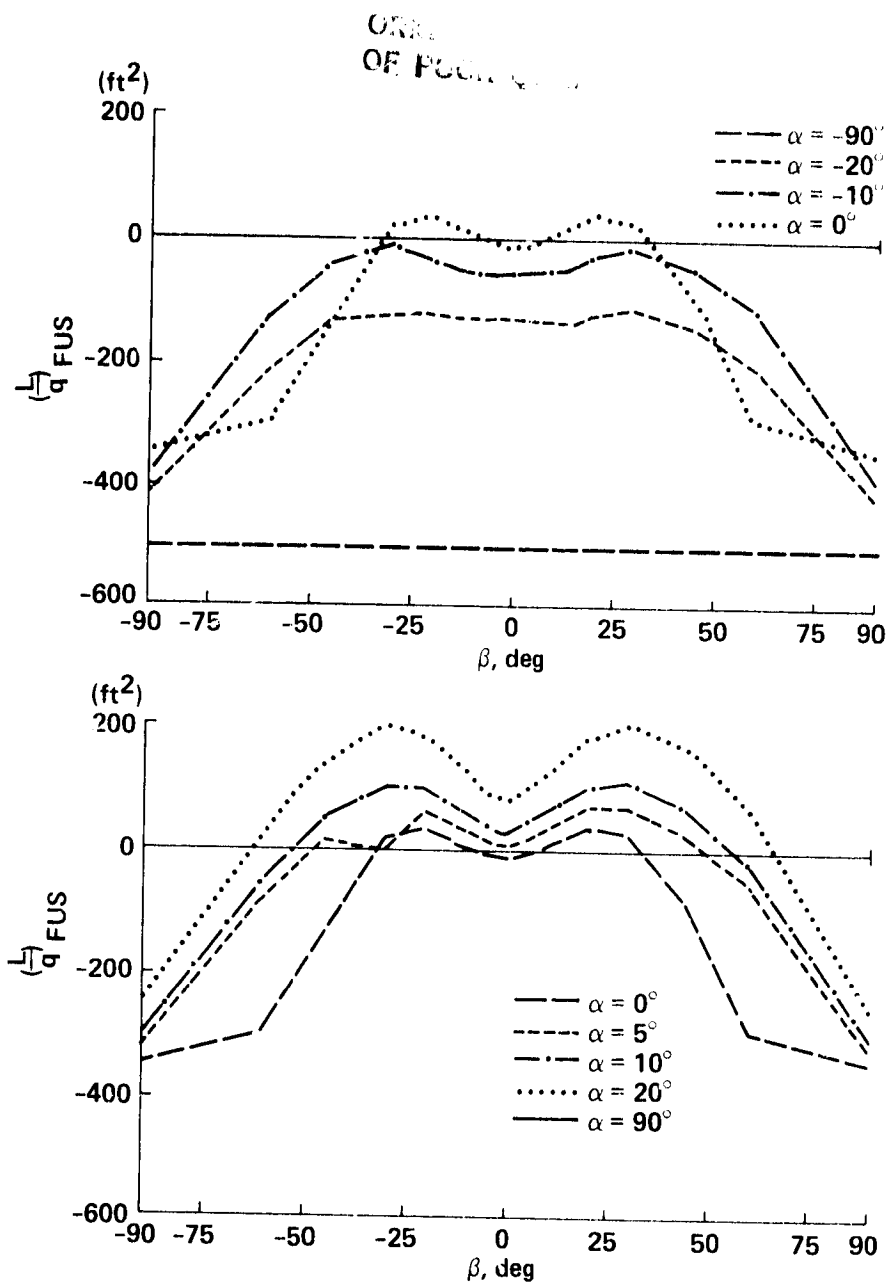


Figure 18.- Fuselage lift data (table: LTOQT).

ORIGINAL  
OF POOR QUALITY

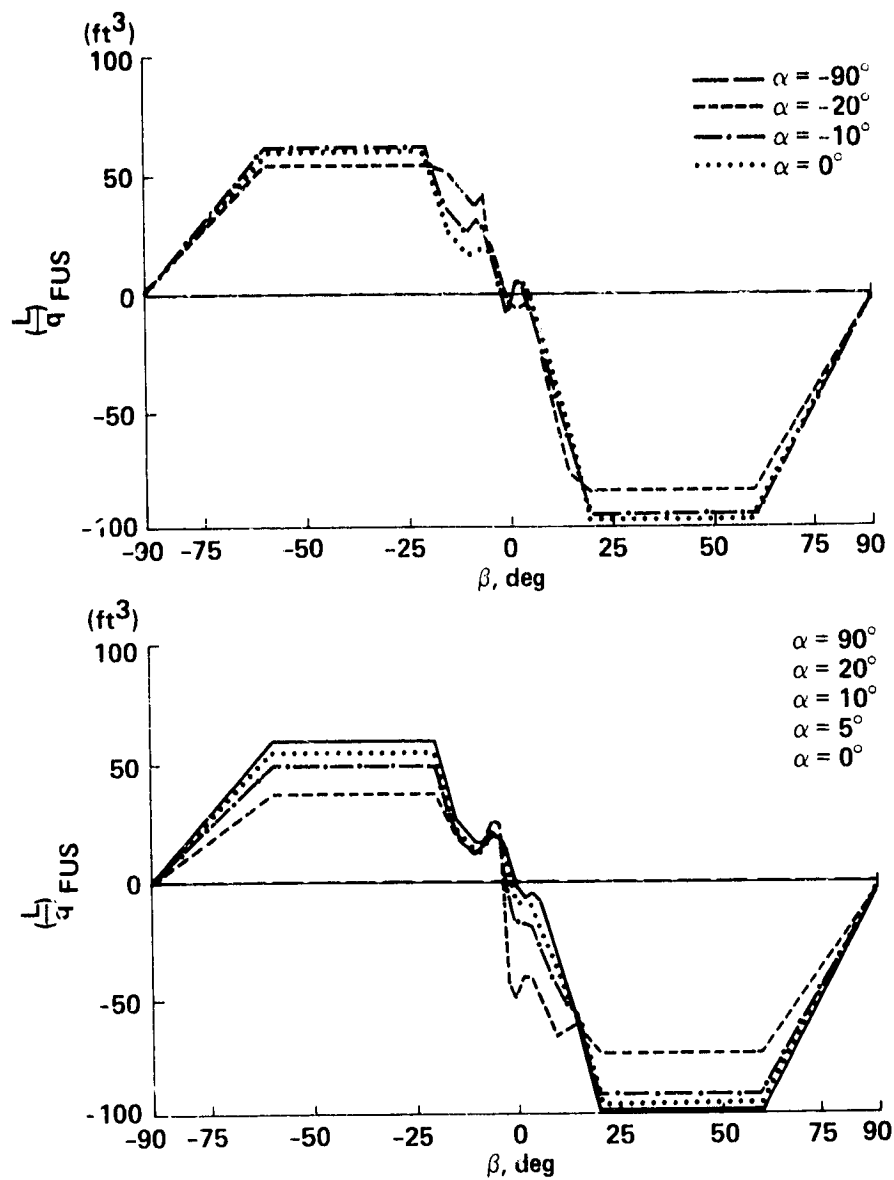


Figure 19.- Fuselage rolling moment data (table: FLOQT).

# OF POOR QUALITY

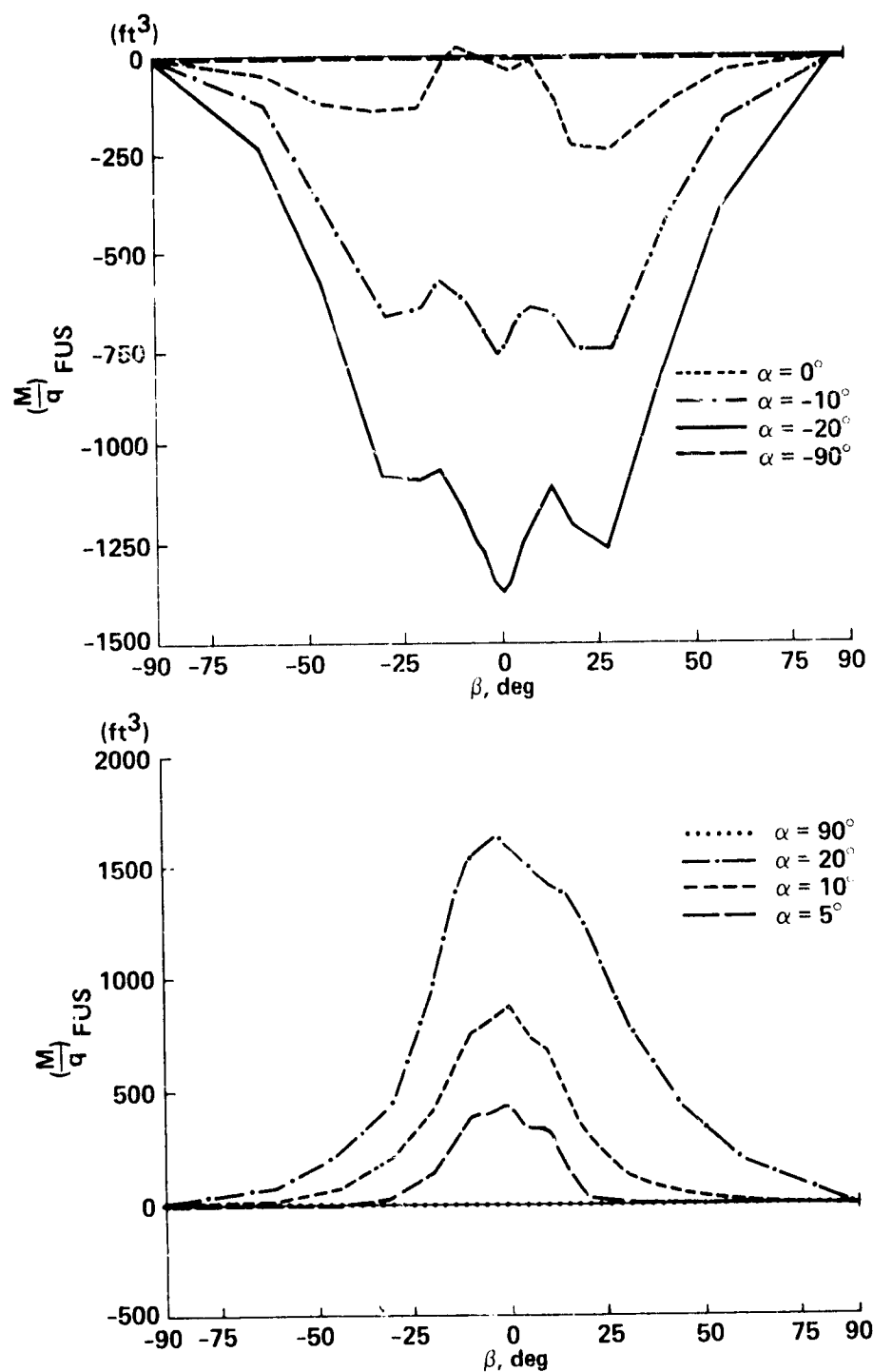


Figure 20.- Fuselage pitching moment data (table: FMOQT).



ORIGINAL DATA  
OF POOR QUALITY

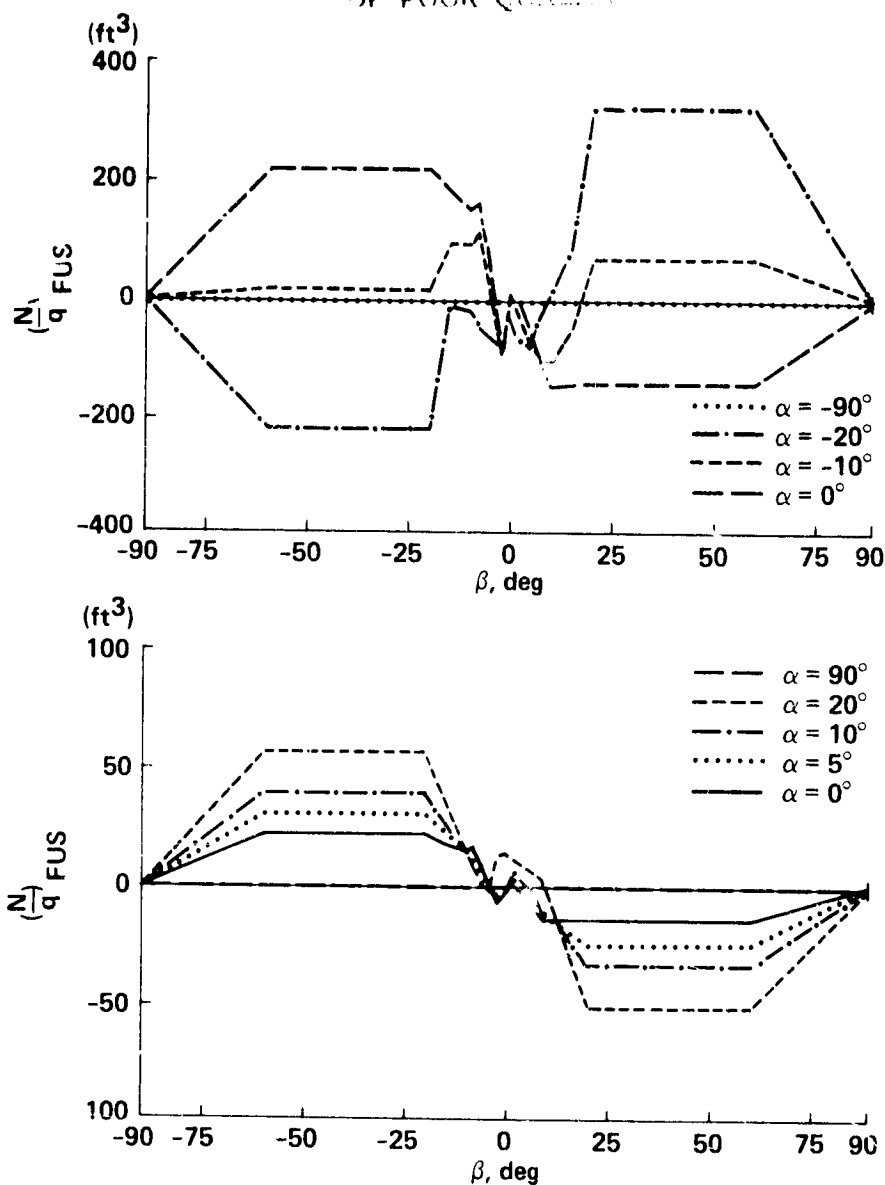


Figure 21.- Fuselage yawing moment data (table: FNOQT).

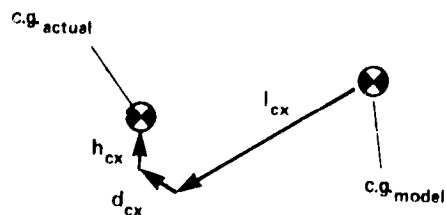


Figure 22.- Actual helicopter versus wind tunnel model center of gravity.

ORIGINAL  
OF POOR QUALITY

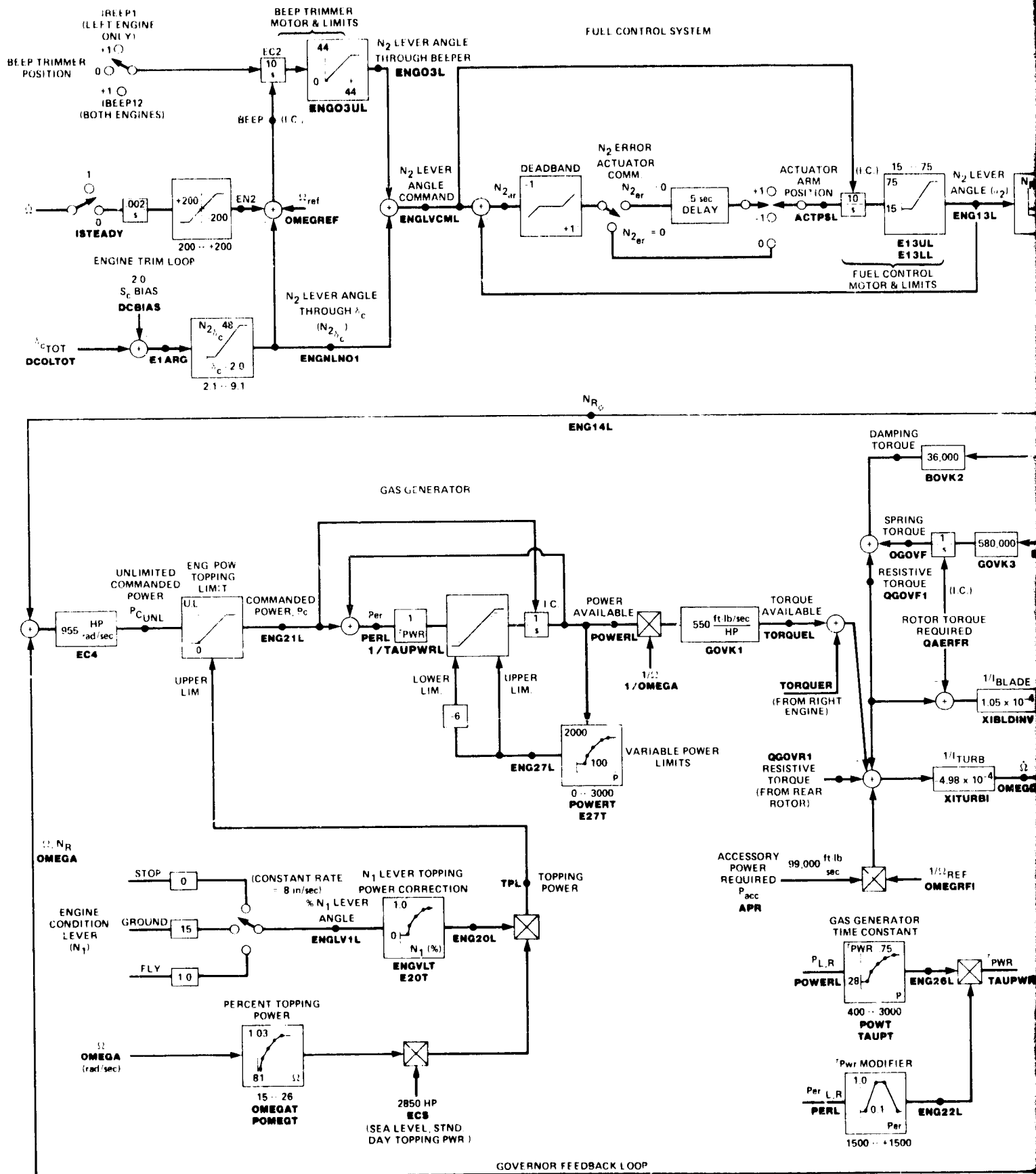


Figure 23.- Engine, governor, and shaft dynamics block diagram.

FOLDOUT FRAME



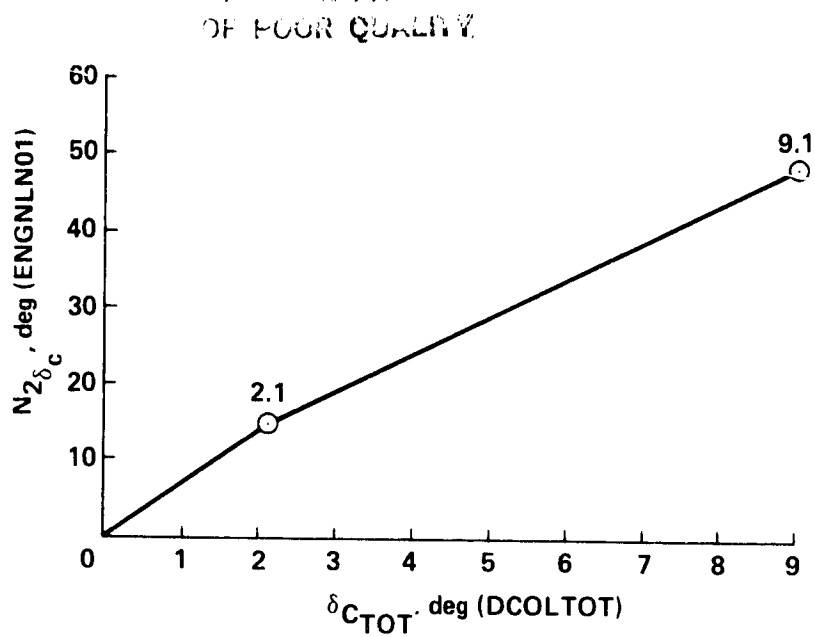


Figure 24.- Computation of  $N_{2\delta C}$  as a function of  $\delta_{CTOT}$ .

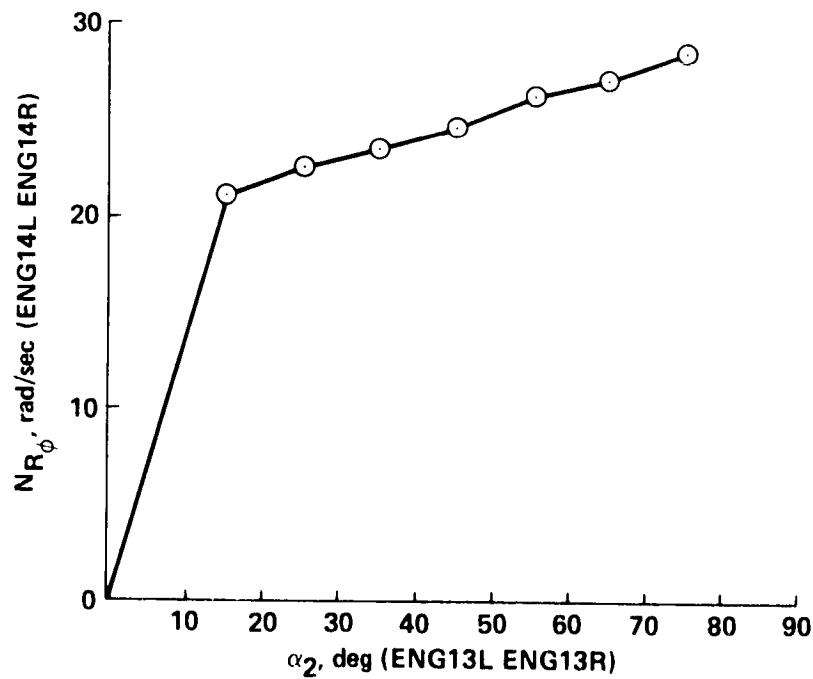


Figure 25.- Determination of fuel control actuator position,  $N_{R\phi}$ .

PRECEDING PAGE BLANK NOT FILMED

ORIGINAL PAGE  
OF POOR QUALITY

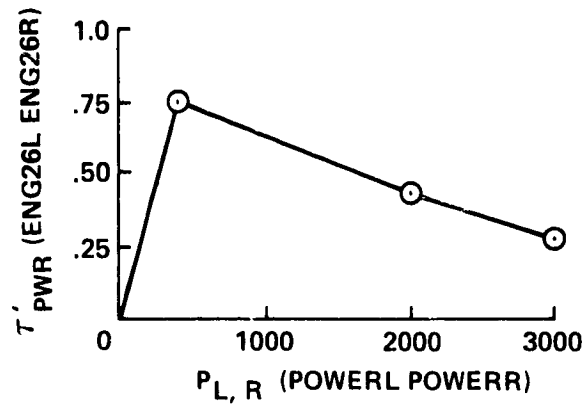


Figure 26.- Power dynamics time constant (table: POWT, TAUPT).

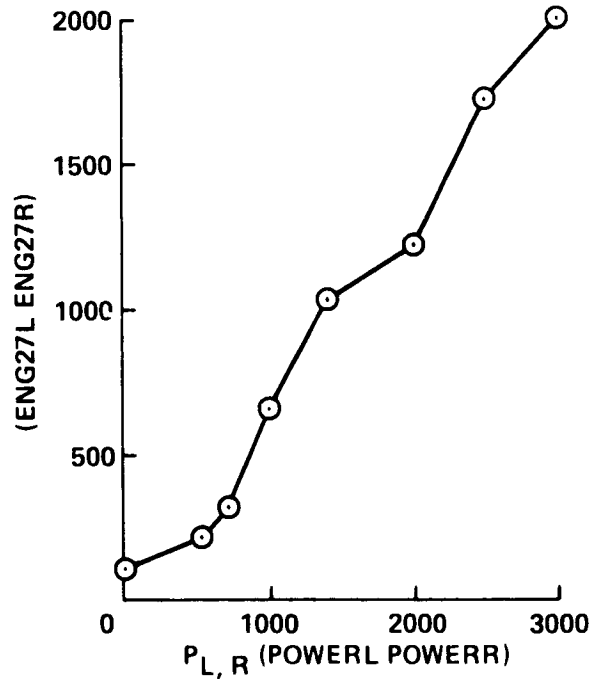


Figure 27.- Variable power limits (table: POWER, E27T).

ORIGINALITY  
OF POOR QUALITY

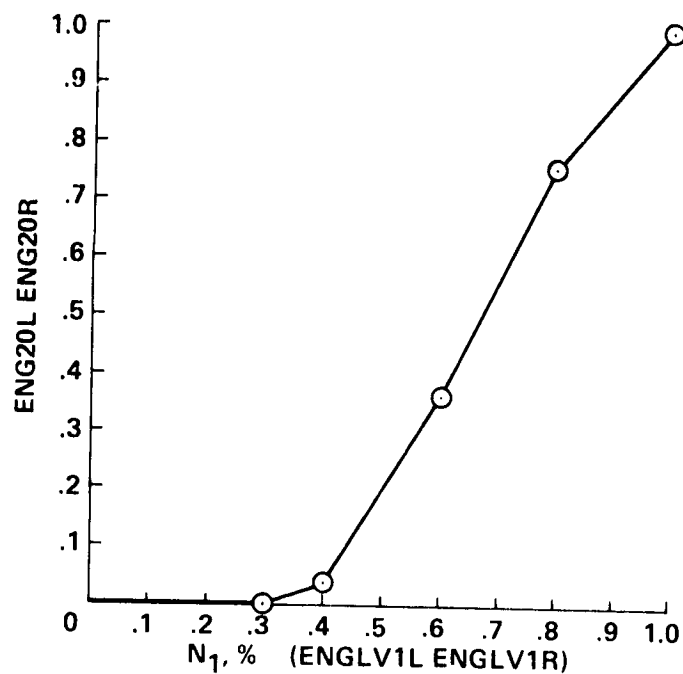


Figure 28.-  $N_1$  lever topping power correction term (table: ENGLVT, E20T).

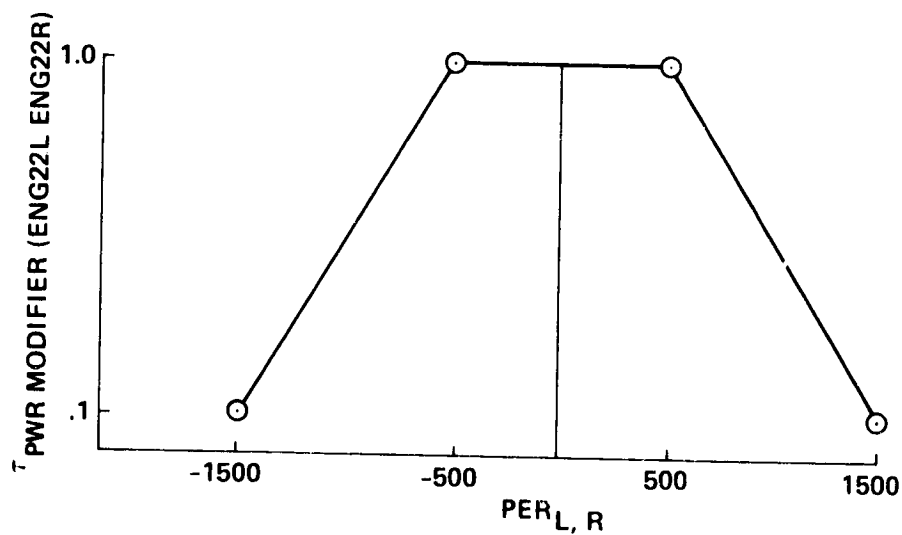


Figure 29.-  $\tau_{pwr}$  modifier (in-line calculation).

ORIGINAL DESIGN  
OF POOR QUALITY

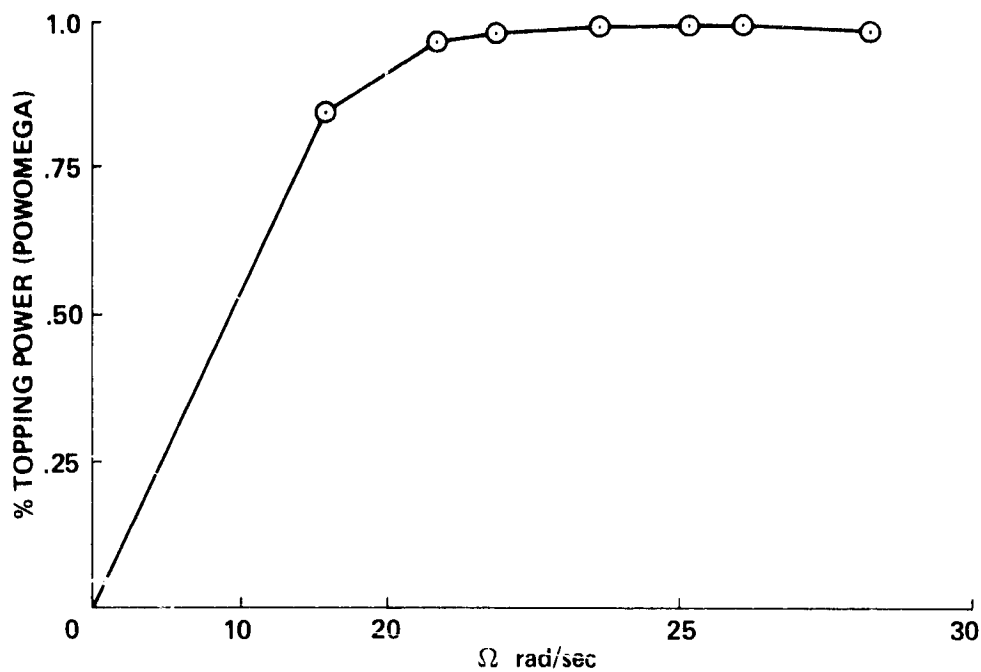


Figure 30.- Percent topping power (table: OMEGAT, POMEQT).

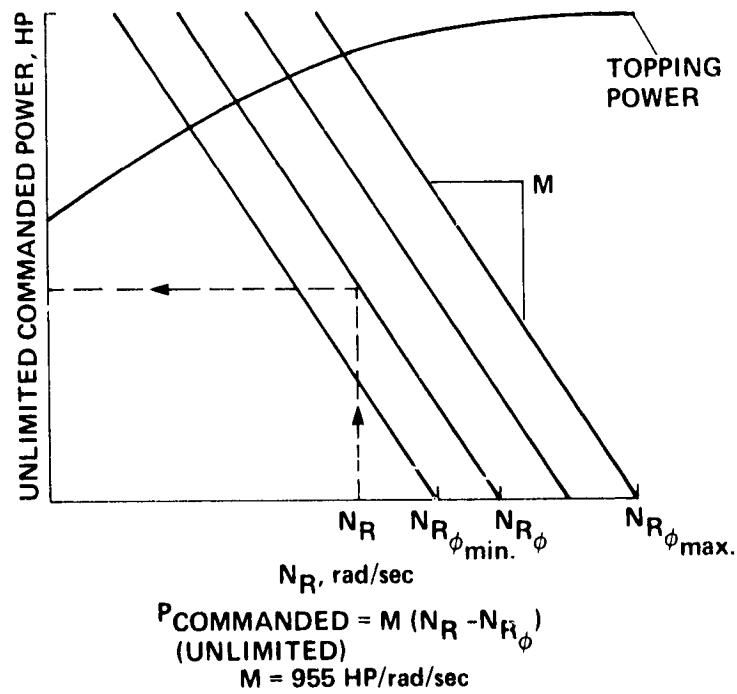
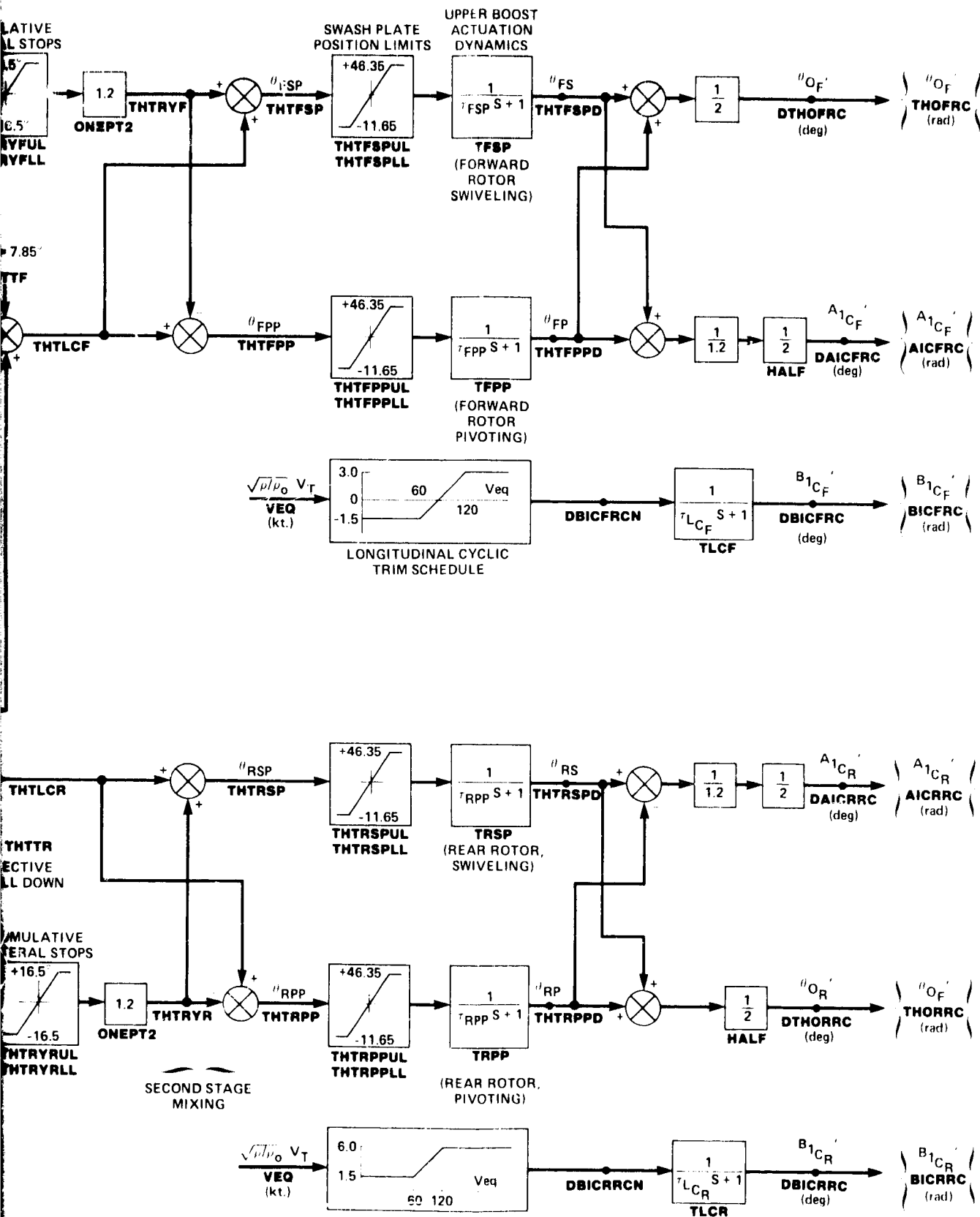


Figure 31.- Unlimited commanded power calculation.







mechanical control system schematic.

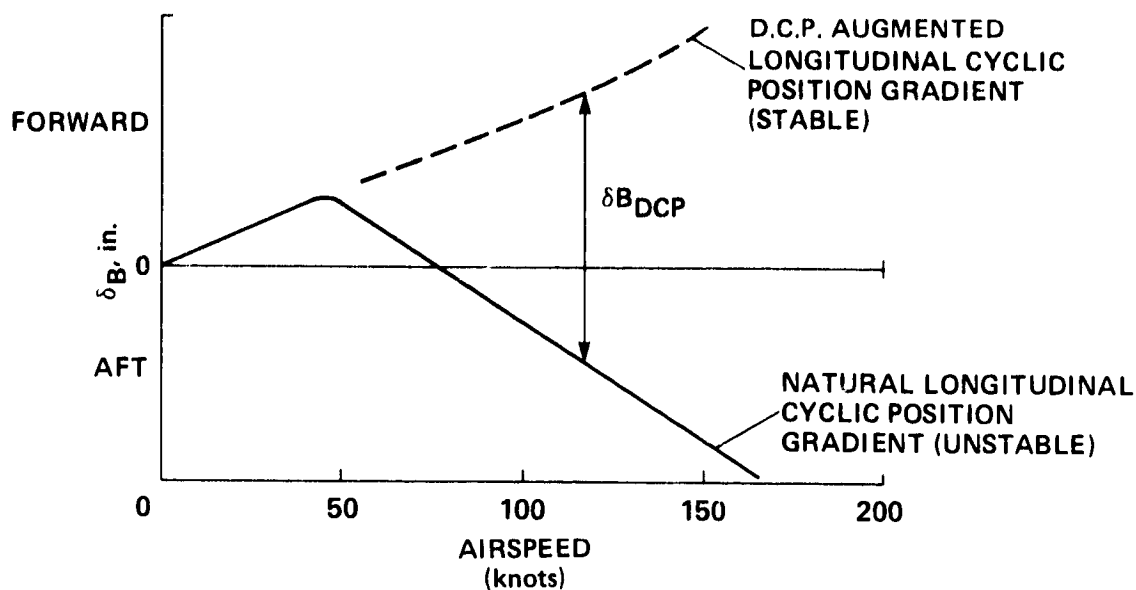


Figure 33.- Longitudinal cyclic position gradient stabilization with differential collective pitch trim.

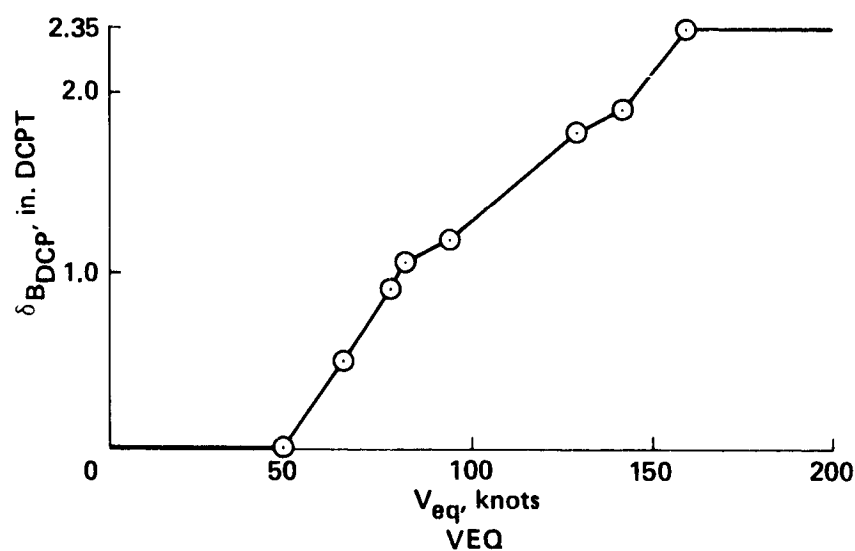


Figure 34.- Longitudinal cyclic differential collective pitch input (table: VDCP, DCPTT).

PRECEDING PAGE BLANK NOT FILMED

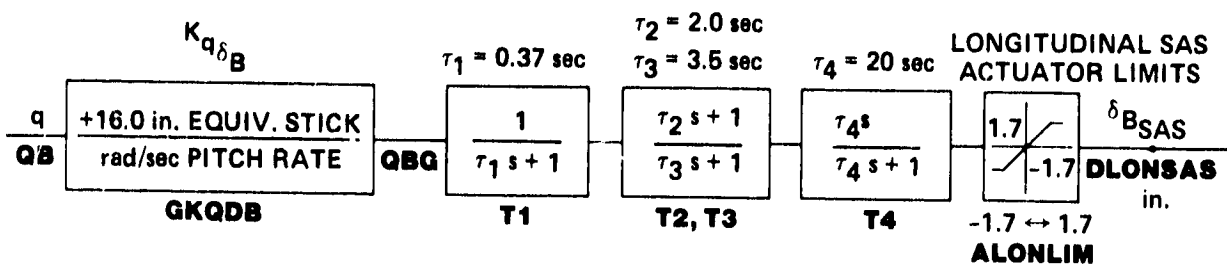


Figure 35.- Longitudinal stability augmentation system.

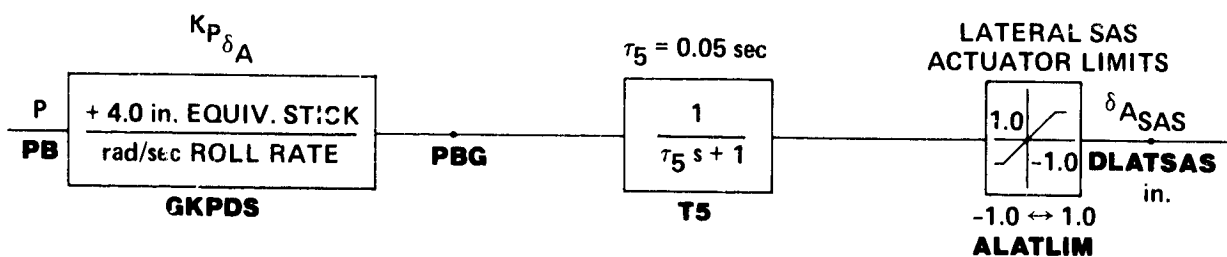


Figure 36.- Lateral stability augmentation system.

# ORIGINAL OF POOR QUALITY

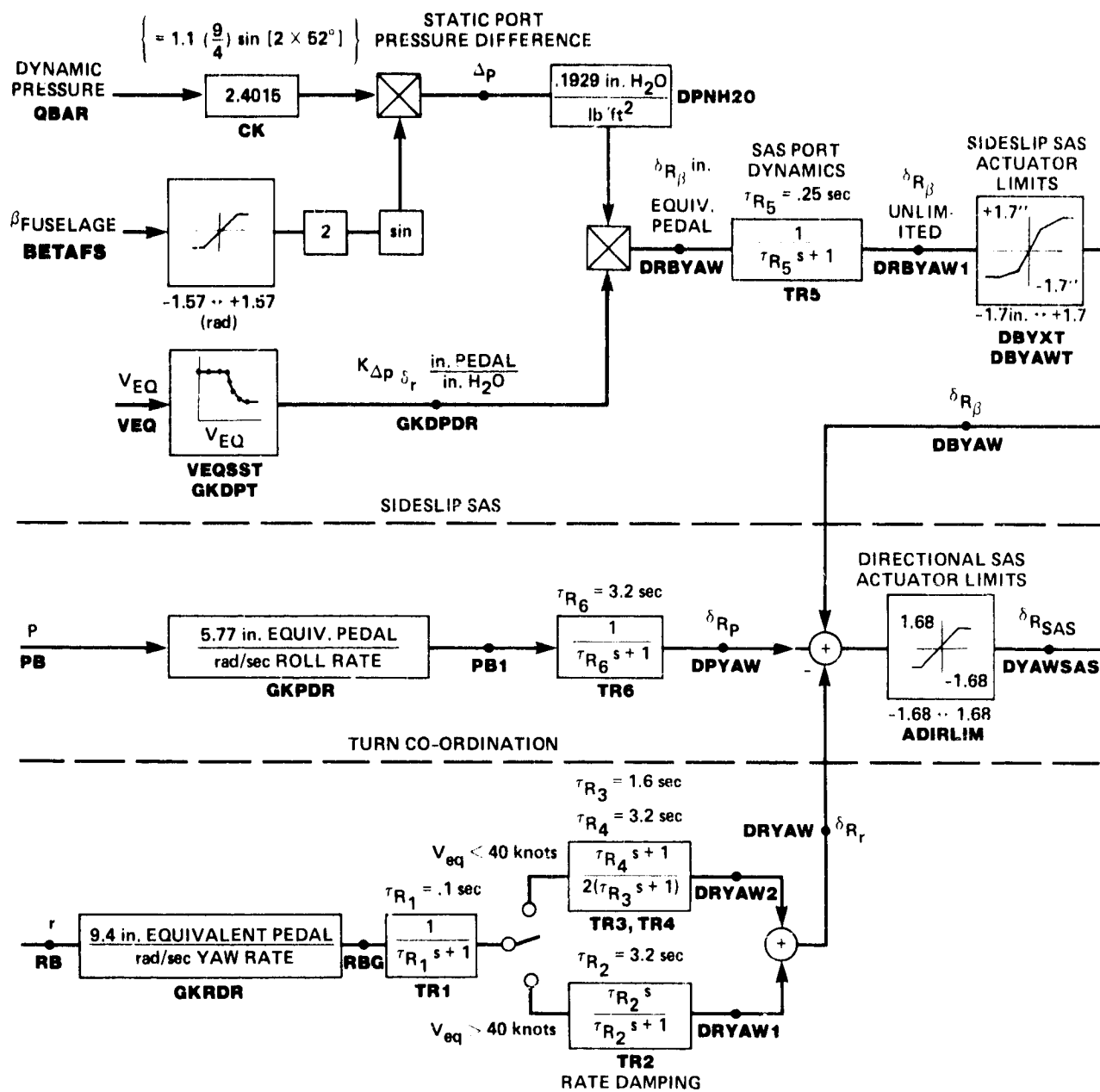


Figure 37.- Directional stability augmentation system.

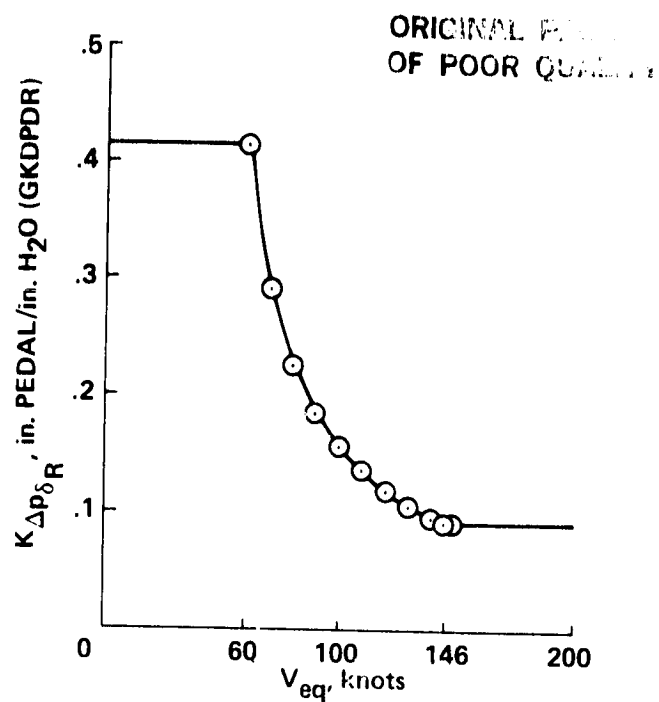


Figure 38.- Velocity dependent sideslip SAS gain (table: VEQSST, GKDPDPT).

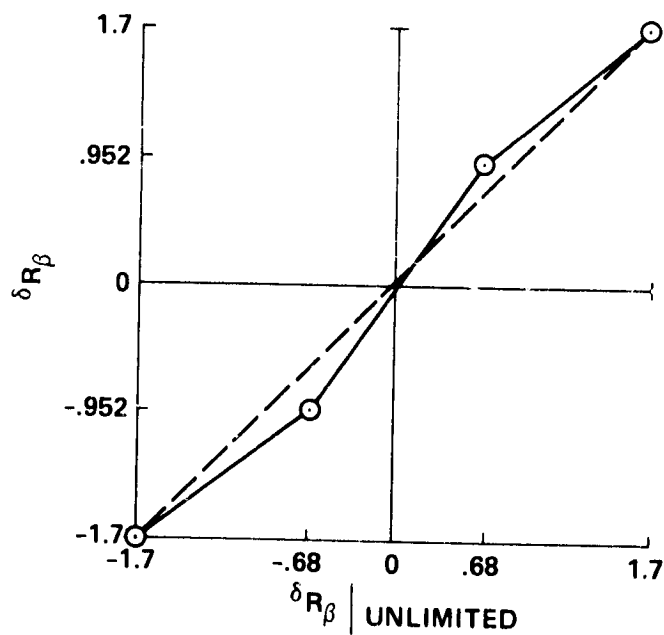


Figure 39.- Sideslip SAS actuator limits.

# ORIGINAL OF FIGURE

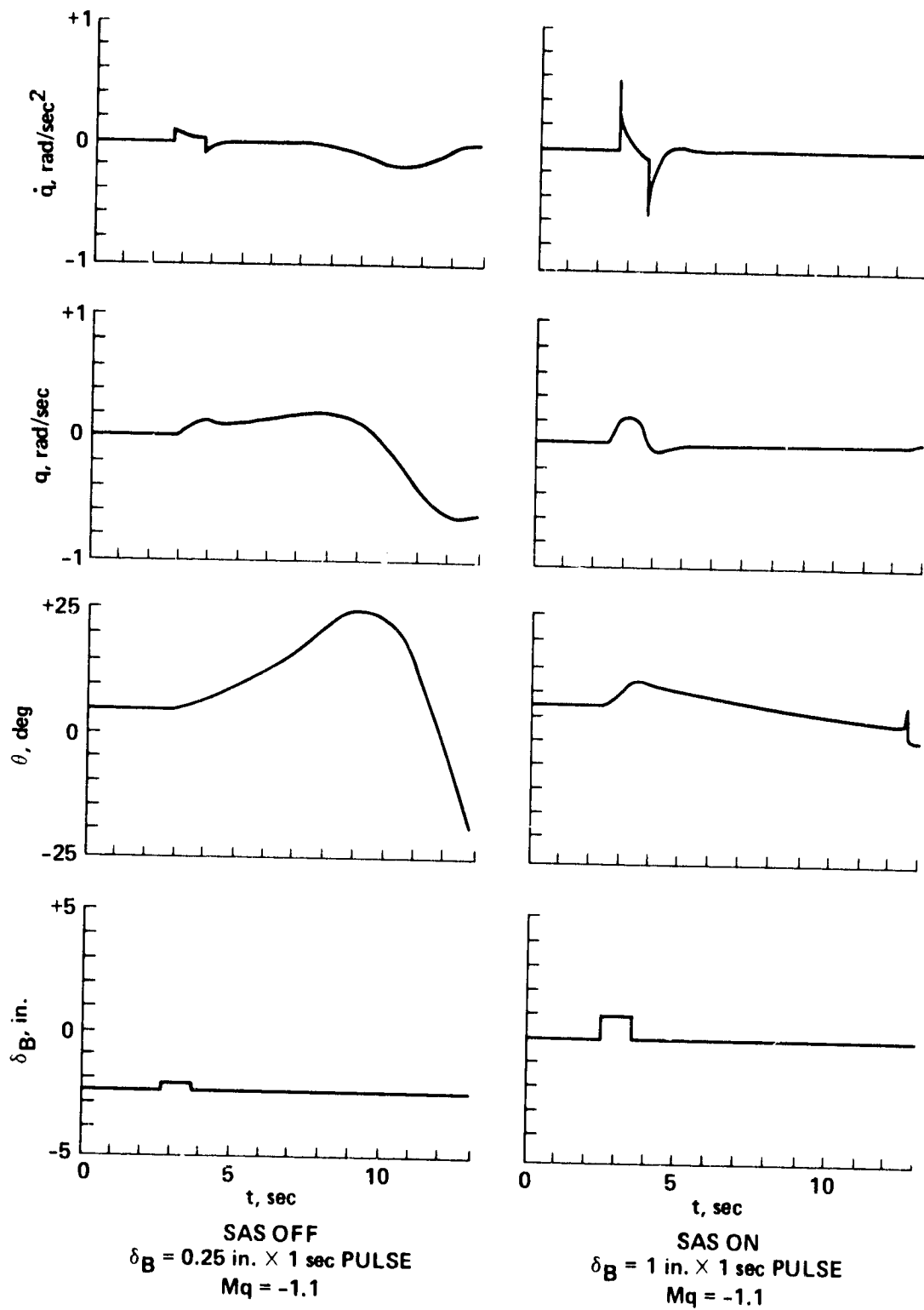


Figure 40.- Longitudinal axis dynamic response SAS OFF and ON;  
hover, weight = 33,000 lb, nominal c.g. position.

ORIGINAL  
OF POOR QUALITY

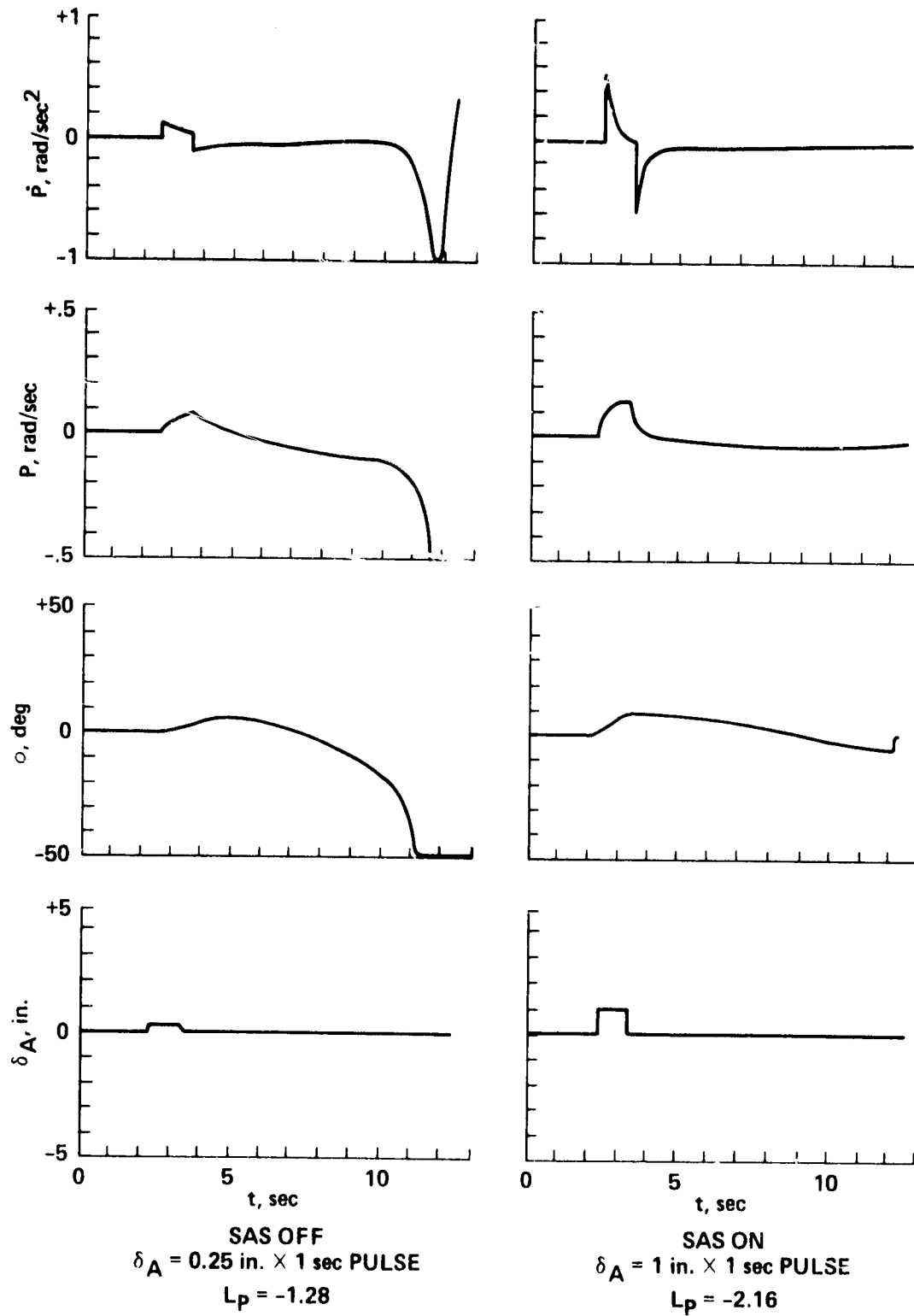


Figure 41.- Lateral axis dynamic response, SAS OFF and On;  
 hover, weight = 33,000 lb, nominal c.g. position.

ORIGINAL PAGE  
OF POOR QUALITY

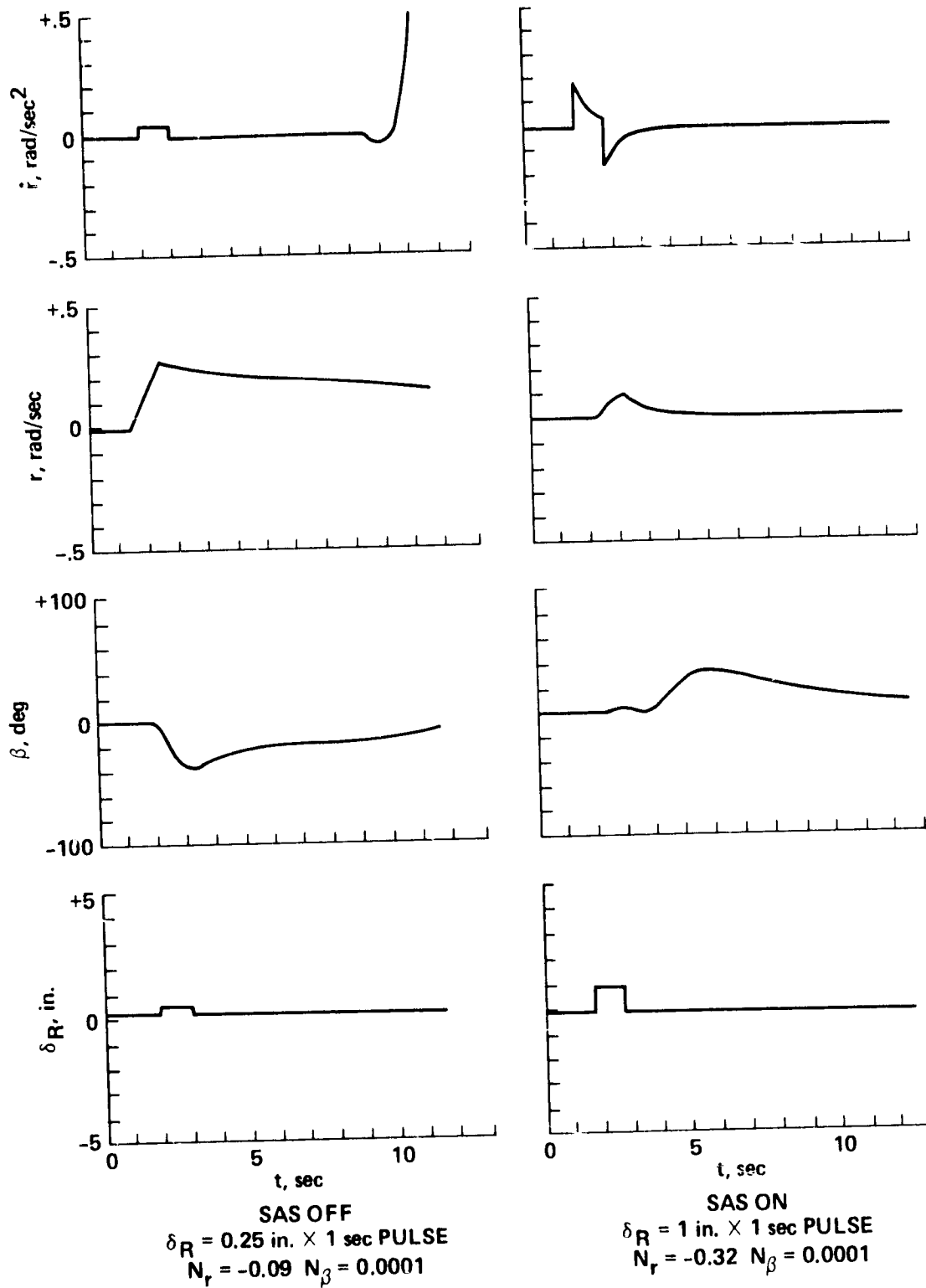


Figure 42.- Directional axis dynamic response SAS OFF and On;  
 hover, weight = 33,000 lb, nominal c.g. position.



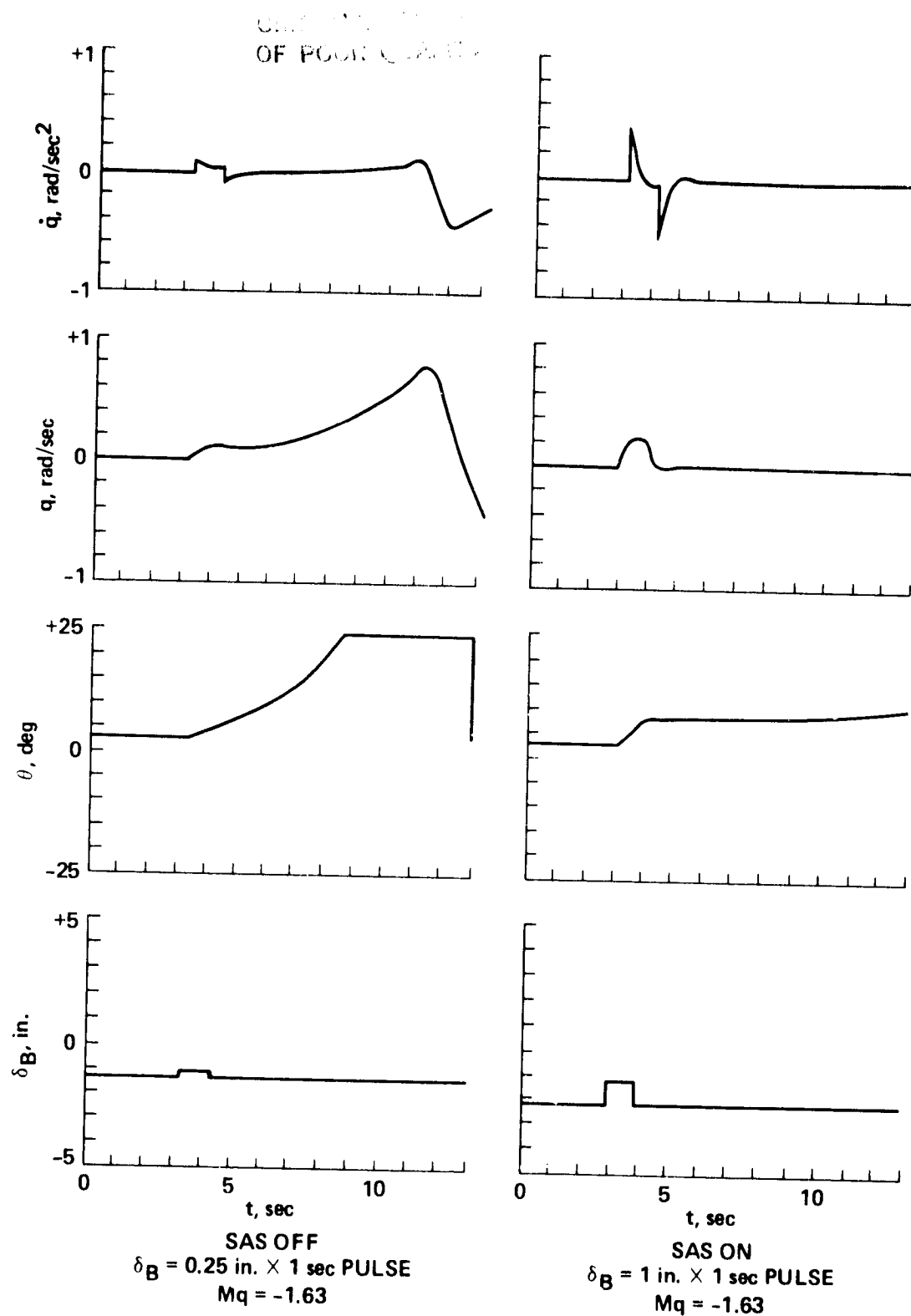


Figure 43.- Longitudinal axis dynamic response SAS OFF and On;  
 $V_{eq} = 75$  knots, weight = 33,000 lb, nominal c.g. position.

# ORIGINAL RECORD OF PDR 000000

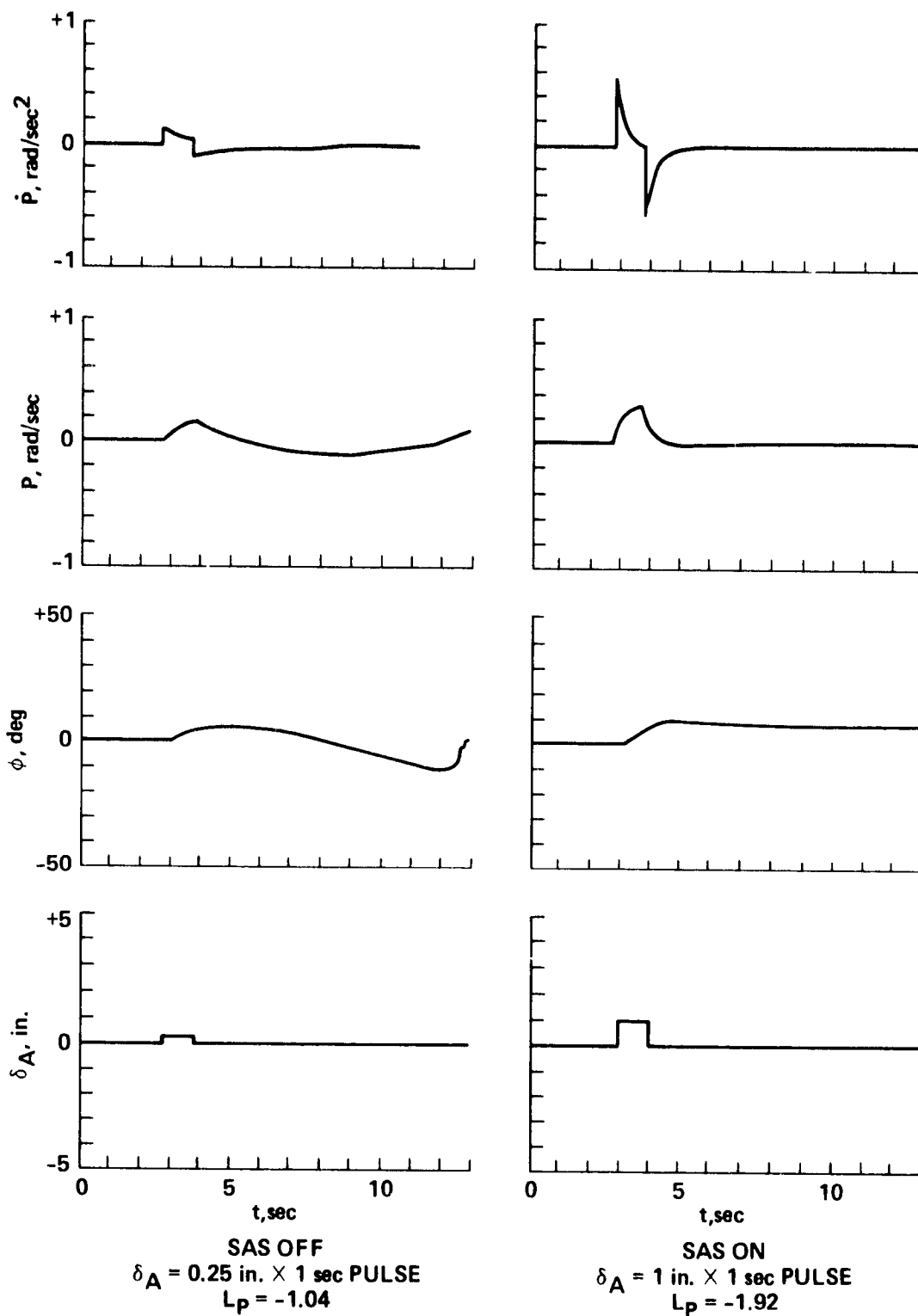


Figure 44.- Lateral axis dynamic response SAS OFF and ON;  
 $V_{eq} = 75 \text{ knots}$ , weight = 33,000 lb, nominal c.g. position.

ORIGINAL PAGE 19  
OF POOR QUALITY

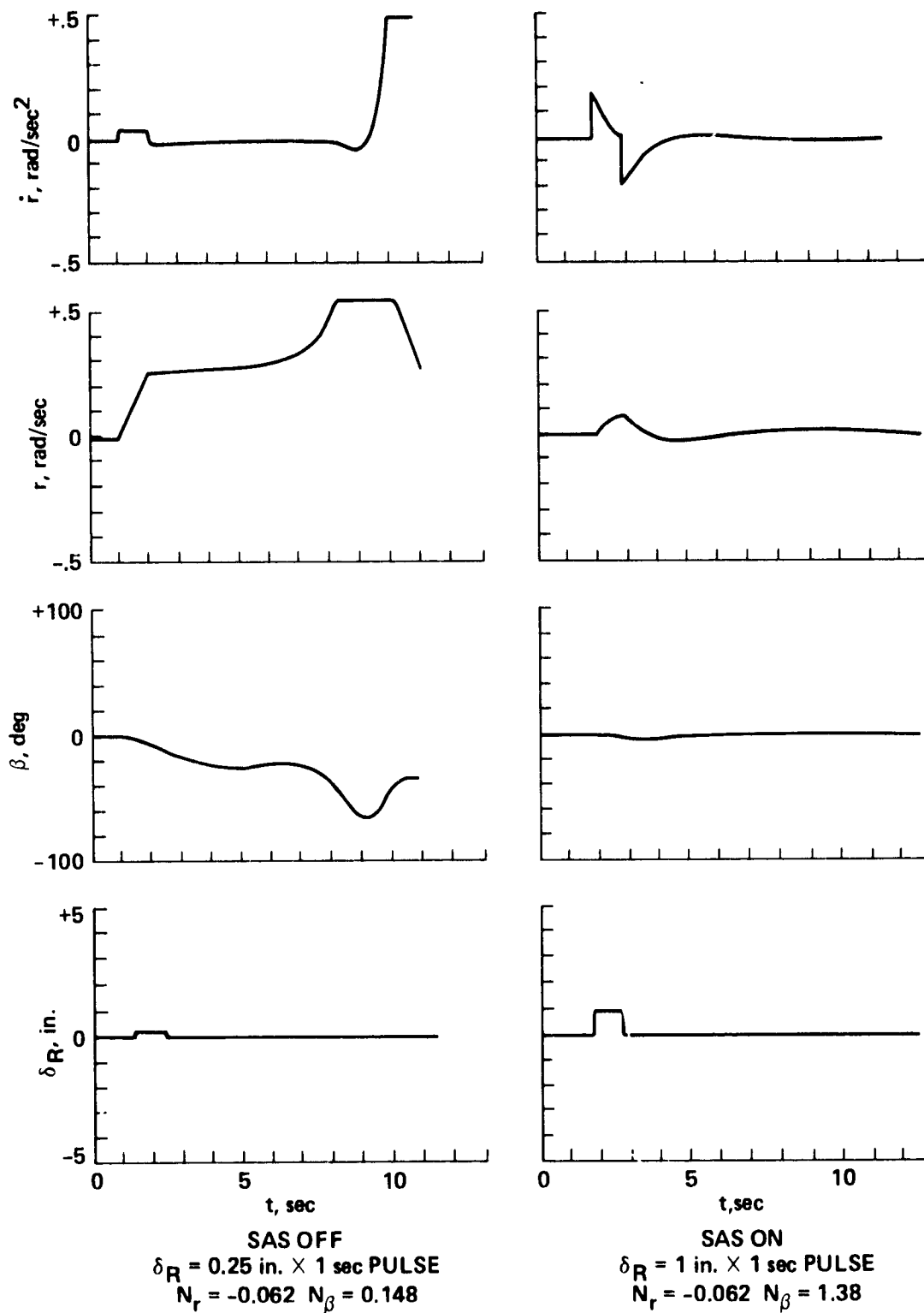


Figure 45.- Directional axis dynamic response SAS OFF and ON;  
 $V_{eq} = 75$  knots, weight = 33,000 lb, nominal c.g. position.

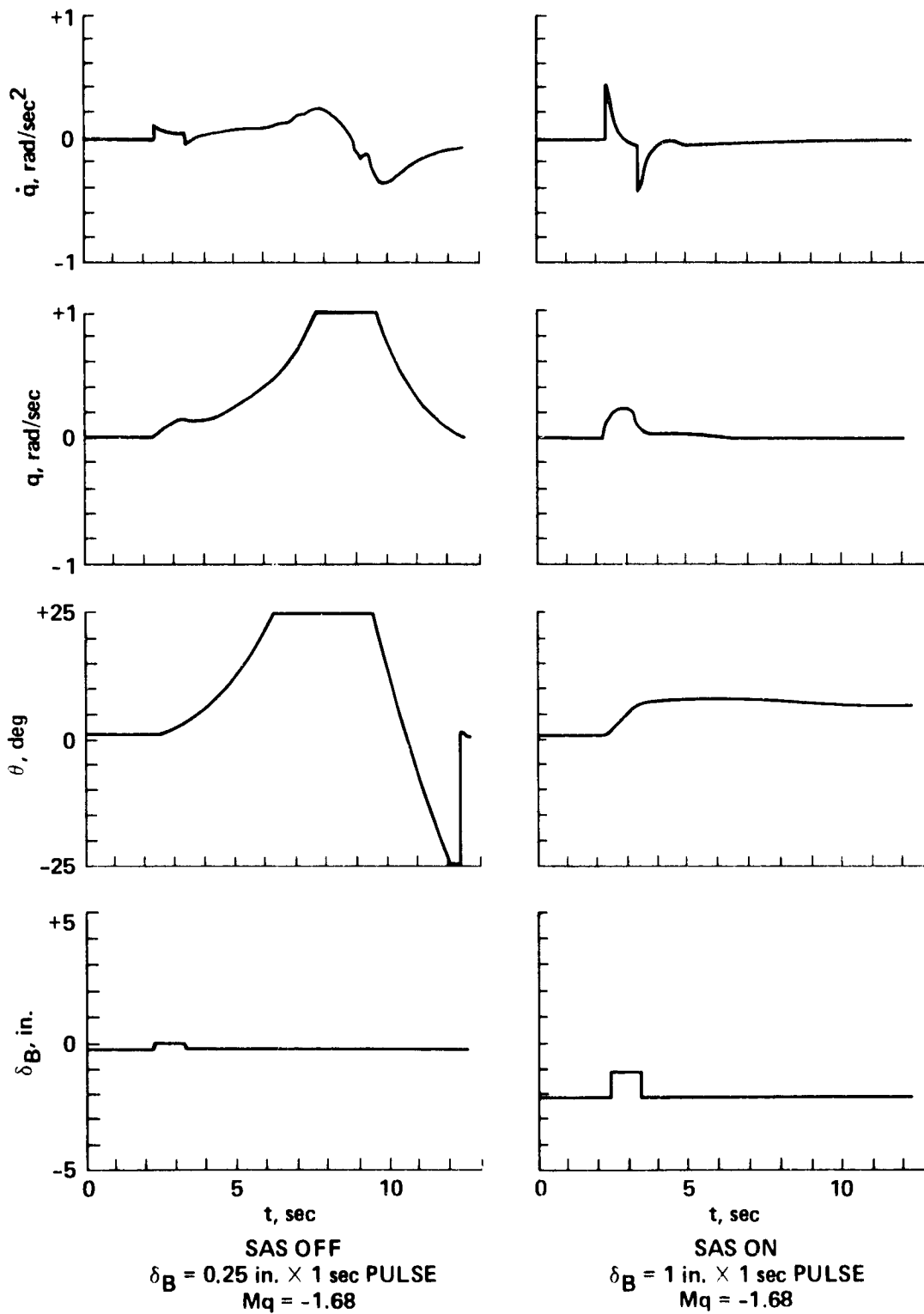


Figure 46.- Longitudinal axis dynamic response SAS OFF and ON;  
 $V_{eq} = 130$  knots, weight = 33,000 lb, nominal c.g. position.

ORIGINAL PAGE IS  
OF POOR QUALITY

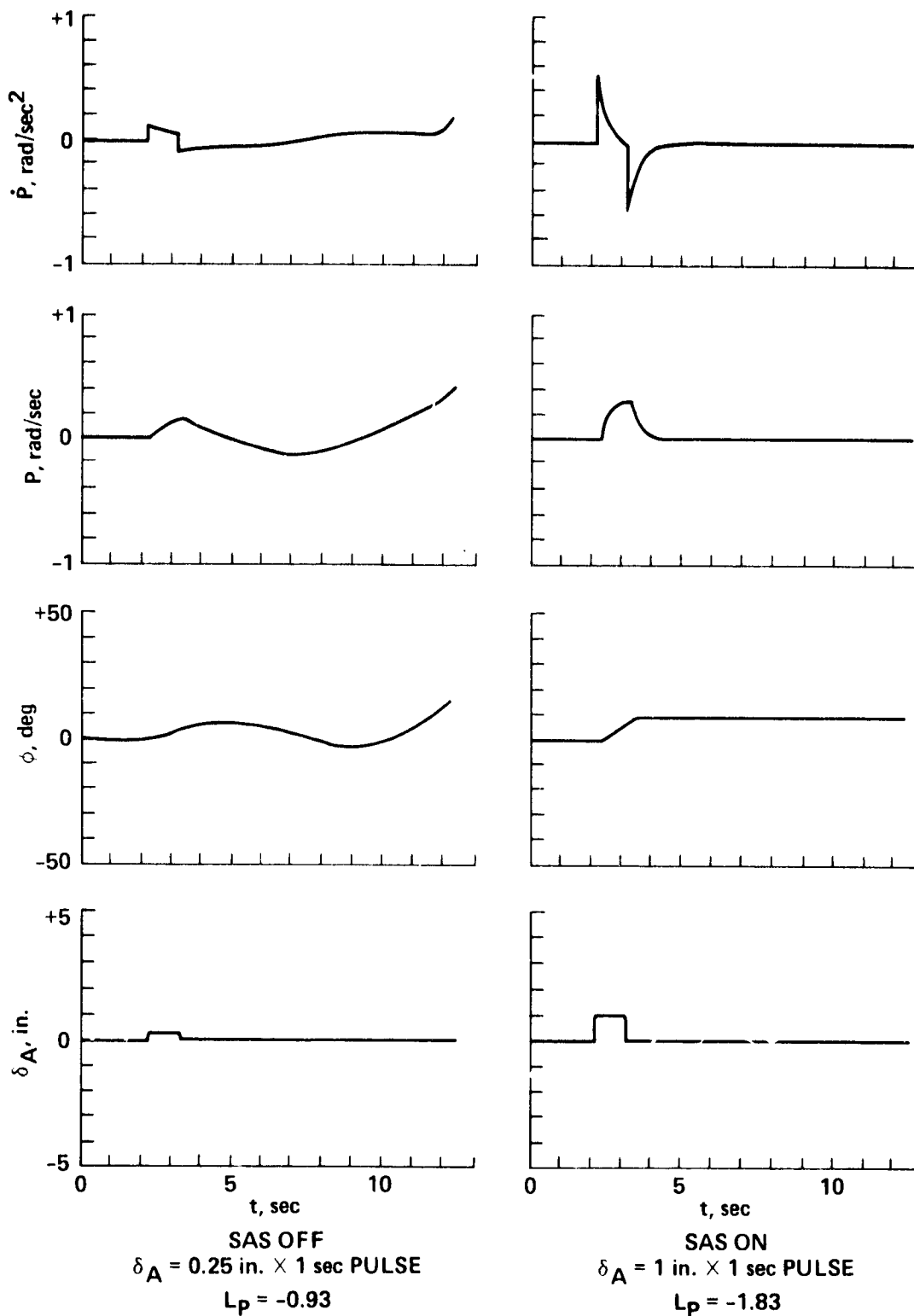


Figure 47.- Lateral axis dynamic response SAS OFF and ON;  
 $V_{eq} = 130 \text{ knots}$ , weight = 33,000 lb, nominal c.g. position.

# Dynamic Response OF POOL

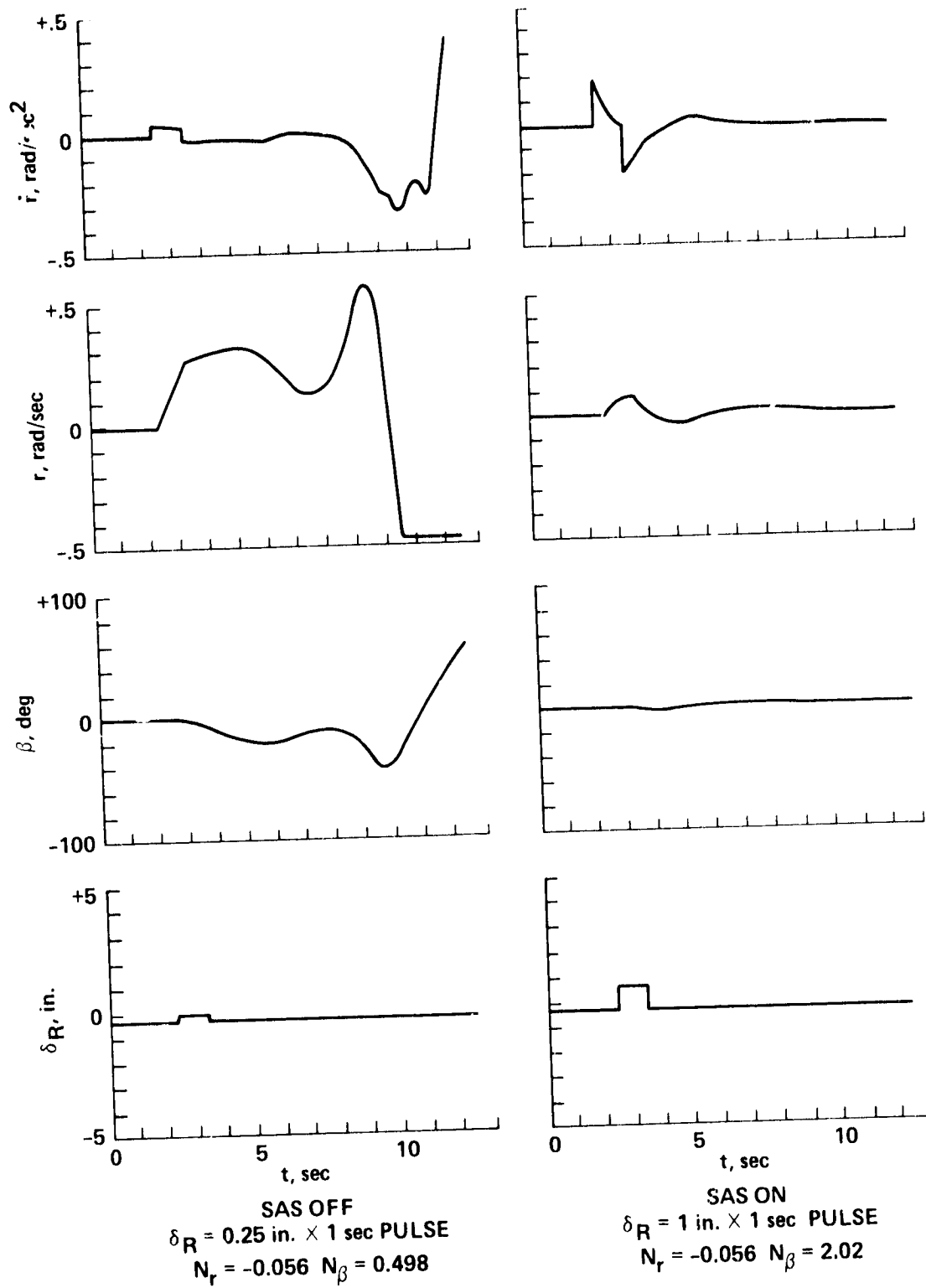


Figure 48.- Directional axis dynamic response SAS OFF and ON;  
 $V_{eq} = 130$  knots, weight = 33,000 lb, nominal c.g. position.

ORIGINAL PAGE IS  
OF POOR QUALITY

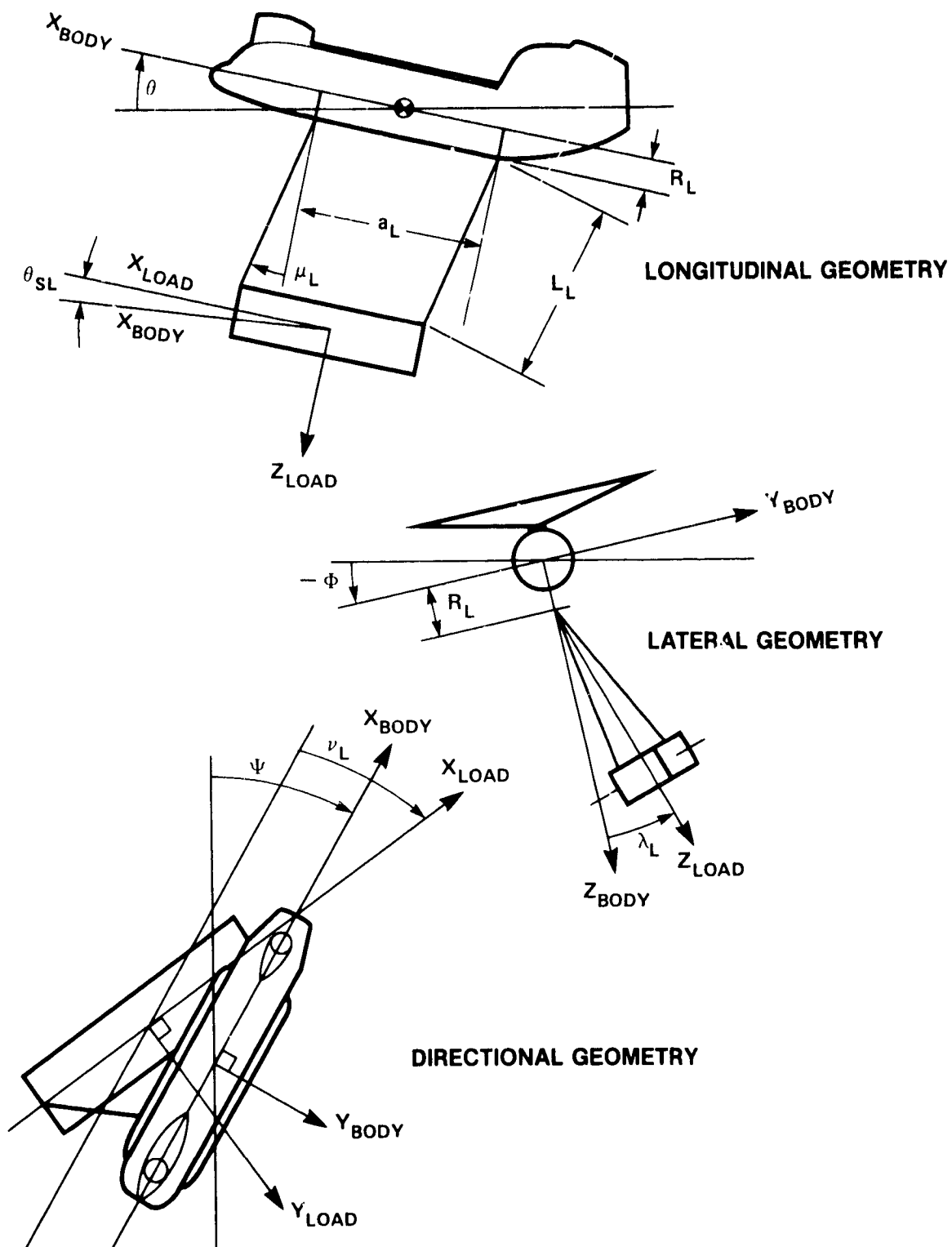


Figure 49.- Slung load geometry (fig. 6.1 of ref. 1).

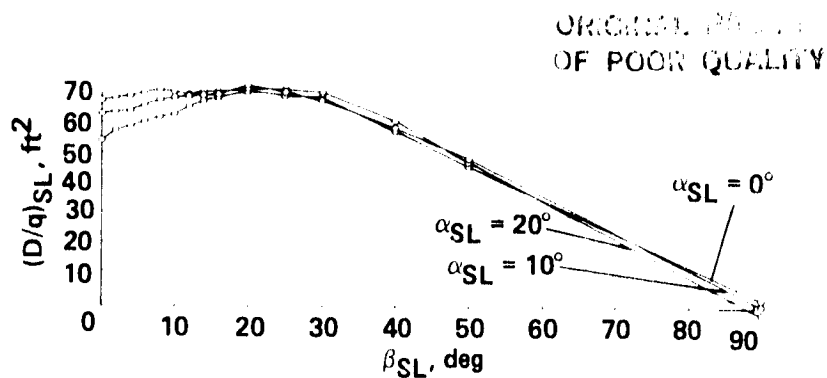


Figure 50.- Slung load drag force (table: SLDQT).

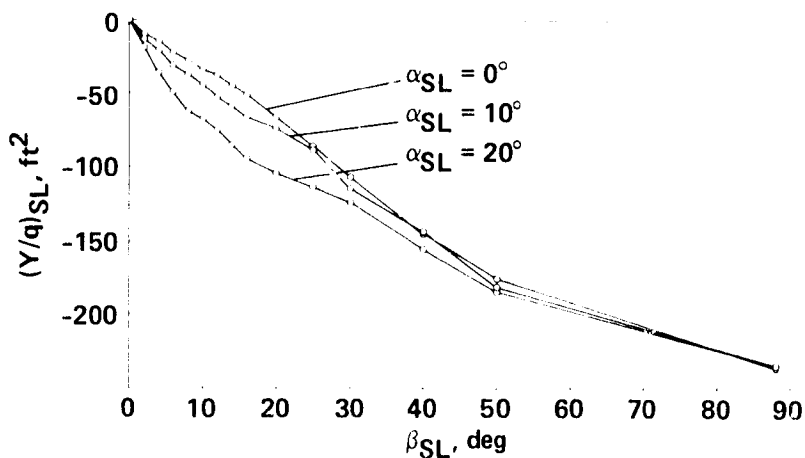


Figure 51.- Slung load side force (table: SLYQT).

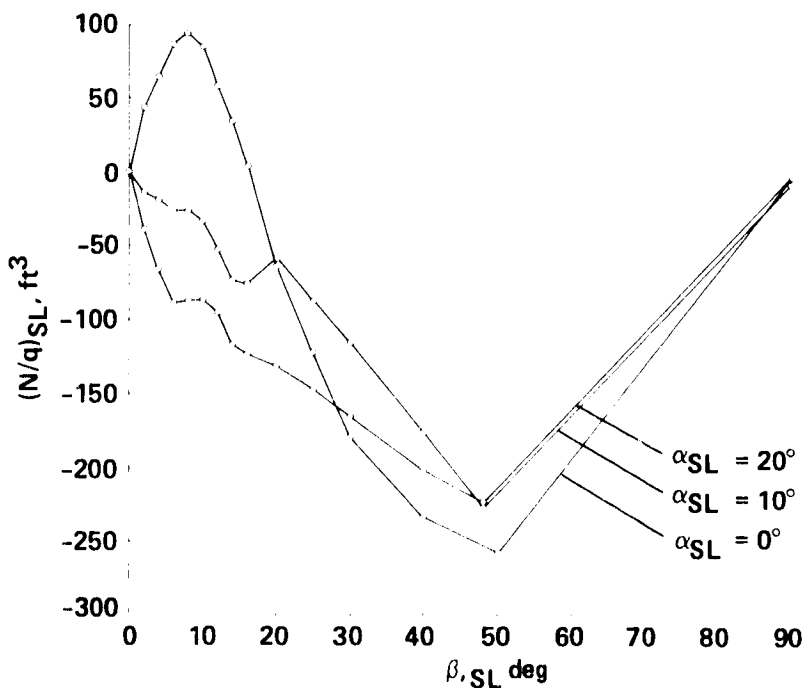


Figure 52.- Slung-load yawing moment (table: SLNQT).